University of Newcastle Upon Tyne

Department of Civil Engineering

Physically-based Mathematical Modelling of Catchment Sediment Yield

by

Jon M Wicks

NEWCASTLE UNIVERSITY LIBRARY

088 23203 9

Thesis L3442

Thesis submitted for the degree of Doctor of Philosophy

December 1988

ABSTRACT

A physically-based, distributed sediment yield component has been developed for the SHE hydrological modelling system. This new component models the hillslope processes of soil detachment by raindrop impact, leaf drip impact and overland flow, and transport by overland flow. If the eroded soil reaches a river system it is routed downstream along with any mobilised river bed material. Deposition on land or in a river is simulated and the river bed material size distribution is continuously updated with allowance for armour layer development.

The equation developed for soil detachment by raindrop and leaf drip impact was successfully tested using data from a field plot with a range of soybean canopy covers and rainfall intensities. The soil detachment coefficient in this equation was determined for a range of soil types and showed a variation consistent with that which may be expected from a consideration of the physics of a soil's resistance to detachment.

At present two soil detachment coefficients need calibration. In order to investigate the variation in these coefficient values, as well as to test the component, various applications were carried out. The hillslope sub-component was applied to rainfall simulator plots with a variety of surface conditions. Two sets of calibration parameters, distinguishable on a physical basis according to the degree of soil disturbance, were found to be appropriate for all the plots. To investigate scale effects, parameters calibrated at the rainfall simulator plot scale were transferred to a 1-ha rangeland sub-catchment. With no further calibration, the catchment response for four events was poorly simulated for both water and sediment. However, with reasonable

variations in the antecedent soil moisture content but no variation in plot calibrated sediment parameters, the sediment yield for two of the four events could be successfully simulated. These applications suggest that parameter transfer is feasible if the sediment yield characteristics at the different scales are similar.

Further applications of the hillslope sub-component were carried out for two small agricultural catchments. The sediment response could be simulated to at least the same accuracy as achieved by two existing distributed soil erosion models. The channel sub-component was applied to the East Fork River, Wyoming. Although the complex sediment storage/supply effects could not be reproduced completely, the simulated response was nevertheless of similar accuracy to that achieved by two existing alluvial river models.

The new component is considered to be a valuable contribution to sediment yield modelling as a physically-based approach is used for both the hillslope and channel phases of the catchment sediment system, within the framework of an advanced hydrological modelling system.

ACKNOWLEDGEMENTS

I wish to thank my supervisors, Dr J.C. Bathurst and Professor P.E. O'Connell, for their invaluable guidance and support throughout the period of this research.

Data from field and laboratory studies conducted by others have formed an important input to my work. I therefore thank all those who were involved in taking measurements which I have used in my research. In particular Dr W.H. Blackburn, C.W. Johnson and colleagues at the USDA-ARS Northwest Watershed Research Center, Boise, Idaho, for considerable assistance with the Reynolds Creek data, Professor H.P Johnson (Iowa State University) for permission to use the ISU data, and Professor S.C. Jain (Iowa Institute of Hydraulic Research) for supplying the data collected by Mosconi.

I am grateful to a number of people for helpful discussions and for supplying information. These include Professor T.J. Ward (New Mexico State University), Professor R.P.C. Morgan (Silsoe College), Dr R. Bettess (Hydraulics Research, Wallingford), S.A. Nielsen and B. Storm (Danish Hydraulic Institute) and Professor G. Fleming (University of Strathclyde).

Financial support was provided by a Natural Environment Research Council Research Studentship, with the visit to Idaho funded by a NATO Collaborative Research Grant.

To NJM.

TABLE OF CONTENTS

LIST OF FIGURES

LIST OF TABLES

LIST OF MAIN SYMBOLS

(L = length; M = mass; T = time; (-) = dimensionless)

a	coefficient
A	cross-sectional area (L^2)
AD	active layer thickness (L)
b	exponent
B	constant term in the finite difference scheme ($=\Delta t/(\Delta x \Delta y)$) ($T\ L^{-2}$)
C	volumetric sediment concentration (-)
C_C	canopy cover density (-)
C_G	ground cover density (-)
d	raindrop diameter (L)
D_F	soil detachment rate by overland flow ($M\ L^{-2}\ T^{-1}$)
D_n	sediment diameter for which n% of the material is finer (L)
D_R	soil detachment rate by raindrop impact ($M\ L^{-2}\ T^{-1}$)
F_m	proportion of the sediment sample in size fraction m (-)
F_w	water depth correction factor (-)
g	acceleration due to gravity ($L\ T^{-2}$)
g_s	volumetric sediment transport rate per unit width ($L^2\ T^{-1}$)
G	volumetric sediment transport rate ($L^3\ T^{-1}$)
G_{cap}	volumetric sediment transport capacity ($L^3\ T^{-1}$)
h	water depth (L)
I	rainfall intensity ($L\ T^{-1}$)
K	soil erodibility index
K_F	overland flow soil detachment coefficient ($M\ T^{-1}\ L^{-2}$)
K_R	raindrop soil detachment coefficient ($T^2\ M^{-1}\ L^{-2}$)
M_D	momentum squared per unit area per unit time for leaf drip ($M^2\ T^{-3}$)
M_R	momentum squared per unit area per unit time for direct rainfall ($M^2\ T^{-3}$)
P	wetted perimeter (L)
q	water discharge per unit width ($L^2\ T^{-1}$)
Q	water discharge ($L^3\ T^{-1}$)
R	rainfall erosivity
s	specific gravity of sediment particles (-)
S	slope (-)

SD loose soil thickness (L)

t time (T)

v kinematic viscosity of water (L^2 T^{-1})

V water velocity (L T^{-1})

V_s longitudinal sediment velocity (L T^{-1})

V_* bed shear velocity (L T^{-1})

w fall velocity (L T^{-1})

W active bed width (L)

x distance in the x direction (L)

y distance in the y direction (L)

z surface elevation (L)

α coefficient

β exponent

Δt time step (T)

Δx distance step in the x direction (L)

Δy distance step in the y direction (L)

Δz change in surface elevation (erosion if negative) (L)

ϵ dispersion coefficient (L^2 T^{-1})

θ time weighting factor in the finite difference scheme (-)

λ porosity (-)

ρ density of water (M L^{-3})

ρ_s density of sediment particles (M L^{-3})

τ shear stress (M T^{-2} L^{-1})

τ_c critical shear stress for initiation of sediment motion (M T^{-2} L^{-1})

ϕ space weighting factor in the finite difference scheme (-)

Subscripts

i channel node index

i,j position indices in the x and y directions respectively

k channel link index

m particle size fraction index

Superscripts

n time index

CHAPTER 1 - INTRODUCTION

Mathematical models of the catchment sediment system are developed to meet the demands made by various groups for predictive tools to aid the decision making process. In the past the requirements have been for field-scale models to predict the annual soil erosion for soil conservation studies, and for models to predict annual catchment sediment yield for reservoir design studies. While these demands continue, there are now further demands being placed on sediment yield modelling for a wide range of sediment related problems. The sediment problems can occur in three environments: source areas (e.g. fields), transfer areas (e.g. rivers) and sink areas (e.g. reservoirs).

Sediment problems in the source areas are usually associated with land management activities. Increased erosion may be caused by inappropriate agricultural practices, domestic animal overgrazing and removal of the natural cover and disturbance to the soil associated with construction, forestry and mining. The most obvious detrimental effect is the loss of soil nutrients and thus agricultural productivity, but the transport pathways and depositional environment of the eroded soil and any associated chemical pollutants are becoming increasingly important (Walling, 1983, 1988).

The sediment load of a river can be increased by accelerated source area erosion and following man-induced changes to the hydraulic characteristics of the river. Where bed aggradation occurs, this may result in increased dredging costs, increased likelihood of flooding, pollution (particularly if chemicals are adsorbed onto the sediment particles) and have a detrimental impact on the natural wildlife (e.g. clogging of fish spawning grounds). Adverse impacts can also result from a reduction in the sediment load, for example the clear water degradation below a dam.

Many of the world's reservoirs have had their usable storage capacity completely filled by sedimentation after only a few years of operation (Sundborg, 1983). Even in less extreme cases, the reduction in water storage capacity caused by sedimentation will reduce the usefulness of the reservoir for flood prevention, water supply, irrigation, power generation and other uses.

The most appropriate approach for simulating many of the above examples of sediment problems is through physically-based, distributed modelling. Some of the benefits of this approach are discussed below.

(1) The modelling system provides a framework in which an integrated view can be taken of the catchment sediment system. This is important as activity in one part of a catchment can cause problems in another part of the catchment (e.g. Wolman, 1977; Sundborg, 1983; Newson and Leeks, 1987). The model will produce a distributed prediction of the sediment response, and therefore source and sink areas for sediment within the catchment can be identified.

(2) The physically-based approach has the potential for use in ungauged catchments as, in principle, all parameters are measurable in the field and do not require a lengthy record for their calibration.

(3) The approach allows an evaluation of the effects of different land management options on the catchment sediment response. Localised land use changes can be incorporated into

the model owing to its distributed basis.

Other advantages of physically-based, distributed models over the more traditional empirical models include: their potential for greater accuracy, allowance for a continuous simulation of the sediment response at all points within the catchment, and ability to incorporate advances in process equations.

The objectives of the research reported in this thesis were to develop and apply a physically-based, distributed mathematical model of catchment sediment yield. The new model, called SHESED, forms the sediment yield component of the SHE hydrological modelling system.

Structure of the Thesis

In Chapter 2 a literature review of the hillslope and channel processes and process models is presented. The review concentrates on processes where water is the eroding agent. The chapter includes a critical review of some examples of current soil erosion, channel sediment routing and sediment yield models.

The third chapter concerns the SHE hydrological modelling system. A short description of the components of the SHE is presented, along with a discussion of the procedure for applying the SHE to a catchment and some of the problems encountered when using the SHE.

In Chapters 4 and 5 the process equations and routing algorithms used in the SHESED hillslope and channel sub-components are described. The chapters include verification applications of the algorithms for soil detachment by raindrop impact and channel bed armouring. Further details of the model are presented in Appendix E (program structure) and Appendix F (data requirements).

Chapters 6, 7 and 8 describe applications of the SHE system with the new sediment yield component. In Chapter 6 applications to rainfall simulator plots and the transfer of parameter values to a 1-ha rangeland sub-catchment are discussed. Chapter 7 describes the application to two small agricultural catchments in Iowa. Chapter 8 describes the application of the SHESED channel sub-component to the East Fork River, Wyoming.

The final chapter provides a summary of the achievements of the research and highlights the capabilities and limitations of the new model. Recommendations for further research are presented.

CHAPTER 2 - LITERATURE REVIEW

2.1 INTRODUCTION

There is an extensive literature of relevance to the processes and modelling of soil erosion, river sediment transport and sediment yield. For soil erosion, the important review type material includes Kirkby and Morgan (1980), Hudson (1981), Foster (1982), UNESCO (1985), Morgan (1986) and Lane et al. (1988). For river sediment processes and modelling, reviews are provided by Vanoni (1975), Simons and Sentürk (1977), Graf (1984), Dawdy and Vanoni (1986) and Pickup (1988). Sediment yield processes and modelling are covered in many of the above references and also by Bennett (1974), Fleming (1977), Walling (1983), Bathurst and Wicks (1988), Singh et al. (1988) and Walling (1988). In view of this review literature it is not necessary to reproduce here a detailed discussion of the processes which affect the catchment sediment yield. Therefore, in this chapter, only an outline of the major processes is attempted, with a more lengthy review presented of the available process models. The chapter is completed by an appraisal of current soil erosion, river sediment and catchment sediment yield models.

Before beginning the discussion of catchment sediment processes it is worthwhile to bring together some definitions of terms used in this thesis.

The **sediment yield** is usually defined as the total sediment outflow from a catchment, measurable at a cross section of reference and in a specific period of time (Vanoni, 1975). If a physically-based, distributed modelling approach is taken to determine the sediment yield, then the sediment yield can also be considered to represent the net effects of all sediment processes within a catchment. Thus, physically-based, distributed sediment yield models are models of the catchment sediment system and therefore combine hillslope phase and channel phase models.

The term **soil erosion** is used in this thesis to refer to the detachment and transport of soil particles (primary particles and aggregates) by the action of flowing water and raindrop impact on hillslopes. The term **hillslope sediment processes** is used to describe all sediment processes which act on hillslopes such as soil erosion, gully erosion (see Section 2.2.3), mass movement (see Section 2.2.4) and wind erosion (see Section 2.2.5.3).

The ratio of sediment yield to the gross erosion within the catchment is termed the **sediment delivery ratio**. Because of sediment storage effects, the delivery ratio may be less than or greater than unity.

Soil erosion may be divided into rill and interrill erosion. **Rill erosion** is the detachment and transport of soil particles by concentrated overland (i.e. hillslope phase) flow in small ephemeral channels. **Interrill erosion** comprises the processes of soil detachment and transport by raindrop impact, and transport and (to a lesser extent) detachment by sheet flow (broad shallow overland flow). Interrill areas are generally considered to be the source areas for sediment which is subsequently transported downslope by rill flow.

The resistance of a soil to detachment and transport is termed **soil erodibility**, whereas the resistance to detachment alone is termed **soil detachability**. The erosive potential of flowing water and raindrops is called **erosivity**.

Note that in this thesis the hydrology is assumed to be accounted for elsewhere (i.e. by the SHE model) and therefore the factors affecting channel and overland flow are not discussed in detail.

The processes which affect sediment yield are discussed below, under the headings hillslope and channel sediment processes.

2.2 HILLSLOPE SEDIMENT PROCESSES

The important hillslope sediment processes are raindrop induced soil detachment, overland flow erosion, gully erosion and mass movements. These and further minor processes are discussed in this section along with a review of the available mathematical representations.

2.2.1 Raindrop Impact

Raindrop impact can initiate soil erosion by breaking cohesive bonds between soil particles (primary or aggregates) and by launching particles into the air or surface water. If the soil surface is not perpendicular to the rainfall a net movement of the particles downslope can result. Sediment transport caused by raindrop impact for given loose soil and rainfall characteristics will depend on the surface slope, surface water depth and wind conditions. Simple empirical equations exist relating transport to rain intensity and surface slope (e.g. Meyer and Wischmeier, 1969) but on the catchment scale raindrop induced transport is generally very small compared with overland flow transport (e.g. Young and Wiersma, 1973) and can therefore be neglected. The major effect of raindrop impact is thus to detach soil particles.

2.2.1.1 Factors affecting raindrop detachment

Soil detachment by raindrop impact is an important hillslope erosion process. It is influenced by a large number of variables, many of which are interrelated. Predictive equations are usually based on a combination of conjecture and data analysis involving some of the major variables discussed below.

(a) Soil properties. The main soil properties which affect detachment are texture, structure and moisture content. For example, fine particles (clays) are resistant to detachment because of their cohesiveness, and the grains of a loosely structured soil are detached more easily than are those of a dense soil. A suitable procedure for quantifying the relative susceptibility of different soils to detachment by raindrop impact is at present not available. Pall et al. (1982) review some of the research in this area and attempt to identify key soil characteristics. Soil shear strength is the most promising soil characteristic for assessing a soil's detachability by raindrop impact. Al-Durrah and Bradford (1982) present evidence for the use of the undrained shear strength (measured with the falling cone penetration apparatus) to represent a soil's resistance to raindrop detachment. Cruse and Larson (1977) also show that soil detachment by raindrops closely correlates with the shear strength of the soil (measured by the triaxial compression test).

(b) Climate. Rainfall is the most important climatic variable. The force exerted on a soil grain by a raindrop is related to the drop size and impact velocity. Temperature is important because of its effects on soil moisture content and form (frozen ground has a very high resistance to erosion), freeze-thaw action, and type of precipitation occurring (snowfall will not cause detachment, whereas hail will (e.g. Hagen et al., 1975)). Wind will affect raindrop velocities and fall inclinations.

(c) Vegetation. The major role of vegetation in raindrop detachment is the interception of the raindrops so that their kinetic energy is dissipated by the plants rather than imparted to the soil. The terms canopy cover density and ground cover density can be used to describe the amount of high cover (e.g. trees) and the low cover (grass, forest litter, mulch and stones) respectively. This distinction can be important as intercepted raindrops can coalesce to form larger drops which, if they then fall from a sufficient height, are potentially more erosive than the original rainfall (e.g. Mosley, 1982; Morgan, 1985; Vis, 1986). The vegetation may also redistribute the rain resulting in regions of repeated leaf drip impact. Soil resistance to detachment is also increased by root binding.

(d) Human influences. Agricultural activities, forest management, mining and construction can all directly or indirectly affect soil detachment. For example, tillage will loosen the soil thus making it easier to be detached, while soil compaction by traffic may make the soil more resistant to detachment.

(e) Surface water depth. Surface water will affect detachment by dissipating the energy of raindrops once some critical water depth has been reached.

(f) Topography. Both micro-topography and hillside slope may affect detachment. The slope may affect the stability of a cohesionless soil, leading to an increased detachability on a steeper slope. However, an increased slope can lead to a reduction in the normal component of the impact force. It is this normal component that has been taken to be important for detachment by some research workers (e.g. Rowlinson and Martin, 1971; Gilley et al., 1985). The net effect of slope on detachment is problematical, for example, using field measurements Morgan (1978) found that detachment was independent of slope.

2.2.1.2 Modelling raindrop detachment

A common approach to constructing a detachment equation is to express detachment as a product of rainfall erosivity and soil detachability factors, i.e. $D_R = K_R R$, where D_R = rate of soil detached by raindrop impact per unit area; K_R = raindrop soil detachment factor; R = rainfall erosivity factor. This expression is then multiplied by factors which account for secondary effects, such as ground cover, canopy cover and surface water. While it is recognised that this approach ignores any interactions between factors, it does allow the findings of studies which have considered only one or two of the factors to be used. Suitable components of an equation for soil detachment by raindrop impact are discussed below.

(a) Soil Detachability. As discussed in Section 2.2.1.1, there is currently no generally accepted expression, based on soil properties, to quantify a soil's susceptibility to detachment by raindrop impact. This leaves the options of either using adjusted existing erodibility indices (i.e. indices expressing a soil's resistance to detachment and transport by raindrops and flowing water) or calibrating the raindrop soil detachment factor with measurements. By far the best known soil erodibility index is the Universal Soil Loss Equation (USLE) K value (Wischmeier and Smith, 1978). Until a more appropriate index is documented, it may seem expedient to use the large amount of information relating soil type to erosion acquired for the USLE to formulate an expression relating soil detachability by raindrop impact to the USLE K factor. This approach was taken by Foster (1982), among others, who needed to make such assumptions as: (1) interrill erosion equals rill erosion for average USLE plot conditions; and (2) rainfall intensities can be typified by a value of 63.5 mm h^{-1}. Foster also suggests that if a soil seems especially susceptible to rill erosion then K should be decreased by one third, and if the soil is not susceptible to rilling K should be increased by one third. However, adjusting USLE K factors in this manner is not recommended as it is likely to lead to large errors; the USLE K factor is an average annual value that combines resistance to detachment and transport by both raindrops and overland flow, it accounts for the infiltration characteristics of the soil, and is intrinsically tied to the USLE erosivity index.

In view of the difficulty of using existing indices, most current, physically-based, soil erosion models leave the soil detachment factor as an unknown to be determined at the model calibration phase.

(b) Rainfall characteristics. Gilley and Finkner (1985) compared the performance of several rainfall parameters for estimating soil detachment by raindrop impact using data available in the literature. They found that the rainfall parameter which provided the best statistical fit was the product of drop circumference and kinetic energy. This product is equivalent to the fifth power of drop diameter. They developed the relationship to form the practical regression equation given below.

$$D_R = 1.299 \times 10^{-5} K_R I^{1.368} \qquad (2.1)$$

where D_R = soil detached by raindrop impact (kg m^{-2} s^{-1}); K_R = raindrop soil detachment coefficient (s m^{-5}); I = rainfall intensity (mm h^{-1}).

Based on a simple model for inelastic collision, Styczen and Høgh-Schmidt (1988) showed that soil detachment by raindrop impact is proportional to the sum of the squared momenta of each drop in a rain event. Using the Marshall and Palmer (1948) raindrop size distribution, they calculated that momentum squared is proportional to $I^{1.83}$ for rainfall intensities below 100 mm h^{-1} and to $I^{1.43}$ for intensities between 100 and 250 mm h^{-1}. They report that the momentum squared approach yields better agreement with the data of Morgan (1985) than do equations based on energy or intensity.

Many of the existing process-based soil erosion models assume rainfall erosivity to be proportional to I^2 (e.g. Li, 1979; Foster, 1982; Rose, 1985). Experimental data tend to confirm this value, although there is usually a range of exponent values, for example Meyer and Harmon (1984) found the exponent to vary between 1.63 and 2.15, with 12 out of 18 values within 10% of 2.

(c) Ground and canopy cover. The effect of ground and canopy cover on detachment by raindrop impact can be included in a detachment equation by multiplying by a simple reduction factor representing the proportion of the soil surface not covered by vegetation, stones or mulch. An alternative expression is necessary where importance is given to the regain of erosive potential by coalesced drops falling from the canopy. For example:

$$D_R = K_R \, [R_D C_C + R_R(1 - C_C)](1 - C_G) \tag{2.2}$$

where R_R = rainfall erosivity for the unaltered rainfall; R_D = rainfall erosivity for drops falling from the canopy; C_G = ground cover density; C_C = canopy cover density. This expression assumes ground cover to be uniformly distributed below the canopy cover which may not be the case; also it does not allow for more than one canopy height.

(d) Surface water. The functions to account for the effect of a surface water layer on soil detachment by raindrop impact reported by Li (1979), Park et al. (1982), and Gilley et al. (1985) are

Li (1979)

$$\begin{aligned} F_w &= \left[1 - \frac{h}{3d}\right] && \text{if } h < 3d \\ F_w &= 0 && \text{if } h \geq 3d \end{aligned} \tag{2.3}$$

Park et al. (1982)

$$F_w = 1 \qquad \text{if } h \le d$$

$$F_w = e^{(1 - h/d)} \qquad \text{if } d < h \le 5h \tag{2.4}$$

$$F_w = 0 \qquad \text{if } h > 5h$$

Gilley et al. (1985)

$$F_w = \left[\frac{d}{h}\right]^{1.83} \tag{2.5}$$

where F_w = water depth correction factor (such that $D_R = K_R F_w R$); h = water depth; d = median raindrop diameter.

Figure 2.1 shows a comparison of these three functions with the data of Palmer (1965). The functions perform approximately equally well, perhaps not surprisingly since Palmer's data were used in the derivation of all three functions.

2.2.2 Overland Flow Erosion

Overland flow erosion is usually considered as a combination of sheet and rill erosion, with both processes being able to detach and transport sediment. Sheet erosion can be thought of as the removal of a sheet of sediment of uniform thickness, whereas rill erosion involves the removal of sediment by small concentrations of water flowing in channels which are small enough to be obliterated by normal agricultural practices.

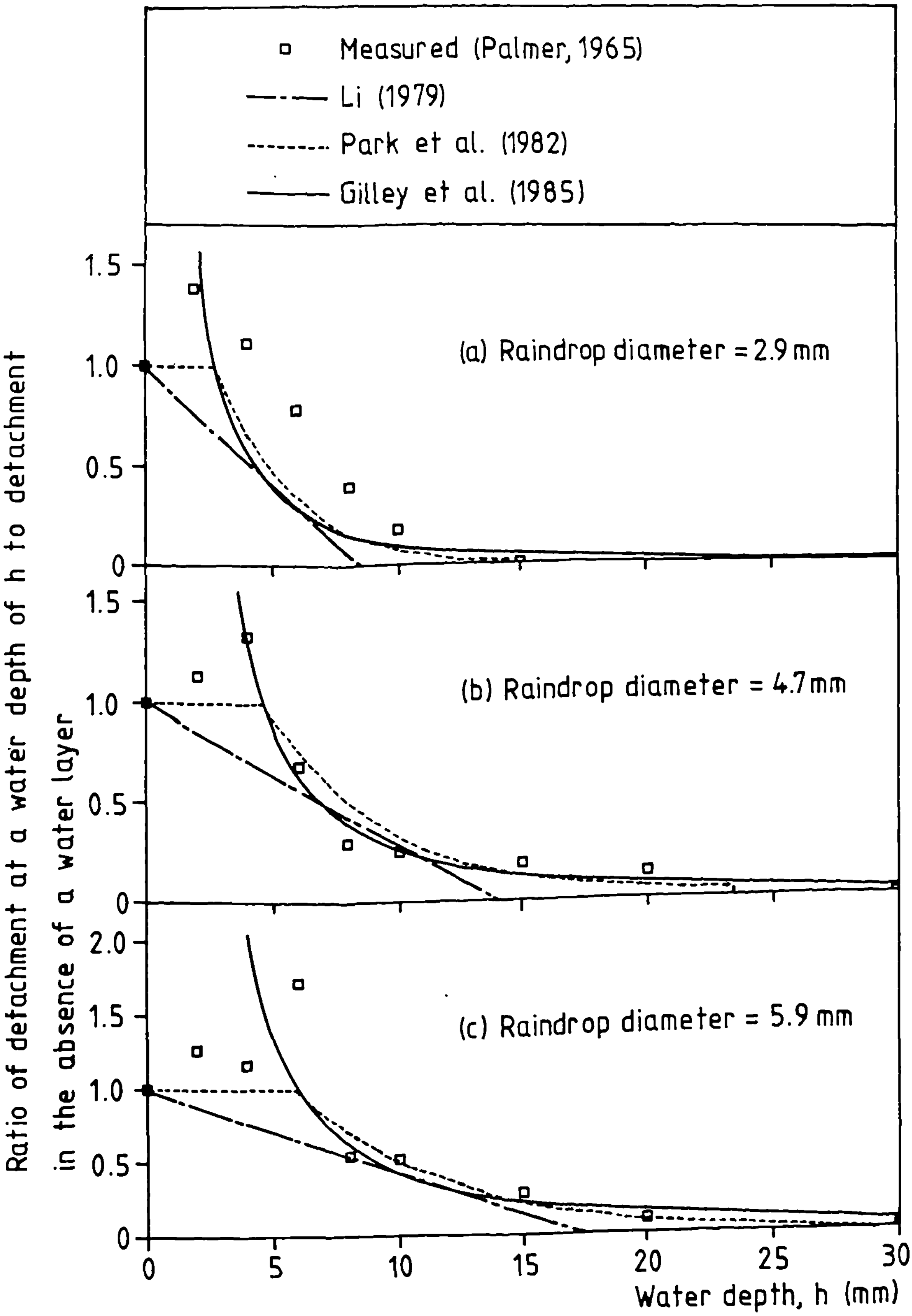

Fig. 2.1 Comparison of three functions to account for the effects of a water layer on raindrop soil detachment using the data of Palmer (1965).

2.2.2.1 Factors affecting overland flow erosion

(a) Overland flow. Overland flow depth and velocity are the most important variables but, as they will be calculated by the overland flow component of the catchment model, they are not discussed here. Turbulence of overland flow is discussed by Julien and Simons (1985) who state that overland flow can be laminar or turbulent depending on the Reynolds number. This would then affect the applicability of alluvial channel sediment transport relationships. Yoon and Wenzel (1971) showed that overland flow with raindrop impact is turbulent even in the conventional laminar Reynolds number range. Turbulence may be assumed for the practical case of sheet flow over natural ground with rainfall.

(b) Soil properties. Soil properties which determine a soil's susceptibility to detachment by overland flow are on the whole the same as for raindrop impact detachment (Section 2.2.1.1), although it is likely that the relative importance of specific properties differ between the two processes. The effect of soil particle size distribution on overland flow erosion has been investigated experimentally by Rowntree (1982), who found that surface armouring effects are important. This is a process where finer material is winnowed from the surface layer, leaving larger and therefore less transportable particles to accumulate on the soil surface, thus shielding the subsurface layers which contain the original mixture of particle sizes.

(c) Vegetation. Vegetation is important owing to its effect on the overland flow; a denser vegetation cover increases flow resistance and therefore reduces flow velocity. It also strengthens the soil by root binding.

(d) Topography. Topography is important, mainly because of its effect on overland flow. Small scale hillslope topography can be important, for example local linear depressions encourage concentrations of flow which may result in regions of increased erosion. Whether a hillside is concave, straight or convex in profile will affect the sediment yield from the hillslope. On a concave slope there may be significant erosion on the upper part but it is possible that all the eroded material will be subsequently deposited on the lower, flatter part. With a convex slope, erosion is more likely to increase with distance downslope. This is an important modelling consideration as an idealised straight slope is unlikely to give the same sediment yield as the convex or concave slope it represents. Regression equations for overland flow erosion consider slope magnitude and slope length as key variables. These variables are, however, being used as substitutes for overland flow depth and velocity and therefore do not need to be included in models where the variation of overland flow in space and time is available.

2.2.2.2 Modelling overland flow detachment

As with raindrop induced detachment, overland flow detachment equations can be considered to consist of the product of a soil detachability factor and an overland flow erosivity factor.

The soil detachability factor can be considered as a function of a soil erodibility index (see Section 2.2.1.2) but is usually left as an unknown to be determined at the model calibration phase.

The flow erosivity factor has been assumed to be a power function of the boundary shear stress

$$D_F = K_F\ (\tau - \tau_c)^b \qquad (2.6)$$

where D_F = soil detached by overland flow; K_F = soil detachability factor for overland flow; τ = shear stress; τ_c = critical shear stress for initiation of sediment motion; b = exponent. Experimental data have been used to determine the exponent and results generally range between 1.0 and 2.0. The critical shear stress may be calculated from experimentally derived relationships such as those given by Smerdon and Beasley (1961), which relate τ_c to soil plasticity, dispersion ratio, mean particle size or percentage clay content. The equation from Smerdon and Beasley with the highest correlation coefficient (r = 0.980) is

$$\tau_c = 0.493 \times 10^{0.0183PC} \qquad (2.7)$$

where τ_c = critical shear stress ($N\ m^{-2}$); PC = percentage clay content of the soil.

Alternatively the critical shear stress may be determined from the Shields curve, although this was derived for material typical of river beds and not cohesive soils. The critical shear stress may also be assumed to be equal to zero or else can be determined by calibration. In equation 2.6 the shear stress should be that which acts upon the soil surface, and not the total shear stress which will act upon both the cover and the soil. Foster (1982) determined the shear stress acting on the soil through partitioning the friction factor between that due to the soil and that due to cover, and then used the Darcy-Weisbach equation to calculate τ using the friction factor due to the soil. Limited experimental data are available to aid the partitioning of the friction factor.

An alternative to using equation 2.6 is to assume that D_F is directly proportional to the difference between the sediment transport capacity and the sediment load (e.g. Li, 1979; Foster, 1982)

$$D_F = \alpha\ (G_{cap} - G) \tag{2.8}$$

where α = coefficient; G_{cap} = sediment transport capacity; G = sediment load.

Equations 2.6 and 2.8 are related. If equation 2.6 is used in conjunction with the Meyer and Wischmeier (1969) transport capacity approach (see Section 2.4.1), then the detachment calculated from equation 2.6 combined with the current sediment load, must not be greater than the transport capacity. This corresponds to equation 2.8 with $0 \leq \alpha \leq 1$.

2.2.2.3 Modelling overland flow transport

The ability of overland flow to transport detached soil particles and aggregates depends on the flow and rainfall characteristics and the sediment particle size, density and availability.

Two types of transport equation have been used: regression equations based on laboratory and field data, and transport capacity equations developed for alluvial channels. Two reported studies have compared many of the available formulae for overland flow conditions.

Alonso et al. (1981) used published shallow depth (0.58 m - 0.0008 m) laboratory and field data to compare nine bed and total load formulae. They recommended that the Yalin (1963) bed load function be used to compute sediment transport capacities for overland flow.

Julien and Simons (1985) derived a general power relationship supported by dimensional analysis and compared this with 13 empirical erosion equations. Their comparison uses no laboratory or field data and is only a test of whether the equations contain the basic variables Julien and Simons consider important. They then transformed 14 alluvial channel sediment transport equations into the same form as their general relationship. The equations were then evaluated in terms of the number of basic variables present and whether the values of the exponents of these basic variables were within the same range as those from the empirical erosion equations. The effect of laminar flow was also included in the analysis. They recommended the formulae of both Engelund and Hansen (1967) and Barekyan (see Simons and Sentürk, 1977, p516) as appropriate for overland flow transport capacity calculations.

Guy et al. (1987) reported experiments which showed that 85% of the transport capacity of rainfall-disturbed overland flow was attributable to raindrop impact, with only 15% attributable to runoff. They suggest that the increased transport capacity was associated with the very large temporary increases in horizontal flow velocities near the raindrop impact locations. None of the formulae recommended by Alonso et al. and Julien and Simons take into account the effect of raindrop impact on transport capacity.

2.2.2.4 Discussion of overland flow erosion modelling

In the review of approaches to overland flow erosion modelling given above, no distinction was made between rill and sheet erosion. There appears to be no way to predict if rills will form for given flow and soil conditions (e.g. see Young and Onstad, 1982). However, rilling has a significant effect on soil erosion and therefore needs to be included in soil erosion models. A number of approaches have been followed for including its effects. The simplest is to ignore the geometric differences between rill and sheet flows, with the effects of rilling being accounted for in the calibration phase (the occurrence of rills being represented by an increase in the soil detachment coefficient). It can be argued that this approach is taken in most current soil erosion models - even those which seem to deal with rills separately. For example, Foster (1982) describes separate equations for processes in rills and between rills, but he also states "rill erosion and flow are assumed to be uniformly distributed across the slope, although physically the flows and erosion are concentrated in small channels". Thus the Foster (1982) type of model is in effect no different from models that assume uniform overland flow depths across the slope. A rill susceptibility factor is another approach for accounting for the effects of rills: for example Komura (1976) multiplied the erosion rate calculated for sheet flow by 5.0 for sheet flow with rills. An alternative approach is to assume that rill pathways will follow furrows in the microtopography; this approach is taken by Khanbilvardi et al. (1983) and by Foster and Smith (1985).

A number of research workers have combined the processes of detachment and transport to produce a single equation for erosion by overland flow, e.g. Li et al. (1973) and Komura (1976). The two works referred to include the assumption that the soil layer is loose and of homogeneous composition. However, they do include a 'fine sediment pick-up rate', which is a power function of the boundary shear stress in exactly the same way as the previously discussed detachment factors.

All the detachment equations referred to so far do not explicitly include particle diameter and density as variables. Their effect is taken to be represented in the soil detachability factor. Only in the alluvial channel transport equations is the sediment diameter and density required as input data. This lack of accounting for particle size prevents formulation of routines to model selective detachment.

Deposition of sediment from overland flow is usually modelled using one of two basic approaches. The first approach is based on the concept that deposition occurs only when the sediment load is greater than the transport capacity (this follows from the work of Meyer and Wischmeier (1969) (see Section 2.4.1)). This approach is used in CREAMS (Knisel, 1980) with the deposition rate calculated from $D = \alpha(G_{cap} - G)$, where D = deposition rate; α = coefficient; G_{cap} = transport capacity; G = sediment load. The coefficient α is estimated from $\alpha = 0.5w/q$, where w = particle fall velocity; q = water discharge per unit width. In the second approach, sediment deposition is assumed to be a continually occurring process owing to sediment settling out under gravity. The rate of deposition is calculated from $D = wC$, where C = sediment concentration (Rose, 1985).

2.2.3 Gully Erosion

Gully erosion has been defined by Vanoni (1975) as the removal of soil by concentrations of flowing water sufficient to cause the formation of channels that cannot be smoothed completely by normal cultivation methods. Typically, they have steep sides, cut into unconsolidated materials and transmit water only during the period of a storm. The erosion of the gully surface can be caused by flowing water, raindrop impact and mass movement. Piest et al. (1975) discuss the relative importance of gully processes and show the effects of different conservation practices on gully development. On the field scale gullying can be spectacular but its contribution to overall sediment production is usually found to be small. For example, in a semi-arid catchment in New Mexico, Leopold et al. (1966) found that gully erosion supplied only 1.4% of the total sediment production. Dunne and Leopold (1978), reporting the findings of Glymph (1957), give gully contributions ranging from 0% - 89%, with three-quarters of the values less than 30%.

2.2.3.1 Modelling gully erosion

In a catchment where gullying occurs, but does not contribute a significant proportion of the total sediment production, one modelling approach is to consider gullying as part of overland flow erosion. It may be appropriate to increase the soil detachability factor, or if present, the rill susceptibility factor. For example, Komura (1976) multiplied the erosion rate calculated for sheet flow by 10.0 for sheet erosion with gullies. If gully erosion is extensive, the feature should be modelled separately. However, at present there are no generally-applicable process-based models of gully formation and growth. Before such a model can be developed, a large amount of research needs to be done; Grissinger et al. (1985) discuss some of these research needs. A process-based model of gully erosion is likely to include process models for surface erosion by raindrop impact and overland flow, mass movement and subsurface erosion. An alternative to process-based models is to use empirical gully growth formulae in conjunction with field measurements to give estimates of gully erosion volumes. A number of these empirical formulae are given by Vanoni (1975, p452).

2.2.4 Mass Movement

Mass movement has been described by Leopold et al. (1964) as the movement of materials on slopes under the influence of gravity without benefit of the contributing force of independent agencies such as flowing water or wind. It can range from being very fast to imperceptibly slow, from persistently active to episodic, with a range of solid/water ratios and involving any amount of sediment.

Mass movement can detach and transport material to a channel or to another part of the hillslope, where it will be stored until moved by another mass movement event or by overland flow. The scars left by some mass movement processes may be subject to increased surface erosion.

The cause of mass movement depends on the type of movement being considered. Rice (1982) states that dry ravel (the down-slope movement by gravity of individual grains or aggregates of soil) can be initiated by animals and birds walking on the slopes, movement of vegetation by strong winds and removal of forest litter barriers by fire. Soil creep (the slow downhill movement of soil) results from freeze-thaw action, moisture content changes and slow plastic deformation under gravity. The various types of slides are caused by high pore water pressures, seismic action and by erosion at the slope base.

2.2.4.1 Modelling mass movement

At present there appear to be no models of mass movement processes which are appropriate for inclusion in catchment sediment yield models. However, in many catchments, mass movement is an important sediment production process. The first stage of a modelling project may be a survey of the catchment to determine which of the mass movement processes occur and if they are likely to be a significant source of sediment. A detailed survey may then be needed, using field work and remote sensing to estimate the volumes and levels of activity involved. For a discussion of the methods of recognition see Dunne and Leopold (1978, p569), Reid (1982) and Megahan and King (1985). A number of possible approaches may then be followed, for example:

(a) The soil mechanics slope stability methods may be applied to individual slopes, or used to give typical critical pore water pressures which can then be compared with measured or simulated pore water pressures. Because of likely uncertainties in input values (e.g. phreatic surface levels and soil and root strength parameters) some form of probability scheme may need to be introduced (e.g. Ward et al., 1981).

(b) If a number of mass movement events are studied then a prediction function can be fitted to the data, along the lines of the method used by Rice and Pillsbury (1982) for landslides in clearcut patches of forest in northwestern California, USA.

(c) Caine (1980) has used published records of rainfall intensities and durations to form a threshold expression for shallow landslides and debris flows. There may be scope to combine this with catchment data to predict volumes mobilised on a storm basis.

2.2.5 Other Hillslope Erosion Processes

Although raindrop detachment, overland flow erosion, gully erosion and mass movement are usually the dominant hillslope erosion processes, a number of other processes may be important in specific catchments. Many of these secondary processes supply sediment which is subsequently acted upon by the main processes e.g. glaciers (Gurnell, 1987) and volcanoes (Collins and Dunne, 1986). Human activities, subsurface erosion and wind erosion are perhaps more universal processes and are therefore discussed below.

2.2.5.1 Human erosion processes

Through agricultural, forest, mining and construction activities, among others, man can cause significant direct erosion as well as influence the main processes discussed previously. For example, minor roads are frequently left unmetalled and so the road surface, as well as roadside ditches and banks, can form a major source of loose material to be transported by another process. Madej (1982) gives sheet wash on road surfaces as the dominant sediment production process in a forested catchment in western Washington, USA. Mining activity can produce vast mounds of loose material and this waste may be routed into streams. If the quantity and particle size and density is known then mining waste can be included in a flexible distributed model.

2.2.5.2 Subsurface flow erosion

Subsurface transport involves both the slow movement of small particles through the soil pore space and a more rapid movement in subsurface pipes and tunnels. The first process is likely to supply only a very small percentage of the total sediment yield, whereas pipes are able to supply significant quantities of sediment (e.g. Jones, 1987). Data on which predictive equations can be based are rare (UNESCO, 1985) and in any case, advances in hydrological modelling of subsurface flow are needed before process-based models of subsurface erosion can be developed.

2.2.5.3 Wind erosion

The main variables affecting wind erosion are the wind velocity, topography, surface roughness, vegetation cover and soil properties. Cole (1985) provides a review of wind erosion modelling. Wind erosion is generally not included in sediment yield studies and is not considered further in this thesis.

2.2.6 Hillslope Sediment Routing

Hillslope sediment routing is the computation of the movement of the sediment load down a hillslope to the point where it may enter a channel. This involves combining the hillslope erosion processes in a way that simulates the actual detachment, transport, deposition and storage processes. There are, however, interactions between processes which are not fully understood, leading to uncertainties in the correct sequencing of erosion operations. Computations are based on the partial differential equation for conservation of sediment mass (Bennett, 1974)

$$\frac{\partial (hC)}{\partial t} + (1 - \lambda)\frac{\partial z}{\partial t} + \frac{\partial (hCV_s)}{\partial x} = \frac{\partial}{\partial x}\left[h\,\epsilon\,\frac{\partial C}{\partial x} \right] \qquad (2.9)$$

where h = depth of flow; C = sediment concentration; λ = porosity; z = surface elevation; V_s = sediment velocity; ϵ = dispersion coefficient; t = time; x = distance in direction of flow.

The dispersion term in equation 2.9 is usually assumed to have a negligible effect and is therefore ignored in most models. Further common simplifications include neglecting the $\partial(hC)/\partial t$ term (therefore assuming quasi-steady conditions), and assuming that the sediment velocity is equal to the flow velocity.

Equation 2.9 needs to be solved numerically, although simplified forms of the equation can be solved analytically.

Methods of solving equation 2.5 are discussed in the sections on existing models (Sections 2.4.1 and 2.4.3), along with a short discussion of the methods for providing the overland flow discharge to transport the sediment.

2.3 CHANNEL SEDIMENT PROCESSES

Sediment is transported in channels because of the hydrodynamic forces exerted on it by the flow of water. Therefore the two main variables are the hydraulic conditions of the flow and the presence of suitable sediment to be transported. If rivers were straight with steady flow and only one size and density of sediment of unlimited availability then modelling would be a relatively simple task. However, natural channels are very dynamic in nature with significant variations in bed and channel form, sediment characteristics and in the sediment and water discharge. The modelling considerations arising from the variable nature of rivers are discussed in the following sections.

2.3.1 Hydraulic and Sediment Characteristics

The primary hydraulic variables which influence sediment transport in channels are velocity, width, depth, slope and water temperature. The important sediment characteristics are size, shape, density, size distribution and availability of transportable particles. The sediment load can be classified according to either the transport mechanism or the origin of the sediment. The transport mechanism is determined by the flow and sediment characteristics; bed load moves by saltation, rolling and sliding on or near the bed, whereas the suspended load is maintained in suspension by the flow turbulence. Bed load is generally composed of large particles (e.g. gravel and sand) with the suspended load comprising of clay, silt and fine sand. The classification by origin divides the sediment load into the wash load (which moves in suspension) which is derived from outside the channel and the bed material load (which moves as both bed and suspended load) which is derived from the channel bed.

A large number of empirical equations have been formed which aim to predict the sediment transport rate from various combinations of the hydraulic and sediment characteristics. These equations can be grouped into those which predict suspended load (not including the wash load), bed load or total bed material load. Details of these equations and evaluations of their applicability can be found in Vanoni (1975), White et al. (1975), Simons and Sentürk (1977), Alonso et al. (1981), Graf (1984) and Bathurst et al. (1987). Equations which have a good reputation include those of Einstein (1950), Engelund and Hansen (1967), Ackers and White (1973), and Yang (1973). As all the equations have an empirical element they should not be applied outside the sediment and flow conditions used in their calibration. Also, they all assume an unlimited availability of sediment, that is they predict the sediment transport capacity. If separate bed and suspended load equations are used then some means has to be incorporated into a model to allow for transfer of sediment between the two transport modes; this was done in the model of Bennett and Nordin (1977).

2.3.2 Sediment Sources

2.3.2.1 Channel-bed sources

The two channel-bed sources are the original bedrock and the material deposited over this by the river or other transport agencies (termed bed material). Where deposited bed material is absent, for example some upstream reaches, the properties of the original bedrock become important. This bedrock may be classified as erodible, (e.g. loose conglomerates), or non-erodible (e.g. granite). Modelling difficulties arise when the exposed bedrock is of a transitional state between loose and non-erodible; this includes cohesive sediments. In this case a detachment equation may be needed such as those used for overland flow detachment.

2.3.2.2 Other sediment sources

In addition to the channel bed there are three major sources of sediment: (1) sediment carried into the reach from upstream and by tributaries joining the channel within the reach; (2) sediment entering the channel by one of the processes discussed in Section 2.2, for example overland flow; and (3) channel bank sources. The first two sediment sources will either be given as input data to a model or be calculated by another part of the model and therefore only bank erosion needs to be discussed here.

Channel bank erosion may introduce a wide range of sediments into a river. The mechanics of bank erosion are complex and involve many variables, such as the water discharge and depth and their variation with time, bank material properties, channel slope in both plan and cross section, wave height, phreatic surface level relative to stream water level and the rate of seepage. Two major processes of bank erosion may be identified: (1) fluvial entrainment - where material is entrained directly from the bank and transported downstream; (2) mass failure - where any proportion of the failed mass may be transported downstream. Thorne (1982a) suggests that fluvial entrainment is best correlated with channel flow conditions and that mass failure be correlated with changes in soil conditions (for example soil moisture). The processes of bank erosion are discussed in more detail by Simons and Li (1982) and Thorne (1982b).

Much research has been done on the prevention of channel bank erosion, and most hydraulics and sediment transport texts include analysis of channel bank stability. However, the methods of analysis are not directly applicable to models of sediment routing, although there is scope for adaptation (for example the use of critical tractive force theory for modelling the process of fluvial entrainment). An adaptation of the supply-based model of VanSickle and Beschta (1983) may also prove to be useful for simulating sediment supply from bank erosion at the catchment scale. Osman and Thorne (1988) present a process-based model of bank erosion which uses slope stability analysis to simulate mass failure and an excess shear stress equation for fluvial entrainment. They do not present a field validation of this model. The IALLUVIAL model (Holly and Karim, 1983) exemplifies the simple approach to bank erosion modelling implemented in current models. In this model, bank erosion is calculated from

$$GB_m = E\ F_m \qquad \text{if } Q \geq Q_{min}$$
$$\qquad\qquad\qquad\qquad\qquad\qquad\qquad\qquad (2.10)$$
$$GB_m = 0 \qquad \text{if } Q < Q_{min}$$

where GB_m = bank erosion rate for size fraction m; E = user specified bank erosion rate; F_m = proportion of size fraction m in the eroded bank material; Q = water discharge; Q_{min} = minimum water discharge above which erosion occurs.

2.3.3 Nonuniform Size Distribution

Nonuniformity of bed material affects sediment transport. The force required to set a large particle in motion is more than that for a smaller particle. Therefore, over time, initially well graded bed material may become poorly graded as the smaller particles are preferentially set in motion. This process is termed sorting. The large particles left on the surface may form an armour layer, protecting finer sub-surface material from further erosion. Even if some fine sediment remains on the surface, the larger particles tend to shield the fine particles lying behind or below them, and thus the fine particles require stronger flows to initiate motion than would be necessary in the absence of the large particles. Conversely, the larger surface particles project into the flow and can therefore be moved by weaker flows than would be necessary in the absence of the smaller particles (the exposure effect). Andrews (1983) has quantified the exposure and shielding effects empirically with field data, giving, for the range $0.3 < D_m/D_{50} < 4.2$

$$F_{*cm} = 0.0834 \left[\frac{D_m}{D_{50}}\right]^{-0.872} \tag{2.11}$$

where D_m = particle size for size fraction m; D_{50} = median particle diameter of the sub-surface material; F_{*cm} = average critical dimensionless shear stress (equation B.1 in Appendix B) for size fraction m.

A further effect is the interlocking of particles which leads to increased resistance to motion. Field studies have suggested that for initiation of motion of interlocked river bed material the value of the critical Shields constant may be increased by a factor of three or more (Reid et al., 1985).

The effects of nonuniformity can be simulated only if sediment is routed by size fraction. This involves using either a sediment transport equation which takes grading into account (e.g. Einstein, 1950; Laursen, 1958; Bishop et al., 1965; Toffaleti, 1969; Proffitt and Sutherland, 1983; Misri et al., 1984; Samaga et al., 1986), or by transforming one of the other equations to route by size fraction (e.g. Day, 1980).

A number of sediment routing models attempt to simulate the armouring process, for example, the models of Bennett and Nordin (1977), HEC (1977), Bettess and White (1981), Borah et al. (1982a), and Holly and Karim (1983). While all these models approach the problem in a slightly different manner, they all use the concept of an active layer, which is usually interpreted as the depth of sediment that can be affected by the flow in the simulation time step. If this layer consists of sediment which is too large to be moved by the current hydraulic conditions, but there is bed material present in layers below the active layer which could be transported, then the bed is considered to be fully armoured. The models differ in the way that they calculate the active layer depth and in the procedure for selective entrainment of sediment from the active layer. For example, Bettess and White (1981) use an active layer thickness equal to the bed form height, which in turn is assumed to be proportional to (in practice equal to) the effective roughness height. Borah et al. (1982a), however, define the active layer thickness as

$$AD = 100\ D_L \ /\ [(1 - \lambda) \sum_{m=L}^{N} F_m] \tag{2.12}$$

where AD = active layer thickness; D_L = diameter of the smallest sediment size fraction that the flow cannot transport; λ = bed porosity; F_m = percentage of fraction m in the layer; N = number of size fractions.

With the current knowledge of bed armouring processes there is a limited scientific basis for choosing between the various methods for simulating armouring.

So far this section has concentrated on the initiation of sediment motion, but nonuniformity also effects deposition. Sediment will be deposited when hydraulic or sediment conditions change so that the transport capacity is less than the sediment load (e.g. on the recession limb of a flood wave, or because of a large sediment inflow from a tributary). In the model of Borah et al. (1982a), deposition begins with the largest size fraction and continues through to the smaller fractions until either the stream is no longer overloaded, or all the fractions in transport have been depleted. The particles will not settle instantaneously, but over a settling time dependent on their quiescent fall velocities, flow velocity and original distance above the bed.

2.3.4 Bed and Channel Form

Bed forms are deformations of the bed profile within the overall channel form and can be classified as either small-scale bed forms (e.g. ripples, dunes and antidunes) or large-scale bed forms (e.g. bars and pool/riffle series). They may be stationary or mobile. Channel form concerns the plan form of the river, the usual classification being straight, meandering or braided. Bed and channel form can influence sediment transport because of the mixing of bed material by mobile bed forms, storage of sediment in bed forms, and the development of variations in the shear stress and velocity.

Two- or even three-dimensional river models are the best approach for dealing with these effects. However, such models are not practicable for catchment scale modelling because of the added computational and data requirements. Attempts have been made to model nonuniform distribution of scour and deposition on the channel bed using one-dimensional river models. These models consider bed shear stress and conveyance in subsections of the channel cross-section. Chen (1979) presents results from such a model; reasonably good agreement is achieved between simulated and measured changes in bed elevations.

2.3.5 Channel Sediment Routing

Channel sediment routing computations involve the calculation of the changes of river bed elevation in, and the sediment discharge from, a channel reach. This is achieved through a consideration of the sediment sources and hydraulic conditions (determined by a water routing model). The sediment sources were described in Section 2.3.2 and include the upstream sediment load, lateral inflow of sediment by hillslope processes and channel bank and bed sources.

Sediment routing is governed by the partial differential equation for conservation of sediment mass, which, if written in terms of the total load, is

$$\frac{\partial(AC)}{\partial t} + (1 - \lambda)\frac{\partial(Wz)}{\partial t} + \frac{\partial(ACV_s)}{\partial x} = \frac{\partial}{\partial x}\left[A\epsilon\frac{\partial C}{\partial x}\right] + g_s \qquad (2.13)$$

where A = flow cross-sectional area; C = sediment concentration; λ = porosity; W = active bed width; z = surface elevation; V_s = sediment velocity; ϵ = dispersion coefficient; g_s = sediment input from overland flow; t = time; x = distance in direction of the flow. This equation can be written for each size fraction in a nonuniform load by adding subscript m (for size fraction m) to the terms C, z, V_s, ϵ, and g_s.

As for hillslope sediment routing, the dispersion term in equation 2.13 is usually assumed to have a negligible effect and is therefore ignored in most models. Further common simplifications include neglecting the $\partial(AC)/\partial t$ term (therefore assuming quasi-steady conditions), and assuming that the sediment velocity is equal to the flow velocity. The simplified equation is usually solved using a finite difference method.

In addition to the equation for conservation of sediment mass, a channel sediment model requires a sediment transport capacity equation (see Section 2.3.1) and an algorithm for keeping track of changes in bed elevation and the bed material size distribution (including the variation in size distribution in the vertical). The models discussed in Section 2.3.3 all include such accounting algorithms.

2.4 CURRENT MODELS

Sediment yield modelling is the calculation of the amount of sediment passed out of a catchment over some time period. This can be determined as the product of the gross erosion and a sediment delivery ratio. However, if the sediment yield is modelled using a physically-based approach, then the processes of detachment, transportation, deposition and storage should be simulated for the whole catchment (hillslopes and channels). Therefore, a physically-based, catchment scale sediment yield model can be considered as a combination of a soil erosion model and a river sediment transport model, with the sediment delivery ratio replaced by the processes of transport, deposition and storage (using the terminology of Walling (1983), illuminating the black box of sediment delivery). In this section existing soil erosion models and river sediment transport models are discussed, followed by a review of sediment yield models.

Many sediment models have been developed and many terms have been used to classify the models. Table 2.1 lists some of these terms in an attempt to assist the appreciation of the differences between models.

Table 2.1 Terms used to describe sediment models

(a) Model aims
- calculate soil erosion
- calculate river bed degradation/aggradation and route sediment
- calculate sediment yield

(b) Applicable land uses
- urban
- agricultural
- forest
- construction sites
- rangeland

(c) End user
- operational; in the field or for office use
- research tool

(d) Tools required for calculations
- graphs and tables
- pocket calculator
- micro-computer
- mainframe or mini-computer

(e) Space scale
- hillslope
- field scale
- small catchment
- river basin

(f) Time scale
- event based
- continuous simulation - short time steps (e.g. minute)
  - long time steps (e.g. day, year)

(g) Modelling approach
- deterministic - empirical (regression)
  - conceptual
  - physically based (parametric, process-based)
- stochastic

(h) Spatial distribution of input data and results
- lumped
- zoned
- distributed

(i) Method of solving the equations
- analytical
- finite difference
- finite element

(j) Dimensions
- 1-dimensional
- 2-dimensional
- 3-dimensional

2.4.1 Soil Erosion Models

Zingg (1940) was the first to develop a soil erosion equation for hillslopes. The equation expressed soil loss as a power function of slope steepness and length. After further significant contributions along the same lines by Musgrave (1947) and Smith (1958), the Universal Soil Loss Equation (USLE) was developed (Wischmeier and Smith, 1965). The USLE has the form

$$E = R.K.LS.C.P \qquad (2.14)$$

where E = mean annual soil loss; R = rainfall erosivity factor; K = soil erodibility factor; LS = slope length and slope steepness factor; C = crop factor; P = conservation practice factor.

In terms of the classification given in Table 2.1, the USLE is an empirical lumped model, giving average annual soil erosion values for field scale agricultural land, it is fully operational and can be used in the field requiring only basic computations aided by tables and graphs. The USLE was designed solely for use on agricultural land in the USA, although many studies have been carried out to determine parameter values for other land uses (e.g. forest and rangeland) and in other parts of the world.

The USLE can be criticised on a number of grounds: it has restricted validity in terms of geographical position (the original data base was the USA east of the Rocky Mountains), slope steepness, crops, soil types and conservation practices; there is interdependence between factors; runoff is not explicitly included; and the only processes dealt with are rill and interrill erosion (deposition, gullying and channel erosion are not accounted for). In spite of these criticisms, the USLE is still regarded as a valuable design tool as long as it is not misused - e.g. used on an event basis or used where parameter extrapolation is necessary.

A considerable conceptual improvement over the USLE is the model of Meyer and Wischmeier (1969). In this hillslope model the processes of soil detachment by rainfall, transport capacity of rainfall, detachment by runoff and transport capacity of runoff are represented by four separate equations. The soil detached by rainfall and runoff for a slope segment is combined with the sediment load from the segment upslope to form the available loose soil, which is then compared with the total transport capacity (runoff plus rainfall transport). If the transport capacity is less than the available loose soil, then the sediment load leaving the segment is equal to the transport capacity. However, if there is insufficient loose soil to fill the transport capacity, then the sediment load leaving the segment is equal to the available loose soil (see Fig. 2.2). Net erosion or deposition for a segment is the difference between the incoming and outgoing sediment loads. This approach is applied to consecutive segments down the hillslope, thus determining the pattern of erosion and deposition for a complete hillslope profile.

The basic concepts introduced by this model (separate equations for detachment and transport capacity, comparison of transport capacity with available loose soil, and the use of the mass continuity equation for sediment) form the basis of most of the current generation of soil erosion and sediment yield models.

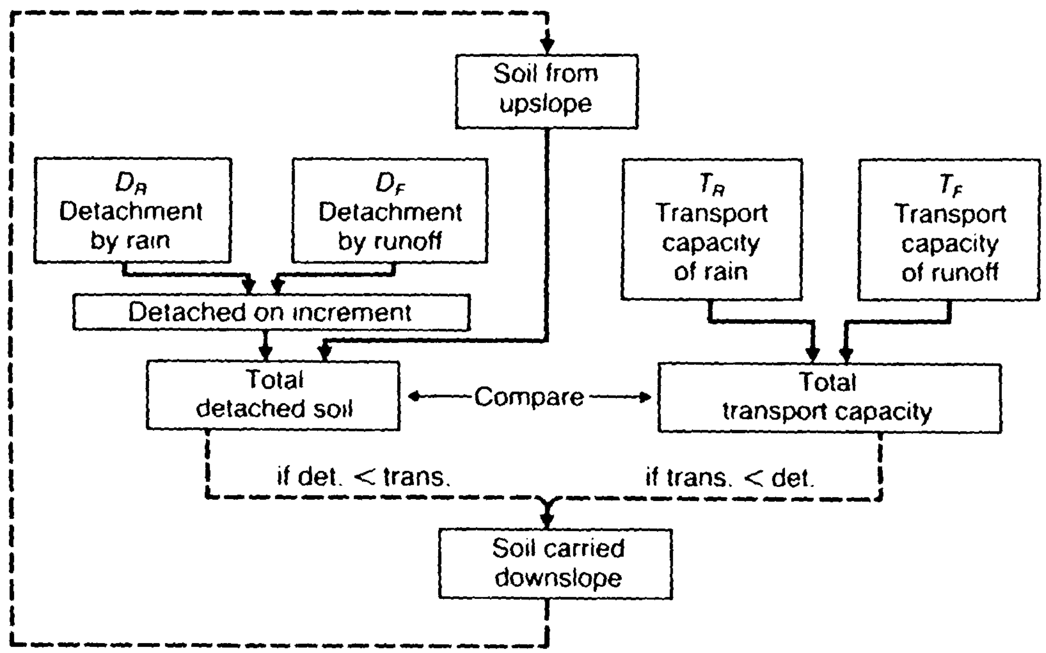

Fig. 2.2 Flow chart for the Meyer and Wischmeier (1969) model. (From Morgan, 1986.)

In fact, the Meyer and Wischmeier model can be considered the first physically-based soil erosion model.

The 1970s saw a plethora of new soil erosion models. Developments occurred in four main areas:

(a) Developments in defining the USLE parameters for further soil types, conservation practices and crops (Wischmeier and Smith, 1978) and for other countries (e.g. Roose, 1977).

(b) Modifications to the structure of the USLE. For example replacing the rainfall erosivity factor with a factor based on rainfall erosivity, total storm runoff and storm peak runoff rate (Onstad and Foster, 1975). A basic problem with this type of approach is that, as the USLE is a regression equation, a change in the definition of one term means that different values now need to be used for the erodibility term. However, in practice when the modifications are made, unaltered erodibility values are used - this must introduce errors, although they are not discussed when these modifications are presented.

(c) Field and hillslope models combining parts of the Meyer and Wischmeier and USLE approaches. The most important example of this type of model is CREAMS (Chemicals, Runoff and Erosion from Agricultural Management Systems) (Knisel, 1980). CREAMS is a daily simulation model that estimates runoff, soil erosion, and plant nutrient and pesticide yields from field-sized areas. The main processes in the erosion/sediment yield component are overland flow, channel flow, and impoundments (ponds). The overland flow component uses modified forms of the USLE to calculate rill and interrill detachment separately, with a modified Yalin equation (Yalin, 1963) used to calculate sediment transport capacity. Channel flow (e.g. grassed waterways and terrace channels, but not gullies or large streams) is modelled using an excess-shear type equation for soil detachment by flow with the Yalin equation again used to calculate sediment transport capacity. The pond component estimates how much sediment settles to the bottom of a pond before the flow passes through the impoundment; regression equations are used.

Some of the advantages of the CREAMS model are that it is designed so that it can be operated without calibration, it includes many agricultural management options, it can calculate the annual amount of soil erosion by summation of event values, and it has had widespread testing (e.g. see Morgan, 1986, p137). Theoretical problems with the CREAMS soil erosion procedure include its use of modified USLE equations to predict rill and interrill detachment separately. The USLE soil erodibility factor, K, is a function of detachability and transportability by combined rill and interrill processes, as well as being a function of infiltration. However, unaltered K values are recommended to be used in CREAMS even though infiltration is dealt with in the hydrology section of the model and a transport capacity equation is used. Also, numerous regression equations are used in the model, some having a very limited data base; these equations should not be used outside the conditions for their evaluation.

(d) Catchment scale hydrological models that include soil erosion routines. These models are usually based on the Meyer and Wischmeier approach, with or without USLE parameters. In general, if the model does not use the USLE soil erodibility factor then the model must be calibrated; if the USLE parameters are used then results must be viewed with suspicion. Because of this need for calibration and the large data and computational requirements, these models have not yet become generally accepted as operational models for soil erosion management. However, this type of model is seen to have the greatest potential for future developments. Catchment scale models are discussed in Section 2.4.3.

The 1980s has seen the continued development of existing and new soil erosion models. However, there now seems to be a realisation that significant improvements in model predictions will only be achieved through a better understanding of the processes, which will hopefully lead to more physically-based process equations. Even if process studies do not produce practical theoretically-based process equations in the short term, the studies will still prove valuable as the data collected can be used to improve the process equations based on regression analysis. Whilst these process studies continue, any new model should be designed so that it can take full advantage of future improvements in process equations. A problem here is that most models have not been designed to treat rill and interrill erosion separately, and therefore improvements in rill detachment and transport modelling may not be able to be included in these models.

Aside from the continued development of catchment scale models which calculate soil erosion (see Section 2.4.3) the 1980s has not seen significant practical developments in soil erosion models, although the WEPP model (currently under development) should prove to have an impact in the 1990s.

The WEPP model (Water Erosion Prediction Project) is being developed by the US Department of Agriculture as a replacement for the USLE (USDA, 1987). The two basic detachment equations used in WEPP are (Laflen et al., 1987): $D_F = K_F(\tau - \tau_c)$, and $D_R = K_R I^2$, where D_F = soil detachment by rills; K_F = rill soil erodibility; τ = shear stress; τ_c = critical shear stress; D_R = soil detachment by raindrops; K_R = interrill soil erodibility; I = rainfall intensity. These equations are not in themselves new; what is innovative is that a major experimental effort is underway to determine K_F, K_R and τ_c values for a wide range of US soil types, whereas past use of the equations relied on dubious adjustment of USLE K factors, or calibration for each application. As the WEPP model is process based, it will be able to be transferred to regions outside the USA if local experimental evaluation of K_F, K_R and τ_c values are undertaken.

2.4.2 River Sediment Models

Many models have been developed for simulating sediment routing in rivers. While the main objective of these models is usually to calculate changes in bed elevation (which is of secondary significance in sediment yield models), the basic equations and methods are applicable to sediment yield modelling. It is therefore useful to discuss some examples of these river sediment models.

(a) HEC-6 (HEC, 1977). This is probably the most widely used alluvial channel model. It is an uncoupled, known discharge model which means that unsteady flows are represented by a sequence of constant discharges with sediment calculations done after flow calculations for each time step. The model attempts to simulate armouring based on the stochastic approach of Gessler

(1971). Sediment transport capacity is calculated using either Toffaleti's application of Einstein's bed load function (Toffaleti, 1969), the Laursen (1958) formula or a user specified regression equation. HEC-6 is also discussed by Thomas (1982) who gives an example application.

(b) Bennett and Nordin (1977). An innovatory feature of this model is the use of different conservation of mass equations for the bed and suspended loads, with a transfer term included in each to allow for exchange of sediment between the two modes of transport. Bed load transport capacity is determined from a form of the DuBoys equation (Graf, 1984) which includes a calibration parameter. The river bed is conceptualised to consist of three layers in the vertical: an active layer, an inactive deposition layer, and the original bed material. The active layer thickness is determined as the product of a calibration parameter (equal to 8 in their example application) and the "D_{50} of the largest size used in simulation" (which Dawdy and Vanoni (1986) interpret to imply the geometric mean of the limits of the largest size fraction). The active layer thickness does not vary during the simulation. A finite difference solution is used for the conservation of mass equation written for each size fraction. Bennett and Nordin present an application of the model to the East Fork River, Wyoming, USA (see Chapter 8 for further details). For this river, which has complex supply effects, they were able to produce a good match of simulated and measured bed load discharges, but the simulated changes in bed elevation bear little resemblance to the measured changes in elevation.

(c) Borah et al. (1982a). Borah et al. developed a one-dimensional model for simulating the movement of well-graded sediment through a stream network. Transport capacity is determined using the Yang (1973) equation for sand (0.1 - 2 mm), a Duboys equation (Graf, 1984) for fine gravel (2 - 4 mm), and the Meyer-Peter and Müller (1948) equation for coarser gravel (≥ 4 mm). Borah et al. introduce the concept of the residual transport capacity, which they define as a measure of the ability of the flow to further entrain material of a given size fraction in the presence of all the fractions already in motion. The definition of the active layer thickness used by Borah et al. was given in Section 2.3.3 (equation 2.12), from which it can be seen that the active layer thickness will change with the flow conditions. A rather elaborate procedure is used for selectively entraining material from the active layer; the procedure includes a calibration parameter which governs the amount of bed degradation. The continuity of sediment mass equation is solved using the method of characteristics. Borah et al. (1982b) present satisfactory simulation results for four applications of the model to laboratory flume and field data (including the East Fork River, Wyoming - see Chapter 8).

(d) IALLUVIAL (Karim and Kennedy, 1982; Holly and Karim, 1983). IALLUVIAL is a one-dimensional, quasi-steady, flow and sediment routing model for simulation of the long term bed evolution of alluvial rivers. The model solves the governing equations in two phases. First, the Saint Venant equations and the Karim and Kennedy (1981) simultaneous equations for sediment discharge and friction factor are solved to give the water surface elevations, velocity and sediment discharge. Then, the sediment continuity equation is solved to give the depth of degradation or aggradation and change in bed material composition. IALLUVIAL allows for the existence of many layers of bed material with different size distributions; more than one of these layers may be incorporated in the active layer. The active layer is assumed to have a thickness equal to the bed form height, which is calculated as an empirical function of shear stress. The model has been applied to the Missouri River for a simulation period of 20 years following the closure of the Gavins Point Dam; close agreement of simulated and measured bed degradation was achieved.

2.4.3 Sediment Yield Models

The sediment yield from a catchment can be determined by one of the following methods.

(a) Measurement of the sediment leaving a catchment by continuous sediment sampling or by reservoir deposition surveys (with some allowance for the trap efficiency). Provided the measurements are reliable and extend over a sufficient time period, this is the most accurate method for determining the sediment yield. However, no information will be available on the likely effects following any changes in land management. Therefore, although this is the best method for obtaining data for reservoir siltation studies and calibrating models, it cannot be used for assessing the impact of different catchment management options on sediment yield and soil erosion.

(b) Short term measurement of sediment and water discharges to determine a sediment rating curve, $C = aQ^b$ (where C = sediment concentration; Q = water discharge; a = coefficient; b = exponent), which is then combined with long term streamflow measurements (or simulated streamflow) to calculate the sediment yield. This method is widely used even though the scatter of data about the rating curve may involve several orders of magnitude and the assumption that there exists a single valued relationship between sediment concentration and water discharge is recognised as a gross approximation.

(c) Use of regional regression equations which express sediment yield as a function of geomorphological, meteorological, hydrological and other catchment characteristics. An example of this type of model is the Flaxman equation (Flaxman, 1972). This expresses sediment yield as a function of the ratio of average annual precipitation to average annual temperature, the weighted average catchment slope, the percentage of soil particles coarser than 1 mm in the soil surface layer, and the soil aggregation index for the soil surface layer. This type of model requires large amounts of data for determining the model parameters and the resulting equations cannot be transferred to situations where there are significant differences in input, catchment processes and output. Also, they cannot be used to assess the likely effects of different land management options.

(d) Use of a soil erosion equation in combination with a sediment delivery ratio. An example of this is the method of Williams and Berndt (1972) who modified the USLE and combined this with a delivery ratio calculated as a function of channel slope. The validity of this method is again restricted to situations similar to those where it was derived. It must also suffer the same criticisms as the USLE (see Section 2.4.1).

(e) Use of mathematical models which require the use of computers for their solution. A wide variety of models can be classified under this heading, ranging from 'conceptual' models in which parameters cannot be determined by direct measurement but must be calibrated from concurrent input and output time series (e.g. Moore, 1984), through an intermediatory category such as the River Basin Model of Fleming (1983/4) in which physically-based process equations are used for some processes but other processes rely on a more conceptual lumped approach, to attempts at fully physically-based, distributed models. The remainder of this section is assigned to a discussion of some examples of this last type of model.

Colorado State University (CSU) model (Shen and Li, 1976; Li, 1979; Simons et al., 1982)

This model was probably the first distributed, physically-based catchment scale sediment yield model. The catchment is discretised using an orthogonal grid network (Fig. 2.3). The model simulates the processes of interception (using a method based on the canopy and ground cover densities and their water storage capacities), infiltration (using a Green-Ampt type equation), and overland and channel flow routing (using the kinematic wave approximation and the Darcy-Weisbach resistance equation). Evapotranspiration, snowmelt and subsurface flow are not modelled. A flow chart for the model is presented in Fig. 2.4.

The simulation of soil detachment by raindrop impact uses the following equation

$$D_{Rm} = F_m \, K_R \, I^2 \left(1 - \frac{h}{3d}\right) (1 - C_G) (1 - C_C) \qquad \text{if} \quad h < 3d$$

$$D_{Rm} = 0 \qquad \text{if } h \geq 3d \qquad (2.15)$$

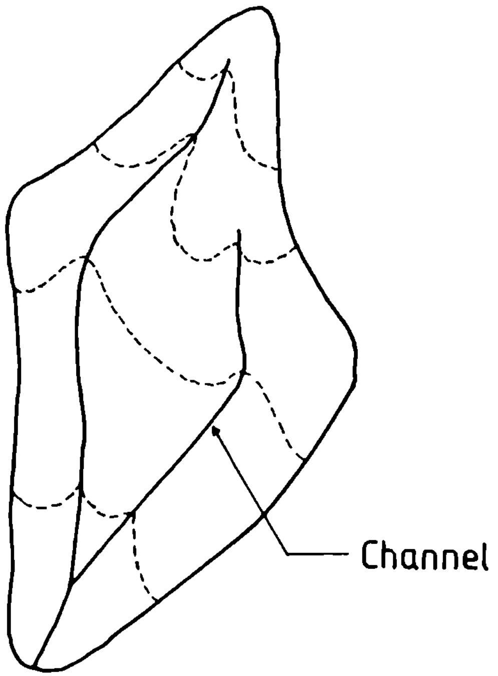

(a) Catchment features

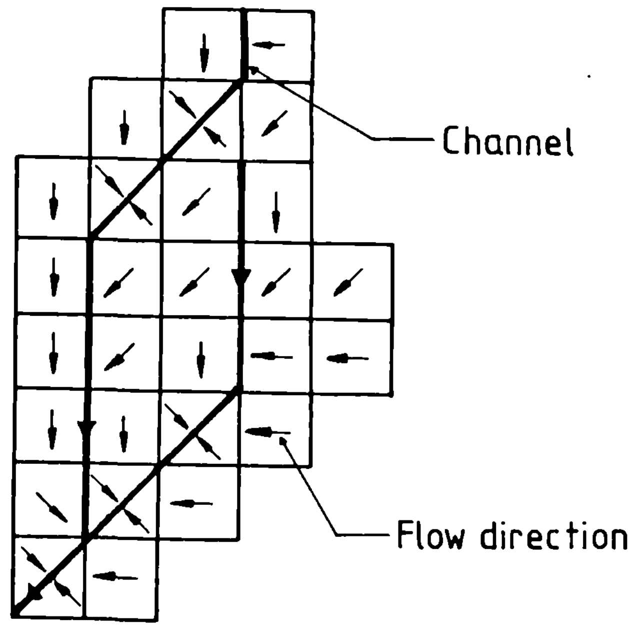

(b) Catchment segmentation

Fig. 2.3 Catchment segmentation in the CSU model. (After Li, 1979.)

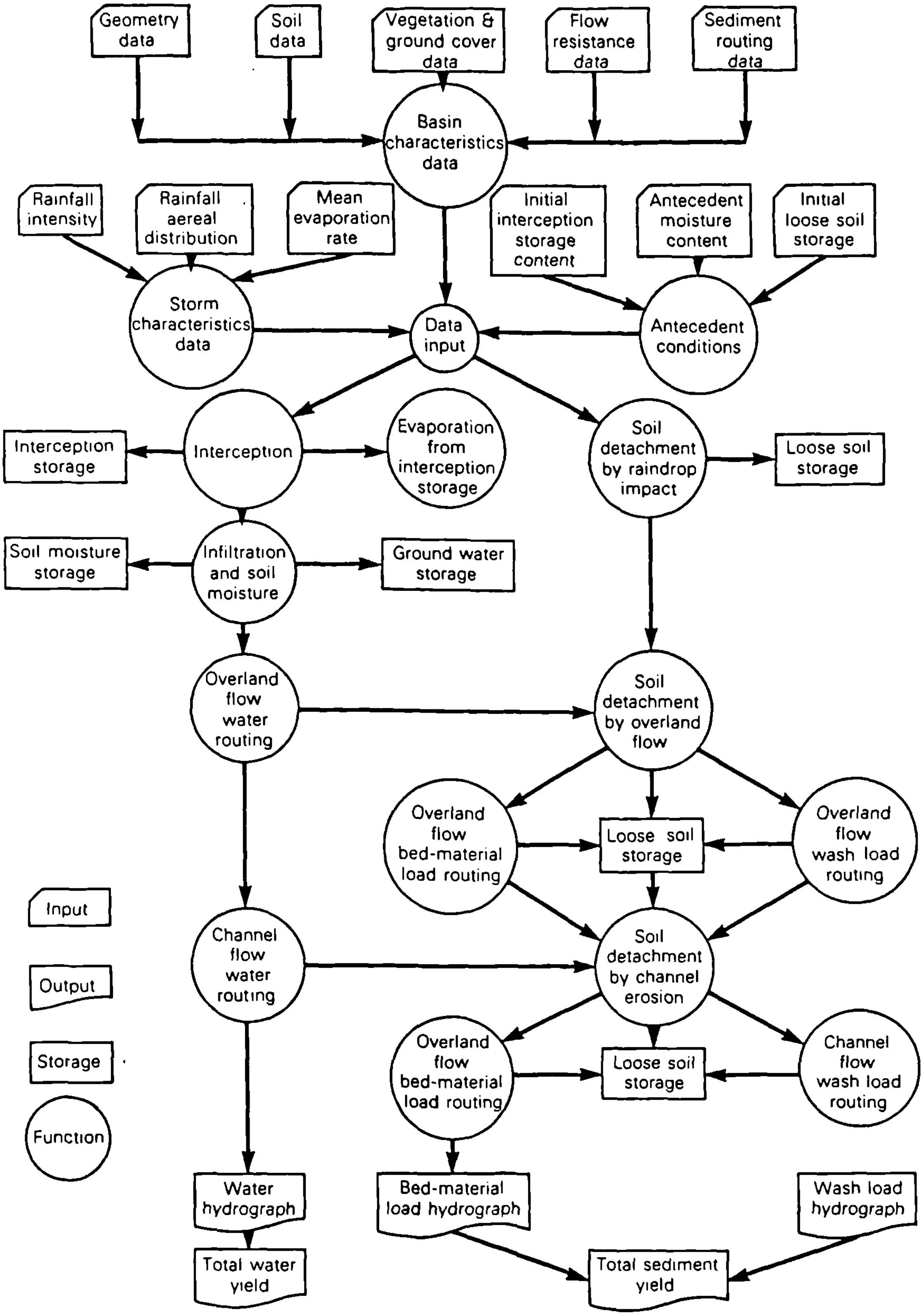

Fig. 2.4 Flow chart for the CSU model. (From Li, 1979.)

where D_{Rm} = potential rate of soil detachment by raindrop impact for size fraction m; F_m = proportion of soil particles in size fraction m; K_R = parameter depending on soil characteristics (calibration parameter); I = rainfall intensity; h = depth of water plus loose soil; d = median raindrop size (calculated as a function of rainfall intensity); C_G = ground cover density; C_C = canopy cover density.

Detachment by overland flow is a function of excess transport capacity

$$D_{Fm} = 0 \qquad \text{if} \quad \Delta z^{pot} < \Delta z$$
$$D_{Fm} = F_m K_F (\Delta z^{pot} - \Delta z) \qquad \text{if } \Delta z^{pot} > \Delta z \tag{2.16}$$

where D_{Fm} = detached soil for size fraction m; K_F = detachment coefficient in the range 0 to 1 depending on soil erodibility (calibration parameter); Δz^{pot} = total potential change in loose soil (calculated from the sediment continuity equation with sediment transport rate set to transport capacity); Δz = total loose soil depth.

Sediment transport capacity is calculated by the Meyer-Peter and Müller (1948) bed load equation and the Einstein (1950) suspended load equation. Sediment routing by size fraction is determined by the mass continuity equation

$$\frac{\partial G_m}{\partial x} + \frac{\partial C_m A}{\partial t} + (1 - \lambda)\frac{\partial P z_m}{\partial t} = g_m \tag{2.17}$$

where G_m = sediment transport rate by volume for size fraction m; C_m = sediment concentration by volume for size fraction m; A = cross-sectional area; λ = soil porosity; P = wetted perimeter; z_m

= depth of loose soil for size fraction m; g_m = lateral sediment inflow (for use with channel routing).

Sediment transport rates and concentrations are related by: $C_m = G_m/Q$ where Q = water discharge. This equation assumes that the velocity of the sediment is equal to the water velocity.

The Meyer and Wischmeier (1969) approach is used for comparing transport capacity with available loose soil to determine if the system is supply or transport limited. A four point finite difference approximation to the continuity equation is used.

FESHM (Ross et al., 1980)

FESHM (Finite Element Storm Hydrograph Model) is a finite element based hydrological model, thus allowing a flexible grid structure as opposed to the more usual finite difference orthogonal network. Infiltration is calculated using a modified Holtan (1961) equation and flow routing is based on the kinematic wave approximation.

Hillslope erosion is based on the methods used in the original ANSWERS model (Beasley and Huggins, 1981) with soil erodibility based on the USLE factors and transport capacity calculated by empirical relationships developed by Beasley et al. (1980). The Meyer and Wischmeier approach is used for comparing transport capacity with detached soil to determine the actual transport rates. Sediment transport in channels is based on the sediment continuity equation. Ross et al. do not present a field validation of their sediment model.

Modified ANSWERS (Park, 1981; Park et al., 1982)

In this model new soil erosion and sediment transport algorithms are incorporated into the ANSWERS (Areal Nonpoint Source Watershed Environment Response Simulation) hydrological model (Beasley and Huggins, 1981). ANSWERS is a distributed model with the hydrological processes represented by simple empirical equations or finite difference solutions to continuity equations. For example, flow routing uses an explicit backward difference approximation to the kinematic wave equation and infiltration is simulated by a modified Holtan (1961) equation.

Soil detachment by raindrop impact is determined as a function of rainfall intensity, surface water depth, surface slope and the erodibility, mulch and crop factors from the USLE. Overland and channel flow erosion is a function of shear stress and the USLE erodibility and crop factors. Various correction factors are incorporated in these equations on the premise that they will allow the use of unaltered USLE soil erodibility and crop factors, and therefore allow the model to be used without calibration. However, the use of USLE factors in these single process equations cannot be expected to give good results.

Sediment transport capacity is calculated using the Yalin (1963) bed load equation or by empirical relationships developed by Beasley et al. (1980). The Meyer and Wischmeier approach is used for comparing transport capacity with potential detached soil to determine the actual transport rates out of the grid rectangles.

Park et al. (1982) show the results of application of the model to eleven events on two small agricultural catchments called ISU1 and ISU2 (see Chapter 7 for further details). The model simulated the measured water and sediment discharges with variable accuracy, even though equation parameters were varied when logic suggests they should have been unchanged (e.g. the exponent of rainfall intensity in the raindrop soil detachment equation was changed from 1.5 to 2.0 for events on consecutive days).

SEM (Nielsen et al., 1986)

SEM (Soil Erosion Model) is a soil erosion model to be used with the SHE modelling system (see Chapter 3 for a short description of the SHE). In general the process descriptions in the SHE are more advanced than those in the other hydrological models described above, for example the Richards equation is used for the unsaturated zone and the diffusion wave approximation to the Saint Venant equations is used for water routing. Thus, given adequate data and a good spatial and temporal definition, the overland and channel flows, which transport the sediment load, are potentially more accurately simulated by the SHE than by most other models.

In SEM raindrop detachment is calculated as a function of the momentum squared of the raindrops, the surface water depth, surface slope, canopy and ground cover and a coefficient depending on soil parameters (used as a calibration factor). Transport capacity of overland flow is calculated from the Engelund-Hansen equation (1967). Overland flow detachment is set equal to the transport capacity multiplied by an entrainment ratio taking a value between 0 and 1 (used as a calibration factor). The sediment routing scheme assumes that the incoming sediment load to a grid rectangle is always deposited in that grid rectangle and thereafter behaves as normal soil (i.e. it must be detached again before being transported). The sediment transport rate out of the grid rectangle is determined from the lesser of the transport capacity and the total amount of detached soil. The simple channel sediment routing algorithm included in the model does not allow for any erosion or deposition.

Nielsen et al. (1986) present results of an application of the model to the ISU1 agricultural catchment (see Chapter 7 for further details). The calibration events presented show a reasonable match between simulated and measured sediment discharges.

<u>SWAM (DeCoursey, 1982; Alonso and DeCoursey, 1985)</u>

SWAM (Small WAtershed Model) is designed to assess the effects of changes in land use or management on the hydrologic, sediment and chemical response of agricultural areas less than 10 km^2 in size. SWAM is a physically-based, distributed modelling system which simulates all the major land phases of the hydrological cycle. The soil erosion component is based on CREAMS2 (Foster and Smith, 1985; Smith and Knisel, 1985) which is a dynamic version of the CREAMS model (see Section 2.4.1). The channel sediment routing component of SWAM is based on the model described by Borah et al. (1982a) (see Section 2.4.2) and therefore represents a considerable advancement over the previous channel sediment routing components of catchment sediment yield models. SWAM is still in the process of development.

2.5 CONCLUSIONS

Physically-based, distributed sediment yield modelling should provide an approach which has universal applicability without the need for calibration. However, it can be argued that all the sediment process equations, on which these models are based, require further development before they can be considered as universal relationships not requiring calibration. In addition to deficiencies in the process equations, there exist problems caused by the structure of the models (e.g. one-dimensional representations of three-dimensional phenomena, and inability to simulate individual rills at the catchment scale) and the lack of test data. In view of these deficiencies it may be instructive to review how well existing soil erosion and sediment transport models predict the observed response. This should be done by looking at validation exercises as opposed to calibration runs (there are usually so many parameters in physically-based models that it may be possible to match any measured response if all parameters are varied). However, very few validation runs have been presented (that is runs for which no calibration for the particular event was allowed). This is true for physically-based soil erosion, river routing and sediment yield models. This lack of validation is a good indicator of the no more than partial success achieved by most current models.

The main objectives of the research reported in this thesis were to develop and apply a physically-based, distributed sediment yield component for the SHE. The new component has the potential for greater accuracy than existing models as it uses state of the art process equations to model both the hillslope and channel phases of the catchment sediment system, within the framework of an advanced hydrological modelling system.

CHAPTER 3 - AN INTRODUCTION TO THE SHE MODELLING SYSTEM

3.1 INTRODUCTION

This chapter is used to introduce the SHE (Abbott et al., 1986a,b), with most emphasis placed on parts of the SHE which interact with the sediment yield componet. It is important to review the SHE as: (a) water is the main transportation agent for sediment, therefore if this is poorly modelled then there is little hope for modelling sediment transport accurately; (b) the structure and philosophy of the sediment yield component are based on those of the SHE, therefore a critical appraisal of the hydrological model will be relevant to the sediment component; and (c) in any application, more effort will be spent on collecting data for and the calibration of the hydrological model, than on purely sediment simulations.

The Système Hydrologique Européen, SHE, is a physically-based, distributed, catchment scale modelling system developed jointly by the Danish Hydraulic Institute, the Institute of Hydrology (UK) and SOGREAH (France). Individual models for particular applications are built from the SHE as required. Each of the primary processes of the land phase of the hydrological cycle are modelled in separate components using either finite difference representations of the partial differential equations of mass, momentum and energy conservation or empirical equations derived from independent experimental research. Spatial distribution of catchment parameters, rainfall input and hydrological response is achieved in the horizontal by an orthogonal grid network and in the vertical by a column of horizontal layers at each grid rectangle (Fig. 3.1).

3.2 COMPONENTS OF THE SHE

3.2.1 Interception and Evapotranspiration Component

Interception of rainfall by vegetation, and drainage from vegetation, is represented by a modified Rutter model (Rutter et al., 1971/72). The vegetation is considered to have a surface storage capacity which is filled by rainfall and emptied by evaporation and drainage. The rate of change of storage is calculated as

$$\frac{\partial C}{\partial t} = Q - k\, e^{b\,(C - S)} \qquad (3.1)$$

where C = depth of water on vegetation; Q = net rate of supply of rain to vegetation (after accounting for evaporation); S = vegetation storage capacity; k and b are drainage parameters; t = time.

Drainage is calculated by a mass balance procedure involving the change in water storage on vegetation, the rainfall input to and the evaporation from the vegetation.

Evapotranspiration is the combined process of evaporation from soil and water surfaces and the water uptake by plant roots that transpires from leaves. A number of options exist in the SHE for calculating the evapotranspiration, the most complex being the Penman-Monteith equation (Monteith, 1965)

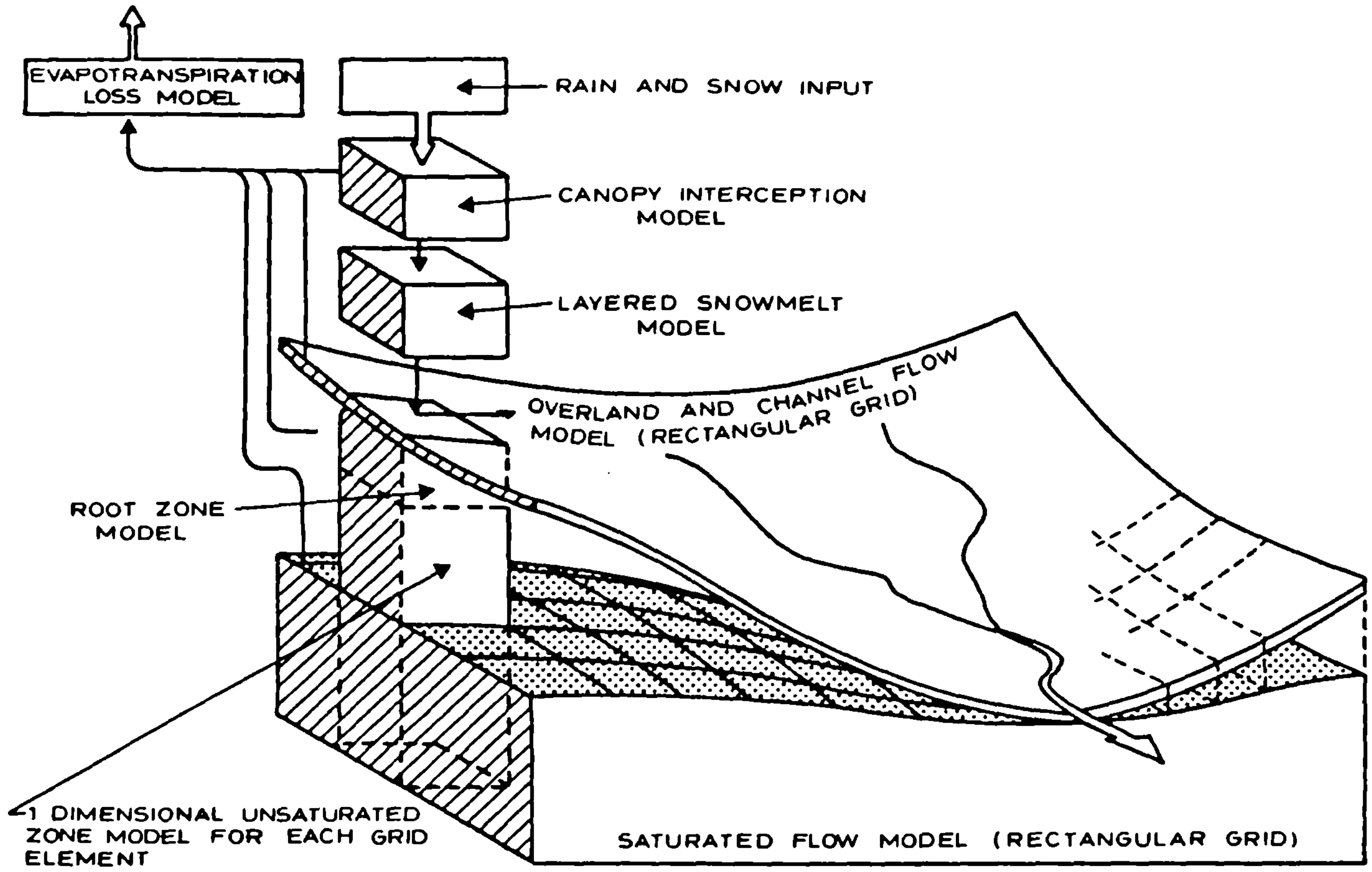

Fig. 3.1 Schematic representation of the structure of the SHE. (After Abbott et al., 1986a.)

$$E_a = \frac{R_n \Delta + \frac{\rho c_p \delta_e}{r_a}}{\lambda \left[\Delta + \gamma (1 + \frac{r_c}{r_a}) \right]} \tag{3.2}$$

where E_a = actual evapotranspiration; R_n = net radiation; Δ = rate of increase with temperature of the saturation vapour pressure of water at air temperature; ρ = density of air; c_p = specific heat of air at constant pressure; δ_e = vapour pressure deficit of air; r_a = aerodynamic resistance to water vapour transport; λ = latent heat of vaporisation of water; γ = psychrometric constant; r_c = canopy resistance to water transport.

3.2.2 Overland and Channel Flow Component

Overland and channel flow is represented by the diffusion wave approximation to the Saint Venant equations.

The following two-dimensional set of equations is used for overland flow

$$\frac{\partial h}{\partial t} + \frac{\partial (uh)}{\partial x} + \frac{\partial (vh)}{\partial y} = q \tag{3.3}$$

$$\frac{\partial h}{\partial x} = S_{ox} - S_{fx} \tag{3.4}$$

$$\frac{\partial h}{\partial y} = S_{oy} - S_{fy} \tag{3.5}$$

where h = water depth; u,v = flow velocities in the x and y directions; q = net precipitation minus infiltration; t = time; x,y = horizontal cartesian coordinates; S_{ox},S_{oy} = ground slope in x and y directions; S_{fx},S_{fy} = friction slopes in the x and y directions.

Applying the Strickler/Manning resistance law for each friction slope to equations 3.4 and 3.5, the relationship between velocities and flow depth may be written as

$$uh = K_x \, S_x^{1/2} \, h^{5/3} \tag{3.6}$$

$$vh = K_y \, S_y^{1/2} \, h^{5/3} \tag{3.7}$$

where K_x, K_y = Strickler roughness coefficients in the x and y directions (the Strickler coefficient is the reciprocal of Manning's n); S_x, S_y = water surface slopes in the x and y directions.

The equations are solved using an explicit finite difference scheme. Equations 3.6 and 3.7 are solved for the flow rate per unit width (uh and vh) at time t based on water depths at time t. Then the water depth in the grid rectangle at time $t+\Delta t$ is calculated from the finite difference version of equation 3.3 using the net rainfall minus infiltration during the time interval Δt and the flow rates across the four sides of the grid rectangle at time t. Thus the flow rates are defined at grid rectangle boundaries while the water depths are defined at the centre of the grid rectangle.

The basic equations for representing channel flow (one-dimensional) are

$$\frac{\partial A}{\partial t} + \frac{\partial (Au)}{\partial x} = q_1 \tag{3.8}$$

$$\frac{\partial h}{\partial x} = S_o - S_f \tag{3.9}$$

where A = cross-sectional area of the channel; u = flow velocity; q_l = source/sink term for overland flow and stream/aquifer exchange; h = water depth; x = distance; S_o = channel bed slope; S_f = friction slope.

The Strickler/Manning equation is again applied, but this time an implicit finite difference scheme is used to solve the equations. The channel system is represented on the boundaries of grid rectangles with a channel link corresponding to a rectangle side. Water depths are defined at the corners of the grid rectangles (computational nodes for channels) with water discharges defined mid-way between the nodes (mid-link position).

3.2.3 Unsaturated Zone Component

The unsaturated zone extends from the ground surface to the phreatic surface and is modelled using the one-dimensional (vertical flow only) Richards equation

$$C \frac{\partial \psi}{\partial t} = \frac{\partial}{\partial z} \left(K \frac{\partial \psi}{\partial z}\right) + \frac{\partial K}{\partial z} - S \qquad (3.10)$$

where C = $\partial\theta/\partial z$ = soil water capacity; θ = volumetric moisture content; ψ = soil moisture tension; K = hydraulic conductivity; S = source/sink term for root extraction and soil evaporation; t = time; z = vertical space coordinate.

This equation is solved using an iterative implicit finite difference scheme.

3.2.4 Saturated Zone Component

Groundwater flow is assumed to be horizontal only, and is modelled by the two-dimensional Boussinesq equation

$$S \frac{\partial h}{\partial t} = \frac{\partial}{\partial x} (K_x H \frac{\partial h}{\partial x}) + \frac{\partial}{\partial y} (K_y H \frac{\partial h}{\partial y}) + R \qquad (3.11)$$

where S = specific yield; h = phreatic surface level; K_x,K_y = saturated hydraulic conductivities in the x and y directions; H = saturated thickness; R = instantaneous vertical recharge in the saturated zone; t = time; x,y = horizontal cartesian coordinates.

Equation 3.11 is solved by an alternating-direction implicit finite difference scheme. Allowance is made for both the complete disappearance of the saturated zone and the rise of the phreatic surface to the ground surface.

3.2.5 Snowmelt Component

The snowmelt component models the snowpack thickness as it is affected by precipitation and melting, and the rate of delivery of meltwater from the snowpack to the soil surface. First the total heat flux is calculated by either an energy budget method or a degree-day method. Then an energy balance equation is used to determine the snowmelt, which is then routed through the snowpack using an empirical equation.

3.2.6 Controlling or FRAME Component

The FRAME component manages the parallel running of the hydrological process components. It controls the sequence in which the other components are called. It manages the exchange of data between components, for example accumulating data from one component which is using a short time step for transfer to another component which is using a larger time step. The FRAME component prints required results at specified intervals and maintains a check on the water mass balance for the whole model.

3.3 APPLICATION OF THE SHE

An application of the SHE generally consists of three stages: (a) collection of data and setting up of data files; (b) calibration and validation using historical events; (c) use of the model for predictive purposes. The first two points are discussed below from the point of view of using the model for sediment yield studies. Possible applications of the SHE have been presented by Beven and O'Connell (1982) and are not reproduced here.

3.3.1 Parameter and Data Requirements

As shown in Table 3.1, a wide variety of parameters are used by the various SHE components. Exact data requirements depend on the application, and there is a facility to use dummy components in place of process components where processes are not significant (e.g. the snowmelt and saturated zone components for many sediment yield studies).

Table 3.1 Data and parameter requirements for each grid rectangle or channel link in the SHE. (From Abbott et al., 1986b.)

Input data and model parameters for each component	
Frame component	
Model parameters	Ground surface elevation
	Impermeable bed elevation
	Distribution codes for rainfall and meteorological source stations
	Distribution codes for soil and vegetation types
Interception component	
Model parameters (for each crop type)	Drainage parameters
	Canopy storage capacity (time varying)
	Ground cover indices (time varying)
Input data	Rainfall rate
Evapotranspiration component	
Model parameters (for each crop type)	Canopy resistance
	Aerodynamic resistance
	Ground cover indices (time varying)
	Ratio between actual and potential evapotranspiration as a function of soil moisture tension
	Root distribution with depth
Input data	Meteorological data
Overland and channel flow component	
Model parameters	Strickler roughness coefficients for overland and river flows
	Coefficients of discharge for weir formulae
Input data	Specified flows or water levels at boundaries
	Man-controlled diversions and discharges
	Topography of overland flow plane and channel cross sections
Unsaturated zone component	
Model parameters (for each soil type)	Soil moisture tension/content relationship
	Unsaturated hydraulic conductivity as a function of moisture content
Saturated zone component	
Model parameters	Porosities or specific yields
	Saturated hydraulic conductivities
Input data	Impermeable bed elevations
	Specified flows or potentials at boundaries
	Pumping and recharge data
Snowmelt component	
Model parameters	Degree-day factor
	Snow zero plane displacement
	Snow roughness height
Input data	Meteorological and precipitation data

Based on the findings of a number of non-rigorous sensitivity analyses, the most important parameters and data for SHE simulations intended for use in sediment yield studies are likely to be:

(a) Overland and channel flow roughness coefficients. These affect water velocity and depth (and the infiltration for overland flow). The roughness coefficients can be estimated from literature values for similar surface conditions, but are likely to need adjusting in the calibration stage.

(b) Saturated hydraulic conductivities for vertical flow and the soil moisture tension/content relationship. These affect the generation of overland flow. In the absence of field data, literature values for similar soil types can be used. The saturated hydraulic conductivities are again likely to be adjusted in the calibration stage.

(c) Interception parameters including percentage vegetation cover. These affect the canopy drainage and input of direct rainfall to the ground surface. The drainage parameters k and b in equation 3.1 are known for a very limited range of vegetation types.

(d) Evapotranspiration parameters and data. These will become important if interstorm periods are simulated to set up initial conditions for following storms.

(e) Surface elevations. These are used for determining overland and channel slopes and have been found to be more important for sediment calculations than for water flow calculations. Their determination is based on map contours, usually with some weighting of point elevations at regular grid positions.

(f) Rainfall input data. For sediment calculations these data need to be available at a timestep which is appropriate to the actual variation in rainfall intensity. This may be as small as one minute for short duration, high intensity storms.

(g) Initial soil moisture content profiles and phreatic surface levels. In the absence of measurements a lead-in simulation period can be used if the necessary soil and meteorological data are available.

(h) A record of the hydrological response for calibrating and validating the model. As a minimum, the catchment water discharge is required, but other data, such as water discharge at internal points, soil moisture contents and phreatic surface levels, will greatly increase the likelihood of obtaining the optimum calibration parameters. Qualitative information on the patterns and mechanisms of the hydrological response (e.g. location of overland flow regions) also assist the calibration.

(i) Distance and time steps. The determination of the optimum distance and time steps involves balancing the requirements of large steps to reduce computational cost and small steps for accurate representation of hydrological response and for stability of finite difference schemes. For sediment studies the important distance steps are the catchment rectangular grid network (which determines the distance step for the river links as well as for overland flow), and the vertical distance step in the root zone (which can influence the time at which simulated runoff commences). The important time steps are those in the overland and channel flow and unsaturated zone components. Time steps and the distance step in the root zone can be easily adjusted and optimum values can be found by trial. The distance steps of the rectangular grid are, however, more time consuming to alter once set. For large catchments (say 10 km^2 and greater) computational limitations may dominate with a grid network of 20 by 20 grid rectangles being typical of applications to date (the exact limit depends on available computer resources, acceptability of long running times, and the size of other arrays used in the model). For catchments smaller than this, uniformity of soil, vegetation and slope may mean that the number of grid rectangles can be significantly reduced without a deterioration in accuracy.

3.3.2 Calibration and Validation

Although in principle all the SHE parameters can be measured in the field, it is usually necessary to calibrate the model for specific catchments. The reasons for this are: (a) it is unlikely that measurements of all parameters will have been taken at the catchment, and therefore values from elsewhere will need to be used which may be poor substitutes; (b) where measurements are made, there will be errors associated with the measurements and limited data on spatial variability; this will affect parameter values, input data (e.g. rain) and hydrological response data; (c) point measurements may be inappropriate for use at the grid scale; (d) the parameter values may need to be adjusted to compensate for errors in the model structure (inappropriate time and distance steps and absence or crudeness of process equations).

Automatic calibration procedures, as used for some lumped models, are not feasible because of the computational cost associated with optimising the large number of parameters for every grid rectangle and the likely complexity of the optimisation response surface. Also, some parameters may be considered to have been well defined from measurements and so not needing adjusting. Further, it is likely that some qualitative information on the actual hydrological response cannot be expressed in a form suitable for automatic calibration.

Currently a typical approach to calibrating a SHE model is based on a trial and error procedure using a limited set of parameters for which the simulation is most sensitive. The set of calibration parameters will also depend on which data were measured effectively and on the objectives of the simulation. The most likely calibration parameters for surface runoff response simulations are the overland and channel roughness coefficients, and the saturated hydraulic conductivity for the unsaturated zone. In addition, initial soil moisture contents and initial phreatic surface levels may form part of the calibration parameter set if measurements are not available. The parameters are then varied within reasonable limits until some calibration criterion is met. This may be a visual match of simulated and measured hydrograph shapes, or a more formal criteria such as minimising the percentage error in predicted peak or total discharge, or minimising the root mean square value of the difference between the simulated and measured discharges at intervals throughout the event.

The match of simulated and measured hydrographs for one calibrated event does not demonstrate that the model will be able to predict the hydrological response for other events. What is needed is a range of events of differing magnitudes and, preferably, methods of response (e.g. surface and subsurface). One or more of these events are used for calibrating the model and the remaining events used to validate the calibration. Only following this split-record calibration-then-validation approach can the calibrated model be used with confidence for prediction.

3.4 PRACTICAL PROBLEMS IN APPLICATIONS OF THE SHE

In many situations there may be significant benefits from using a physically-based, distributed hydrological model, such as the SHE, in place of a traditional lumped model. Indeed many land management issues of current concern can be modelled only by using a SHE type approach. However, although this new class of model has been in existence for a number of years, it has not yet become established as an operational tool. While this remains the case, there is a limited likelihood of the sediment yield component fulfilling its potential as a predictive tool to aid the decision making process in the correction of the important sediment related problems discussed in Chapter 1. As one of the aims of the project reported in this thesis was to produce a model that would be of practical use, it is worthwhile to consider the likely reasons for the limited commercial use of the SHE. Also, because of their common philosophy, many of the reasons for the current limited use of the SHE will apply equally well to the sediment yield component.

The most common reasons for choosing lumped models in preference to the SHE are the large data and computational requirements of the SHE. The problem of insufficient data is likely to persist, even though remote sensing is expected to be able to provide some of the parameter values in a very convenient form. As computer power continues to increase, the computational requirements of the SHE will become less of a problem. The important scientific issues concerning the model which still need to be settled include the means of measuring parameter values at the appropriate spatial scale for representing behaviour at the grid scale, the development of a more rigorous calibration procedure, and the appropriateness of current process theories or of their simplified representation as used in the SHE. These issues are best addressed through research projects. Other problems arise from the complexity of the program which may lead to difficulties in installing and using the program, even after training and with continuing (but remote) support. The model user also needs to have a good general understanding of hydrology, preferably first hand knowledge of the catchment response, an understanding of computing and numerical methods, and a knowledge of data collection methods and likely measurement errors.

None of these obstacles is insurmountable and physically-based, distributed hydrological modelling is expected to replace lumped modelling in many applications and also provide a modelling approach for situations where lumped models cannot be used.

CHAPTER 4 - HILLSLOPE SEDIMENT PROCESSES IN SHESED

4.1 INTRODUCTION

Within a catchment, the erosion, transport and deposition processes can be divided into hillslope and channel phases; this chapter describes the hillslope phase of SHESED, with the channel phase described in the next chapter.

The hillslope phase involves such processes as the erosion and transportation of soil particles and aggregates by raindrop impact, leaf drip impact, flowing water, wind and mass movements. However, owing to lack of process predictors and the structure of the SHE, not all the major hillslope processes can be modelled by SHESED. Those which are included in the model are: detachment of soil by raindrop impact, leaf drip impact and overland flow, and the transport of this material by overland flow. Wind erosion and mass movements are not considered in SHESED, in common with all other physically-based models.

4.2 RAINDROP DETACHMENT

As noted in Section 2.2.1, raindrop impact initiates soil erosion by breaking cohesive bonds between soil particles and by launching particles into the air or surface water. Major factors which affect raindrop detachment are rain characteristics, soil characteristics, ground and canopy cover, surface water depth and surface slope.

4.2.1 Rainfall Erosivity

Rainfall characteristics which affect erosivity and the available process models were discussed in Section 2.2.1.2. For SHESED, the theoretical study of Styczen and Høgh-Schmidt (1988) has been followed, which relates detachment to the sum of the square of raindrop momenta. Although there is no conclusive evidence to suggest that this approach is a significant improvement on the more common functions of kinetic energy and rain intensity, the theoretical basis is more attractive than a purely empirical one.

To calculate the momentum squared, it is necessary to know the distribution of raindrop sizes and the rainfall intensity throughout the storm (assuming the drops are falling at their terminal velocities). Data from storms in various parts of the world are available, but it is unlikely that the drop size distribution will be available for the storm under consideration and therefore a standard drop size distribution needs to be included in the program. One of the most commonly used models for the size distribution of raindrops is that of Marshall and Palmer (1948), where the number of drops per unit volume having diameters between d and Δd is given by $n(d)\Delta d$, where

$$n(d) = n_0 \; e^{-\lambda d} \tag{4.1}$$

where n_0 = known empirical constant; and the slope factor, λ, is given by

$$\lambda = 41 \; I^{-0.21} \tag{4.2}$$

where I = rainfall intensity.

Subsequent research has shown that this expression is not sufficiently general to cover many situations (e.g. Mason and Andrews, 1960; Carter et al., 1974). It is most appropriate for steady rain in temperate continental areas but even then it is not able to describe the distribution of raindrops with diameters less than 1 mm: this is not too great a problem for erosivity calculations as these small drops make a minor contribution to detachment. Alternative functions have been proposed; for example Quimpo and Brohi (1986) found that a lognormal model provided a good fit to a large data set derived from measurements at various sites in the USA. However, guidelines could not be given for parameter values in the function for use at sites with no data. As it is unlikely that site data will be available to calculate these parameters, and the addition of calibration parameters to SHESED is unwelcome, the Marshall-Palmer distribution has been accepted as the default relationship for SHESED.

The use of the Marshall-Palmer drop size distribution to calculate the momentum squared involves a numerical integration, which would be computationally expensive if repeatedly calculated in SHESED simulations. Therefore, the momentum squared, based on the Marshall-Palmer distribution, has been calculated for rainfall intensities in the range 0 to 250 mm h^{-1}, and expressed by the following function for use in SHESED

$$M_R = \alpha I^{\beta} \tag{4.3}$$

where M_R = momentum squared for rain ($(kg\ m\ s^{-1})^2\ m^{-2}\ s^{-1}$); I = rain intensity ($m\ s^{-1}$); α, β = coefficient and exponent as given in Table 4.1. The derivation of these values is given in Appendix A.

Table 4.1 Parameters used in the relationship between momentum squared and rainfall intensity (equation 4.3)

Rain intensity, I ($mm\ h^{-1}$)	α	β
$0 \le I < 10$	3214.9	1.69
$10 \le I < 50$	583.4	1.55
$50 \le I < 100$	133.1	1.42
$100 \le I$	29.9	1.28

4.2.2 Soil Detachability

As discussed in Chapter 2, a suitable predictor of soil resistance to detachment by raindrop impact has yet to be generally accepted and soil detachability is usually accounted for by a coefficient to be determined for the site conditions. In SHESED this coefficient can be evaluated either by applying the whole model at prototype scale (or preferably at a smaller scale as data collection is then easiest and the influence of other processes are at their least), or by applying the raindrop detachment process model to experimental conditions. An example of the first method is presented in Chapter 6, and of the second in Section 4.2.8.

4.2.3 Ground Cover

Ground cover is material which directly shields the soil from the kinetic energy of the rain. It includes litter, mulch, stones, short vegetation and snow. Ground cover is accounted for in the model using an areal reduction factor.

4.2.4 Canopy Cover

Canopy cover refers to taller vegetation which initially dissipates the kinetic energy of impinging drops but allows some of the water to then coalesce on the vegetation surface and fall to the ground as large leaf drips. The influence of leaf drip is included in SHESED using the same momentum squared approach as used for direct rainfall. The extra data needed are fall height, representative drip diameter, percentage canopy cover and proportion of canopy drainage which reaches the ground as leaf drip (as opposed to stem flow and leaf splash). These values change with vegetation type and maturity. Table 4.2 summarises the findings of studies which have either stated these parameters or given data from which the parameters could be determined.

As an example of the methods used to determine the data in Table 4.2, Fig. 4.1 shows how a representative leaf drip diameter can be estimated from graphs of drop size distributions from above and below the canopy (the data of Armstrong and Mitchell (1987) are used). Fig. 4.1(a) shows the untransformed rainfall (in this case produced by a rainfall simulator) with a median drop diameter of 2 mm. Fig. 4.1(b) shows the drop size distribution below a soybean canopy, using the simulated rainfall. The distribution is bimodal, with peaks at 2 mm and 6 mm, and the representative leaf drip diameter can be taken as 6 mm. The determination of the representative leaf drip diameter can be more complicated though, as shown in Fig. 4.1(c). Here, the same simulated rainfall is sampled below a maize canopy, but a more even distribution of drop sizes occurs, the representative leaf drip diameter being in the range 4 - 7 mm.

Table 4.2 Leaf drip parameter values based on published data

Reference	Vegetation	Percent cover	Fall height (m)	Drip diameter (mm)	% drainage as leaf drip
Quinn & Laflen, 1983	Maize	33 - 77	0.5 - 1.1	4.5 - 5.5	35 - 73
Finney, 1984	Brussels sprouts	1 - 40	-	4.5 - 6.3	1 - 23
	Sugar beet	1 - 28	-	4.6 - 6.2	0 - 18
	Potatoes	2 - 27	-	4.7 - 5.9	2 - 21
Vis, 1986	Tropical forest	-	<1, 3-4, 5-6, >10	4 - 6	-
Armstrong & Mitchell, 1987	Maize	66	≤ 2.0	4 - 7	-
	Soybean	97	≤ 0.87	5 - 6.75	-
	Spruce	96	18 - 20	4 - 7	-
	Sycamore	92	20 - 30	3 - 7	-

Note: the dash signifies that insufficient data were available to determine the value.

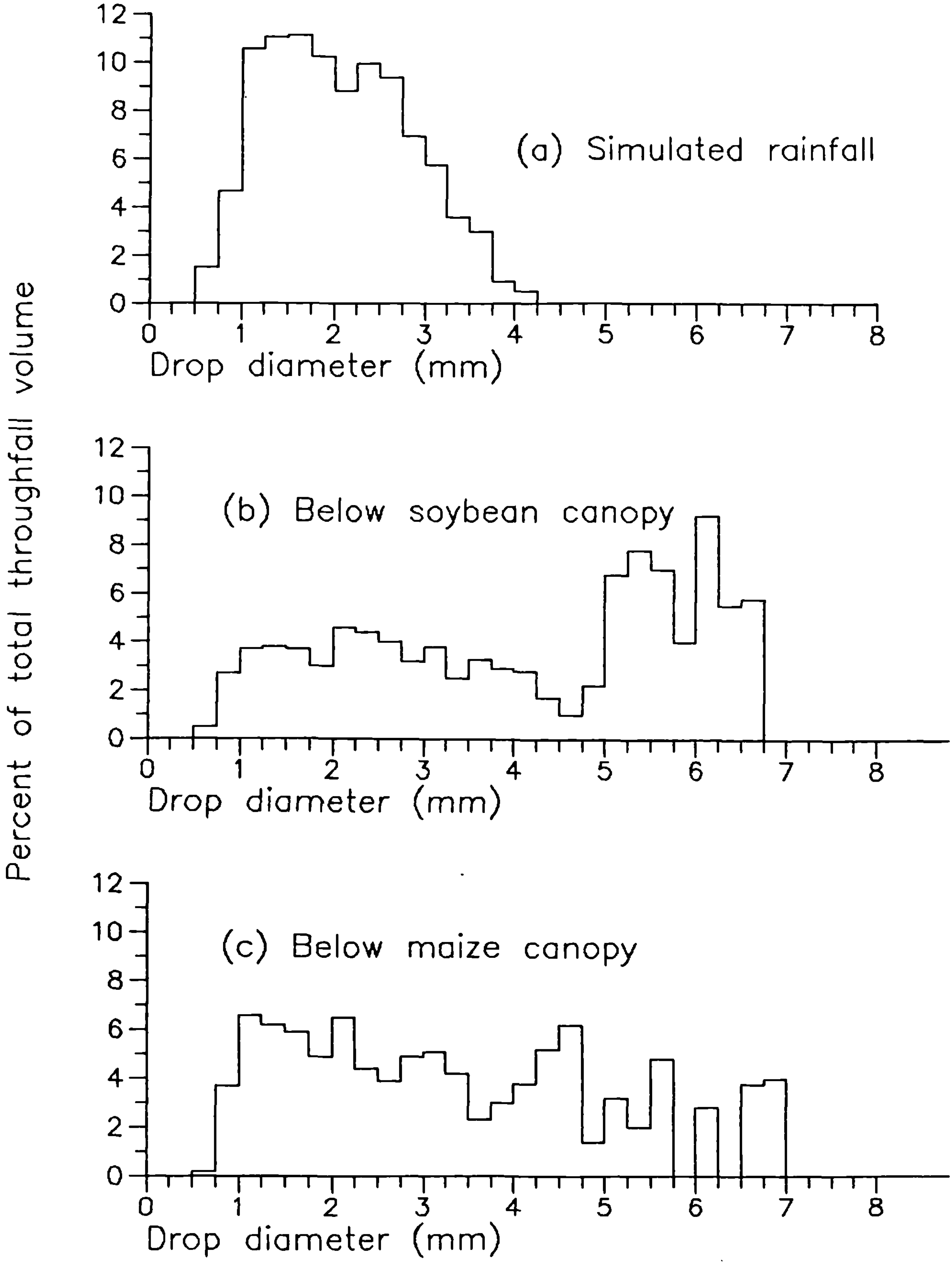

Fig. 4.1 Drop size distributions for simulated rainfall and for rainfall transformed by soybean and maize canopies. (After Armstrong and Mitchell, 1987.)

The momentum squared for leaf drip is calculated by the following function

$$M_D = \frac{\left[\frac{V \rho \pi d^3}{6} \right]^2 DRIP\% \ DRAINA}{\left[\frac{\pi d^3}{6} \right]} \tag{4.4}$$

where M_D = momentum squared for leaf drip ((kg m $s^{-1})^2$ m^{-2} s^{-1}); V = leaf drip fall velocity (m s^{-1}) (calculated by an approximation to the Epema and Riezebos (1983) method); ρ = density of water (kg m^{-3}); d = leaf drip diameter (m); DRIP% = proportion of drainage which falls as leaf drip; DRAINA = canopy drainage (as calculated by the SHE for the grid rectangle) (m s^{-1}). The derivation of equation 4.4 and its implementation in SHESED are presented in Appendix A.

4.2.5 Surface Water

Surface water depths greater than a critical depth dissipate the energy of rain, thus reducing the hydrodynamic forces exerted on the soil by raindrops. The effect is accounted for in the model by the following expression (based on the method of Park et al. (1982), to fit the data of Palmer (1965))

$$\begin{aligned} F_W &= e^{(1 - h/d_m)} \qquad \text{if } h > d_m \\ F_W &= 1 \qquad \text{if } h \le d_m \end{aligned} \tag{4.5}$$

where F_W = water depth correction factor; e = base of natural logarithms; h = water depth; d_m = median raindrop diameter. The median raindrop diameter is either determined from $d_m = 0.00124 x I^{0.182}$ (Laws and Parsons, 1943) where I = rainfall intensity (mm h^{-1}); and d in metres, or set equal to the leaf drip diameter if canopy drainage continues after the direct rainfall has ceased.

As was shown in Fig. 2.1, the Park et al. expression is an adequate model for the Palmer data, although there is little evidence to suggest that it is superior to the other equations shown in the figure.

4.2.6 Surface Slope

A slope effect term is included in some process-based soil erosion models. This is not thought to be appropriate for inclusion in the raindrop detachment equation derived here, as SHESED does not account for either the wind effect on raindrop fall inclination or the microtopography, both of which are considered to be of more significance than the mean surface slope.

4.2.7 The Raindrop Detachment Equation

Combining the above sub-process descriptions leads to the following equation to predict raindrop detachment

$$D_R = K_R F_W (1 - C_G) [(1 - C_C) M_R + M_D] \tag{4.6}$$

where D_R = soil detached by raindrop impact (kg m^{-2} s^{-1}); K_R = raindrop soil detachment coefficient (J^{-1}); C_G = proportion of soil covered by ground cover; C_C = proportion of ground covered by canopy cover, with other terms defined previously. As the SHE gives average canopy drainage for the grid rectangle, the M_D term in equation 4.6 applies to the full grid rectangle and not just the area below the canopy.

4.2.8 Application of the Raindrop Detachment Equation for Determining Soil Detachment Coefficients

Equation 4.6 was applied to several published experimental data sets to try to establish ranges of K_R values for different soil types (Table 4.3). It must be stressed that the experimental conditions varied greatly from those ideal for determining K_R values and that certain missing data had to be estimated. Even if the ideal experimental conditions are used to determine K_R values, it will probably still be necessary to adjust the K_R values for any particular application of SHESED because of scale effects (see Section 4.6.3), different soil conditions (e.g. volume and state of soil moisture), effects of animals (e.g. compaction by grazing cattle), human effects (e.g. tillage) and vegetation effects (e.g. root binding). Although there was a wide variation in experimental conditions, e.g. soil disturbance, vegetation and effects of overland flow, the K_R values shown in Table 4.3 are reasonably consistent within the soil texture classes (except for the high clay result from the data of Bradford et al.). The sand and sandy loam samples show high K_R values as might be anticipated (corresponding to low soil cohesion and relative ease of detachment). This contrasts with indices which include transportability, such as the USLE K factor, which exhibit low values for coarse sand because the relatively large sand particles are more difficult to transport than clay and silt particles.

Table 4.3 Values of the raindrop soil detachment coefficient, K_R, calculated from experimental data using equation 4.6

Data source	Mean K_R coefficient (J^{-1}) for soils of texture							
	Clay	Silty clay	Silty clay loam	Silt	Silt loam	Loam	Sandy loam	Sand
Meyer & Harmon 1984	19.0	18.2	16.2	29.8	39.8	28.2	32.0	
Morgan 1985						30.0		
Bradford et al. 1987a,b	73.5		22.2		25.7	37.6	34.4	62.4
Verhaegen 1987					24.7	23.4	30.0	

Table 4.3 is significant as it provides a data base of parameter values, albeit with a range of error, which should allow the use of SHESED with minimal calibration. At present the data base is limited, but as more data become available it is hoped that K_R values can be taken from tables such as 4.3 in a similar way as is currently done with Manning roughness values.

Additional attempts to calculate K_R values were made using data from the single drop experiments of Bubenzer (1970) and Al-Durrah and Bradford (1982). However, the K_R values obtained showed more variation with drop diameter than with soil type. It is not clear whether this is caused by deficiencies in the model, an incorrect interpretation of the data, or a basic problem in using single drop data for this purpose.

4.2.9 Field Test of the Raindrop Detachment Equation

The ability of equation 4.6 to account for the effects of differing rain intensities, canopy cover and canopy height on raindrop induced soil detachment is illustrated by applying the equation to field data from Morgan (1985) for a soybean plot with a loam soil. Figure 4.2 shows the good agreement obtained between simulated and measured soil detachment rates. Each point has different experimental conditions within the ranges of canopy cover varying from 0 to 90 %, canopy height from 0 to 0.8 m and simulated rainfall intensities from 42.6 mm h^{-1} to 109.8 mm h^{-1}. A constant K_R value of 30 J^{-1} was used for all these conditions (determined by a least squares analysis). This value for the loam soil is within the range of the K_R values for loams given in Table 4.3 (23.4 to 37.8 J^{-1}). If the K_R values are calibrated for each data point, then 76% of the individually calibrated K_R values are within ±25% of 30 J^{-1}. Note that three experimental data points (at a canopy cover of 90%) were excluded from this analysis. For these points the measured intensity below the canopy was significantly higher than the intensity above the canopy. This was probably caused by redistribution of the rainfall towards the sampling points.

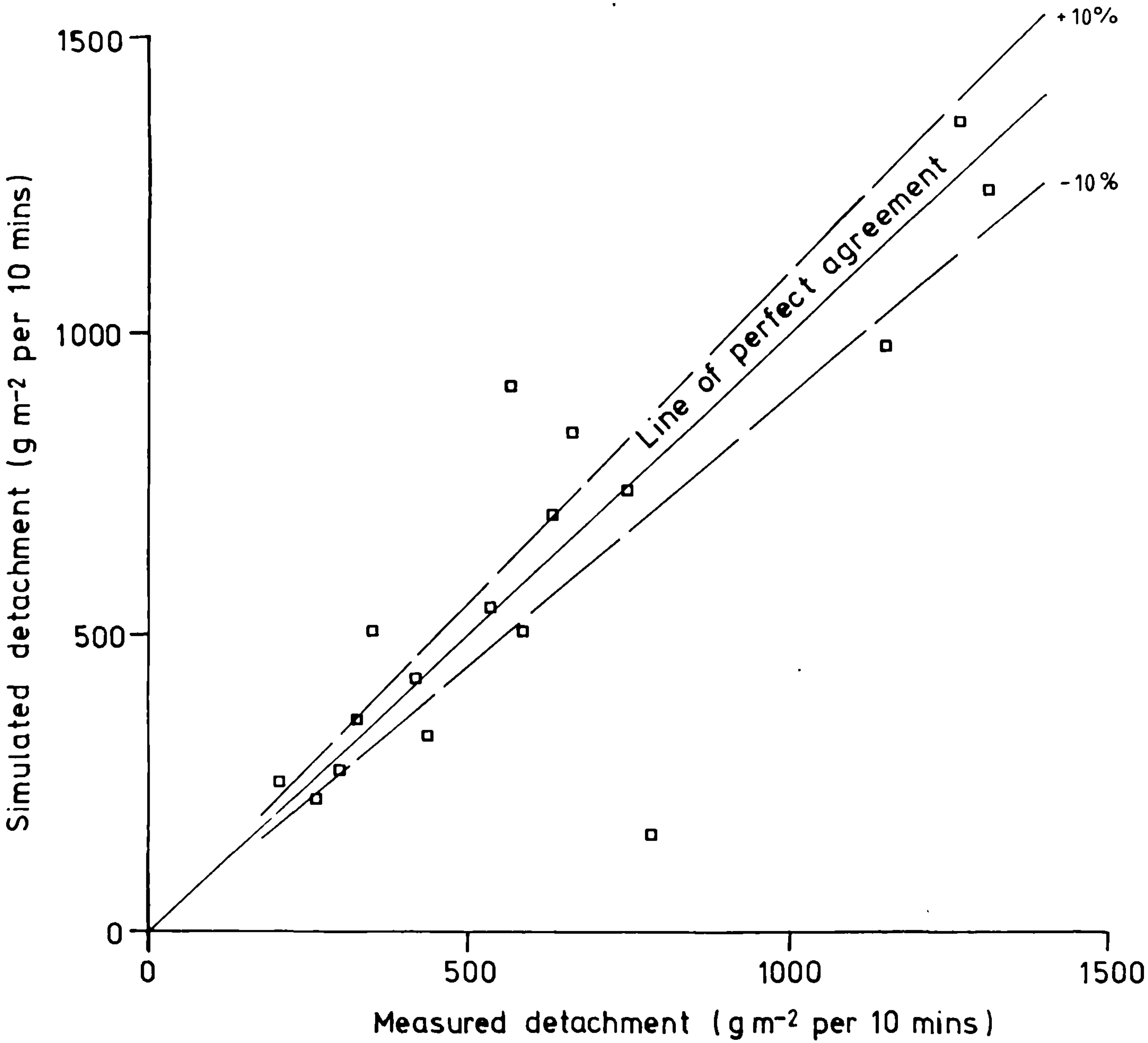

Fig. 4.2 Simulated and measured detachment rates for the field experiments of Morgan (1985).

Owing to lack of data, the following assumptions had to be made in the modelling study: (a) The Marshall-Palmer drop size distribution was appropriate for the rainfall simulator; (b) The representative leaf drip diameter was 5 mm; (c) The canopy drainage (DRAINA in equation 4.4) is given by the reported rainfall intensity collected below the canopy minus the product of the rain intensity above the canopy and the proportion of bare ground; (d) All canopy drainage falls as leaf drip. This means that leaf splash is assumed to make an insignificant contribution to the total drainage volume. Stem flow was not measured and therefore does not need to be eliminated from the data; (e) Surface water and ground cover have no influence on the soil detachment (i.e. $C_G = 0$ and $F_W = 1$ in equation 4.6).

4.3 OVERLAND FLOW DETACHMENT

For modelling soil erosion, overland flow is best described by a combination of sheet and rill flows. However, with the present structure of the SHE, the important hydraulic variables of flow depth and velocity are available only as values averaged over the SHE grid rectangle. Consequently it is not possible to simulate the separate processes of rill and sheet flow, and therefore a fully physically-based overland flow detachment predictor applicable to rilled surfaces cannot as yet be included in the model. In view of this, it was decided to use the following simple equation to predict overland flow detachment (e.g. Ariathurai and Arulanandan, 1978)

$$D_F = K_F \left[\frac{\tau}{\tau_c} - 1 \right] \qquad \text{for } \tau > \tau_c$$
$$D_F = 0 \qquad \text{for } \tau \leq \tau_c \qquad (4.7)$$

where D_F = overland flow detachment (kg m^{-2} s^{-1}); K_F = overland flow soil detachment coefficient (kg m^{-2} s^{-1}); τ_c = critical shear stress from Shields curve extended by Mantz (1977) for small particle sizes (see Appendix B); and τ = shear stress ($\tau = \rho ghS$ where ρ = water density; g = acceleration due to gravity; h = water depth; S = water surface slope).

As discussed in Section 2.2.2.2, the shear stress should be that which acts upon the soil surface, and not the total shear stress which will act upon both the cover and the soil. However, in SHESED the total shear stress is used; partitioning the shear stress would involve introducing another calibration parameter.

The use of the Shields curve, a relationship for non-cohesive sediment, to calculate the critical shear stress, τ_c, for generally cohesive soils is recognised as a likely weak element. The alternatives are to assume a τ_c value of zero, determine τ_c during the model calibration, or use one of the published empirical equations, which are usually based on limited data (e.g. Smerdon and Beasley, 1961). It is considered that none of these alternatives will significantly increase the accuracy of the predicted overland flow detachment rates and this is identified as an area where further research is needed.

The overland flow soil detachment coefficient, K_F, can be predetermined by experiment only where sheet flow exists in the absence of rills, and this value is then applicable only if the SHE grid network is sufficiently refined to be able to predict overland flow depths accurately. As these situations are rare, the K_F coefficient is best thought of as a calibration coefficient, although as experience in applying SHESED grows, the K_F value may be able to be predicted from a knowledge of the soil and overland flow characteristics.

4.4 OVERLAND FLOW TRANSPORT CAPACITY

The ability of overland flow to transport detached soil particles and aggregates depends on the flow, rainfall and sediment characteristics. In the absence of a general sediment transport equation derived for the small water depths and large slopes typifying overland flow, alluvial channel sediment transport equations must be used. Studies by Alonso et al. (1981) and Julien and Simons (1985) have recommended the equations of Yalin (1963) and Engelund-Hansen (1967) as being appropriate for overland flow (these transport equations are presented in Appendix B). Both of these equations are included in SHESED for the calculation of overland flow transport capacity.

Although there is widespread use of alluvial channel sediment transport equations for overland flow, it must be stressed that overland flow conditions vary greatly from those used in the derivation of these equations. A major factor here is the increase in overland flow turbulence caused by raindrop impact, which allows greater suspension of sediment relative to the case with no rainfall but otherwise similar flow conditions (e.g. Novotny, 1980; Guy et al. 1987). There is an urgent need for a theoretically-based equation to predict overland flow sediment transport capacity for overland flow with rainfall.

4.5 HILLSLOPE ROUTING

4.5.1 Sediment Continuity Equation

Hillslope sediment routing involves the calculation of the movement of the sediment load down a slope to the point where it may enter a channel. Computations are based on the partial differential equation for conservation of sediment mass, which, if expressed in two space dimensions, is

$$\frac{\partial(hC)}{\partial t} + (1 - \lambda)\frac{\partial z}{\partial t} + \frac{\partial g_x}{\partial x} + \frac{\partial g_y}{\partial y} = 0 \qquad (4.8)$$

where h = water depth (m); C = sediment concentration ($m^3\ m^{-3}$); λ = soil surface porosity; z = soil surface elevation (m); t = time (s); g_x = volumetric sediment transport rate per unit width in the x-direction ($m^3\ s^{-1}\ m^{-1}$); g_y = volumetric sediment transport rate per unit width in the y-direction ($m^3\ s^{-1}\ m^{-1}$). (The dispersion term discussed in Section 2.2.6 has been neglected in this equation.)

4.5.2 Finite Difference Scheme

The sediment continuity equation is solved numerically using a finite difference method based on the four-point scheme shown in Fig. 4.3 (where F represents any physical quantity). The four-point scheme is extended to two space dimensions with the notation adjusted as shown in Fig. 4.4(a).

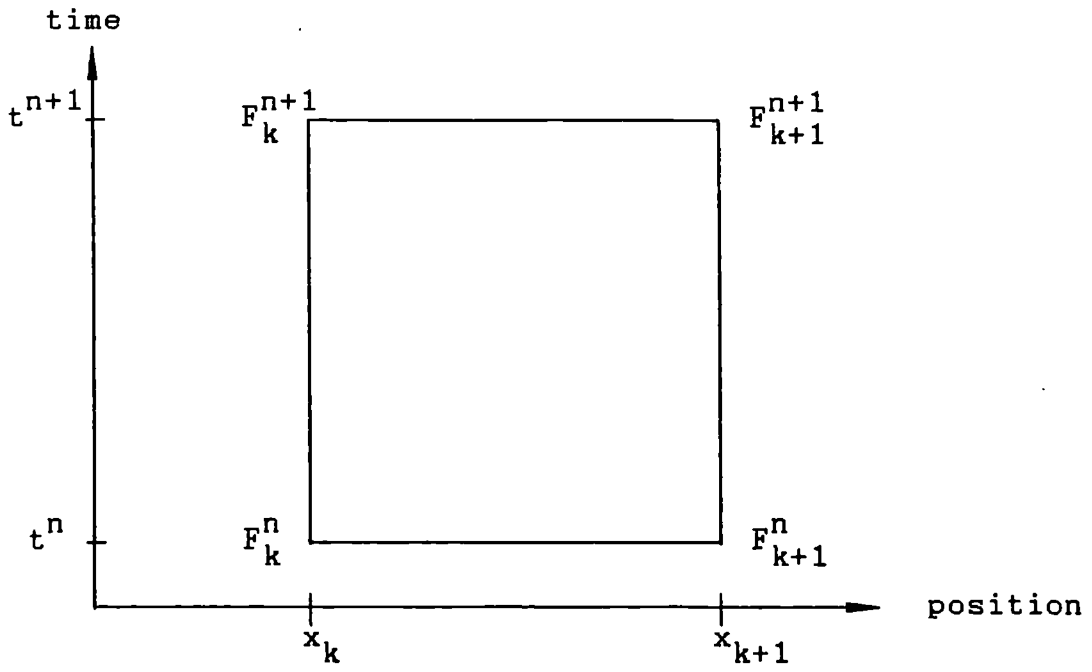

$$\frac{\partial F}{\partial t} \approx \frac{1}{\Delta t}\left[\phi(F_{k+1}^{n+1} - F_{k+1}^{n}) + (1 - \phi)(F_k^{n+1} - F_k^n) \right]$$

$$\frac{\partial F}{\partial x} \approx \frac{1}{\Delta x}\left[\theta(F_{k+1}^{n+1} - F_{k}^{n+1}) + (1 - \theta)(F_{k+1}^{n} - F_k^n) \right]$$

$$\Delta x = x_{k+1} - x_k \qquad \Delta t = t^{n+1} - t^n$$

Fig. 4.3 Four-point finite difference scheme.

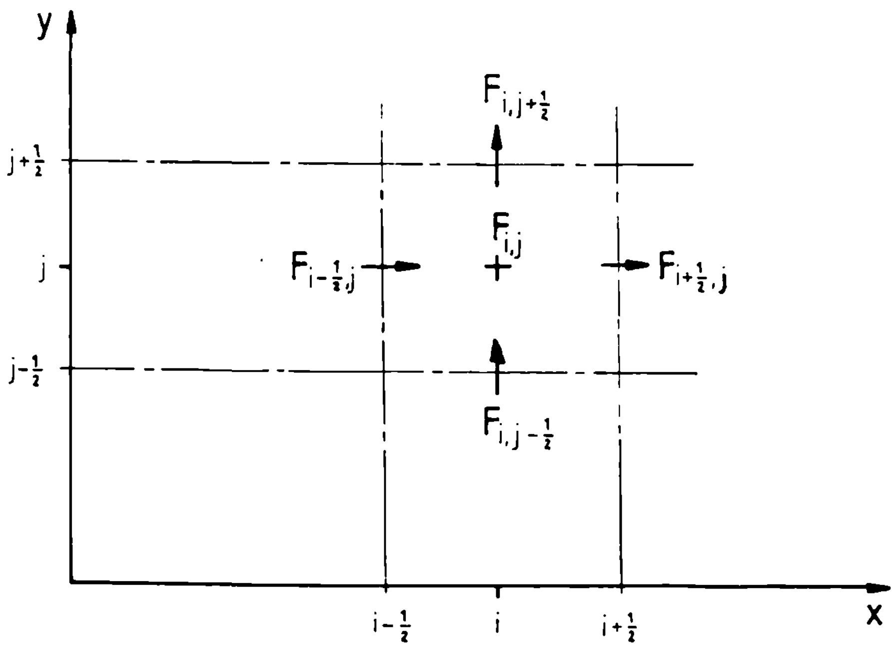

(a) Notation for the finite difference grid in two space dimensions.

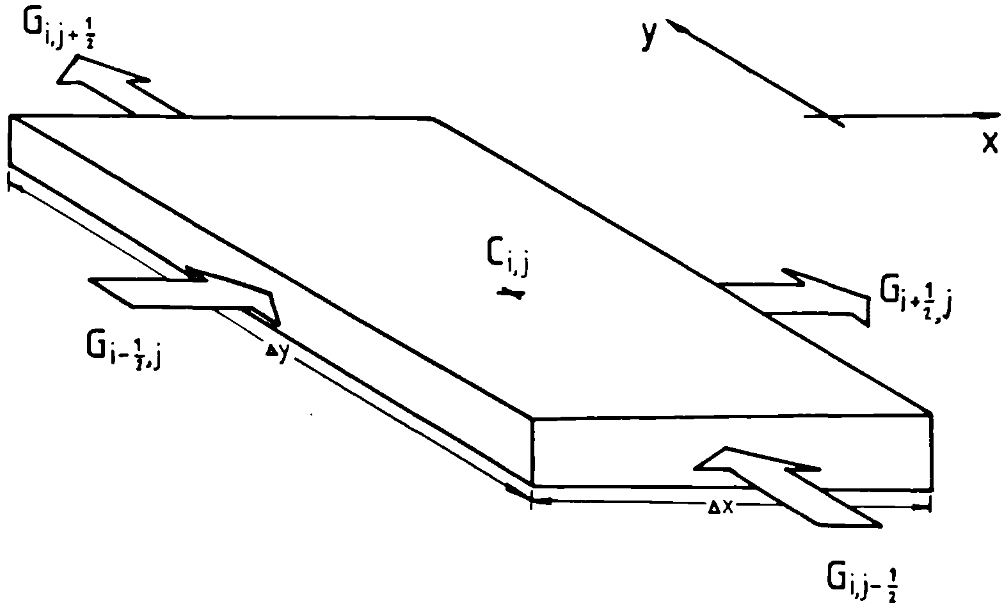

(b) Schematic representation of the definitions of sediment transport rate, G, and concentration, C, for a SHE grid rectangle.

Fig. 4.4 Finite difference grid in two space dimensions.

In terms of the SHE grid network, a variable defined at the centre of a grid rectangle (e.g. sediment concentration, water depth and changes in surface elevation) is represented by $F_{i,j}$, whereas a variable defined at the edge of a grid rectangle (e.g. water and sediment discharges and slope) is represented with the notation for the staggered grid, e.g. $F_{i+½,j}$. Fig. 4.4(b) shows a schematic representation of these definitions for the sediment concentration, C, and sediment transport rate, G.

Expressing the sediment transport rates per unit width (g_x and g_y) as the sediment transport rate divided by the width of the grid rectangle in the x and y directions, and noting that the space weighting factor, ϕ, is not relevant because z and C are defined at the centre of the grid rectangle, the finite difference version of equation 4.8 is

$$\frac{1}{\Delta t}\left[(hC)^{n+1}_{i,j} - (hC)^{n}_{i,j}\right] + (1-\lambda)\frac{\Delta z_{i,j}}{\Delta t}$$

$$+ \frac{1}{\Delta y \Delta x}\left[\theta\left[G^{n+1}_{i+½,j} - G^{n+1}_{i-½,j}\right] + (1-\theta)\left[G^{n}_{i+½,j} - G^{n}_{i-½,j}\right]\right]$$

$$+ \frac{1}{\Delta x \Delta y}\left[\theta\left[G^{n+1}_{i,j+½} - G^{n+1}_{i,j-½}\right] + (1-\theta)\left[G^{n}_{i,j+½} - G^{n}_{i,j-½}\right]\right]$$

$$= 0 \qquad (4.9)$$

where Δt = computational time step; Δz = change in surface elevation over Δt (erosion if negative); Δy = the SHE grid rectangle width in the x direction; Δx = the SHE grid rectangle width in the y direction; θ = time weighting factor; G = volumetric sediment transport rate; n and n+1 refer to the start and end of the time step respectively; i and j are the position indices in the x and y directions respectively (see Fig. 4.4).

4.5.3 Solution Procedure

An explicit solution of equation 4.9 is possible if the calculations start at the grid rectangle with the highest surface elevation and then progress to the next highest grid rectangle and so on. The significance of this is that all inflows to the current grid rectangle are known at the times t^{n+1} and t^n. The various stages of the overland flow sediment routing calculations are shown below for one grid rectangle at one time step.

(1) Calculate the transport capacity (see Section 4.4) for flows out of the current grid rectangle using variables defined at the edges of the grid rectangle and for the time t^{n+1}.

(2) Calculate the potential sediment concentration (i.e. assuming an excess of sediment supply) for the grid rectangle using

$$C_{i,j}^{n+1} = \frac{1}{4}\left[\left[\frac{G}{Q}\right]_{i+\frac{1}{2},j}^{n+1} + \left[\frac{G}{Q}\right]_{i-\frac{1}{2},j}^{n+1} + \left[\frac{G}{Q}\right]_{i,j+\frac{1}{2}}^{n+1} + \left[\frac{G}{Q}\right]_{i,j-\frac{1}{2}}^{n+1} \right] \qquad (4.10)$$

where Q = water discharge; G = either the sediment transport rate into the grid rectangle, or the transport capacity for flows out of the grid rectangle. Equation 4.10 assumes equality of volume concentration and transport concentration (G/Q), thus implying that the sediment is transported at the water velocity. As eroded soil is usually fine grained, this should not introduce too large an error.

(3) Using the potential sediment concentration from equation 4.10, equation 4.9 can be rearranged to give the potential change

in surface elevation

$$\Delta z^{pot}_{i,j} = \Bigg[-B \Big[\theta[G^{n+1}_{i+½,j} - G^{n+1}_{i-½,j}] + (1 - \theta)[G^{n}_{i+½,j} - G^{n}_{i-½,j}] \Big]$$

$$- B \Big[\theta[G^{n+1}_{i,j+½} - G^{n+1}_{i,j-½}] + (1 - \theta)[G^{n}_{i,j+½} - G^{n}_{i,j-½}] \Big]$$

$$- [(hC)^{n+1}_{i,j} - (hC)^{n}_{i,j}] \Bigg]$$

$$/ (1 - \lambda) \qquad (4.11)$$

where $B = \Delta t/(\Delta x \Delta y)$; G = either the sediment transport rate into the grid rectangle, or the transport capacity for flows out of the grid rectangle.

(4) Calculate, $\Delta z^{ava}_{i,j}$ the depth of soil available to be eroded

$$\Delta z^{ava}_{i,j} = -SD_{i,j} - \frac{\Delta t(D_{R_{i,j}} + D_{F_{i,j}})}{\rho_s (1 - \lambda)} \qquad (4.12)$$

where SD = initial loose soil depth; D_R = soil detached by raindrop impact (from equation 4.6) (kg m^{-2} s^{-1}); D_F = soil detached by overland flow (from equation 4.7) (kg m^{-2} s^{-1}); ρ_s = density of the soil particles (kg m^{-3}). The inclusion of the initial loose soil depth term allows for previously detached soil particles to remain on the surface in storage until the water can transport the material. Thus, sediment detached by rainfall before runoff has started is available to be transported if runoff occurs. Deposited sediment is also included in this term.

(5) Compare $\Delta z^{pot}_{i,j}$ and $\Delta z^{ava}_{i,j}$. If $\Delta z^{pot}_{i,j}$ is positive (denoting deposition) or the potential depth of erosion is less than the available depth of erosion ($\Delta z^{pot}_{i,j} > \Delta z^{ava}_{i,j}$, as erosion is negative), then erosion is limited by transport capacity. The predicted $\Delta z_{i,j}$ is as calculated from equation 4.11 with the predicted sediment transport rates equal to the transport capacity values (calculated in step (1) above) and the sediment concentration $C^{n+1}_{i,j}$ equal to that calculated from equation 4.10.

However, if the potential depth of erosion is greater than the available depth of erosion ($\Delta z^{pot}_{i,j} < \Delta z^{ava}_{i,j}$, as erosion is negative), then erosion is supply limited and the predicted $\Delta z_{i,j}$ is as calculated from equation 4.12. The predicted sediment concentration, $C^{n+1}_{i,j}$, is determined from a rearrangement of equation 4.9

$$C^{n+1}_{i,j} = \Bigg[(hC)^{n}_{i,j} - \Delta z_{i,j}(1 - \lambda)$$

$$- B \Big[\theta\big[\sigma G^{n+1}_{i+\frac{1}{2},j} - \sigma G^{n+1}_{i-\frac{1}{2},j}\big] + (1 - \theta)\big[G^{n}_{i+\frac{1}{2},j} - G^{n}_{i-\frac{1}{2},j}\big] \Big]$$

$$- B \Big[\theta\big[\sigma G^{n+1}_{i,j+\frac{1}{2}} - \sigma G^{n+1}_{i,j-\frac{1}{2}}\big] + (1 - \theta)\big[G^{n}_{i,j+\frac{1}{2}} - G^{n}_{i,j-\frac{1}{2}}\big] \Big] \Bigg]$$

$$/\Big[h^{n+1}_{i,j} + \theta B\big[(1-\sigma)Q^{n+1}_{i+\frac{1}{2},j} - (1-\sigma)Q^{n+1}_{i-\frac{1}{2},j} + (1-\sigma)Q^{n+1}_{i,j+\frac{1}{2}} - (1-\sigma)Q^{n+1}_{i,j-\frac{1}{2}}\big]\Big] \tag{4.13}$$

where $B = \Delta t/(\Delta x \Delta y)$; $\sigma = 1$ if the accompanying flow is into the grid rectangle, or $\sigma = 0$ if the accompanying flow is out of the grid rectangle. (The accompanying flow is that at the grid position represented by the indices of the Q or G value which is multiplied by σ.)

The sediment transport rates out of the grid rectangle are then calculated from G = CQ, e.g.

$$G^{n+1}_{i+\frac{1}{2},j} = C^{n+1}_{i,j}\, Q^{n+1}_{i+\frac{1}{2},j} \tag{4.14}$$

Thus the sediment transport rates out of the grid rectangle and the sediment concentration and change in surface elevation at the centre of the grid rectangle are determined. Finally the loose soil depth, SD, is either increased to include any deposited sediment or detached soil that could not be transported, or reduced if soil was transported from this storage.

4.5.4 Initial and Boundary Conditions

The solution of the sediment continuity equation requires that initial sediment concentrations or transport rates are given for all grid rectangles and that data on inflows of sediment to the modelled area are provided. However, SHESED sets all these values to zero and therefore, in its current form, SHESED should be run from the start of the event and the area to be modelled should include no inflows of sediment transported by overland flow. SHESED does allow the initial depth of loose sediment to be specified at the start of the simulation. This may prove useful for modelling erosion of stores of loose material such as mining waste.

4.5.5 Numerical Behaviour

The behaviour of the numerical solution depends on the relative importance of the processes occurring, the value of the time weighting factor, and the Courant number ($V\Delta t/\Delta x$). The weighting factor for time, θ, is set to 0.65, thus ensuring some light damping to eliminate long-term instability. However, a time weighting factor not equal to 0.5 will introduce some numerical diffusion which can become significant. To restrict this numerical diffusion, the time step should then be selected so as to produce a Courant number near to unity.

Near the start and end of an event, the numerical solution of the sediment continuity equation may produce physically meaningless negative concentrations (the causes of which are discussed in Appendix D). These negative concentrations are of minor significance in terms of the mass of sediment involved and are a characteristic common to a number of finite difference schemes (e.g. see Holly and Preissmann, 1977). However, they cannot be accommodated within the explicit solution technique used in SHESED. To overcome this problem the weighting factor is temporarily increased to 1.0 and the calculations repeated for the grid rectangle. Alternatives to this approach are: (1) to convert the negative values to zeros, thus accepting some mass balance error; and (2) to increase the weighting factor by a small increment (e.g. 0.02), repeat the calculations, and if negative concentrations are still obtained then increase the weighting factor again, recalculate and repeat until the negative concentrations do not occur. This second method may result in large increases in the computational time.

4.6 DISCUSSION

This discussion concerns three important aspects of the hillslope phase of sediment yield which have received little attention so far in this chapter: soil particle size distribution, sediment deposition, and spatial averaging of processes with particular reference to the effect of this on rill and sheet flow modelling.

4.6.1 Soil Particle Size Distribution

The current version of SHESED does not simulate the effects of hillslope processes on the soil particle size distribution. The assumption made in SHESED is that the particle size distribution defining each soil type can be used as the particle size distribution of the sediment input to a channel reach from overland flow. Thus the enrichment of the sediment load with finer sizes (clays), surface armouring, and the likely preferential deposition of larger sizes cannot be predicted.

If the model were to be altered to consider these effects, then a number of issues which are currently not well understood need to be addressed. The main uncertainties concern the adjustment of the raindrop impact detachment, flow detachment and transport capacity equations to consider the selective detachment and transport of particular particle sizes.

Any transport capacity equation can be used to give transport capacity for a particular size fraction: the transport capacity is calculated using the size fraction diameter and density and then multiplying by the percentage of that size fraction in the soil surface (or sediment load if known). A more elaborate modification to the Yalin (1963) equation has been developed (Foster et al., 1980). However, the only reported testing of this modified equation was inconclusive (the equation apparently worked well for deposition of a sample with two fractions of sand and coal of the same fall diameter but did not work well for a sand-coal mixture where the two particle fractions had different fall diameters (Foster, 1982, reporting Davis, 1978)). There is no intrinsic reason to expect that transport capacity equations so modified will produce more accurate results than those obtained by using the representative particle size suggested by the original developer of the equation. Indeed the opposite is more likely, as the equations are being used in a form different from that in which their empirical elements were determined.

Raindrop detachment equations are usually unselective with respect to size of sediment particle detached. When used to calculate the amount detached for a particular size fraction, the total detached sediment is multiplied by the percentage of the size fraction in the original soil surface. An alternative to this approach is presented by Wright (1987), who uses a physically-based analysis of the mechanisms of particle entrainment caused by raindrop impact in combination with the Bagnold (1966) equation to predict the differential erosion of different particle size fractions. Wright's model relies on the Bagnold equation (a total load equation derived for alluvial rivers) to determine the transport in the high speed lateral flow occurring immediately after raindrop impact. He uses an unspecified modification to Bagnold's equation to determine the proportion of different particle sizes that are entrained.

Flow detachment equations are also generally unselective with respect to size of sediment particle detached. The methods currently used either involve multiplying the total flow detachment by the percentage of the size fraction in the original soil, or are related to the flow transport capacity for each size fraction.

None of the above methods takes into account the effect of cohesion on selective detachment and transport; also very little testing of the methods with field or laboratory data has been reported. In view of the above discussion, it is not thought worthwhile to route sediment by size fraction in the hillslope phase of the current SHESED as this will greatly increase computational time and storage requirements with no guarantee of improved results. However, routing by size fraction will eventually need to be added to the program in order to model the transport of contaminants adhering to soil particles.

4.6.2 Sediment Deposition

As discussed in Section 2.2.2.4, there are two basic approaches used in soil erosion modelling to deal with sediment deposition. The first approach is based on the concept that net deposition occurs only when the sediment load is greater than the transport capacity. The second is based on the concept that deposition is a continually occurring process owing to sediment settling out under gravity and the deposition is therefore mainly a function of particle fall velocities.

The first approach is used in SHESED, and therefore deposition is simulated by the model only when the transport capacity is less than the sediment load. The sediment load is defined here as the inflow of sediment to the current grid rectangle over the computational time step plus the sediment concentration in the grid rectangle at the start of the time step minus the sediment outflow from the grid rectangle over the time step.

When deposition occurs, the material is added to the depth of loose soil storage and is available for transport at subsequent time periods without having to be detached again. The opposite assumption has been made in some models (e.g. Foster, 1982; Nielsen et al., 1986), that is detachment of deposited sediment requires the same energy input as does detachment of the original soil. This may be true if deposited sediment is stored for extended periods of time, or is compacted by traffic; however, during an event, or series of events, deposited sediment is likely to remain loose and therefore does not need re-detaching. For situations between the two extremes, some function (e.g. exponential decay) needs to be introduced to account of the reduction in the loose soil storage with time.

4.6.3 Spatial Averaging

A distributed model, such as SHESED, can be considered as a matrix of interconnected lumped models, each lumped model being a grid rectangle. Within each grid rectangle, uniformity of characteristics is assumed. Problems associated with the grid scale include: non-coincidence of natural boundaries (e.g. between vegetation types) and grid boundaries, use of a grid scale larger than one characteristic of the processes occurring, and the inappropriateness of data obtained at the point scale for representing parameters or response at the larger grid scale. The scale problem is receiving much attention in hydrology although only a limited literature on the problem is available in the field of soil erosion modelling (e.g. Walling, 1983; Julien and Frenette, 1986).

Two important aspects of the scale problem in soil erosion modelling which have received little written comment to date are the representation of rills and the use of grid average slopes; these are discussed below.

(1) Rilling is recognised as one of the main processes which lead to increased removal of soil. However, rills are difficult to represent explicitly in a catchment scale model such as SHESED (see Section 4.3) and even some of the field scale models which claim to simulate rill and interrill flow separately (e.g. CREAMS, Foster et al., 1980 and Foster, 1982) in fact make effectively no explicit distinction between rill and interrill flow (see Section 2.2.2.4).

The problem remains that we need to account for the likely increased soil loss from rilling, but that rills cannot be included in the model in a physically-based sense. A comparable problem exists when macropores cause rapid movement of water in the unsaturated zone but are not included explicitly in the hydrological model. In that case the saturated hydraulic conductivity can be increased from that expected based on soil samples. Similarly, to account for the effect of rills, the overland flow soil detachment coefficient could be increased from values appropriate to sheet flow. However the magnitude of the increase is not clear and, as rills are ephemeral features, the value is likely to change with time. The problems associated with modelling rill erosion remain one of the major difficulties encountered in soil erosion modelling.

(2) SHESED assumes a uniform surface slope between grid rectangles where in fact the slope profile may be a complex combination of concave and convex segments with local depressions. This could lead to the model predicting net erosion from a grid rectangle, where in reality, soil eroded from a steep part of the profile is deposited within the grid rectangle in a local depression. This is a problem caused by using too large a grid size; however, it may not be possible to reduce the grid size if computer and/or data requirements become excessive. If this is the case, calibration parameters are likely to take different values at different grid scales.

Another problem associated with the model representation of the topography involves the determination of the representative land surface elevation for each grid rectangle. This is used to determine the ground surface slopes between adjacent grid rectangles. Based on simulations carried out during the development of SHESED, the elevations have a minor influence on the overland flow discharge, but can be very important for the determination of the distribution of net soil erosion and deposition. Current methods for determining the representative surface elevations are based on averaging a predetermined set (usually four or five) of point elevations within a grid rectangle. This may lead to overland flow directions which are different from those which occur in the catchment, or to gentle slopes between grid rectangles where steeper slopes may be more appropriate (or vice versa).

Thus, modelled flow pathways may be longer than actual ones, or inappropriate slope gradients between grid rectangles may lead to the prediction of deposition or erosion where none should occur. This problem with distributed soil erosion models requires greater attention, although the lack of distributed data on erosion and deposition zones may hinder progress in this area.

A third aspect of the scale problem, the transfer of parameter values obtained at the small scale to larger scales, is the subject of one of the field tests of SHESED presented in Chapter 6.

CHAPTER 5 - CHANNEL SEDIMENT PROCESSES IN SHESED

5.1 INTRODUCTION

The channel sub-component of SHESED routes the sediment load through the channel network. The sediment load consists of sediment carried into the channel by overland flow, entrained from the channel bed, and transported into the study reach at an upstream boundary of the model. Deposition and some of the effects of nonuniform bed material are also simulated. These processes are simulated using algorithms which determine the transport capacity of the flow, the supply of sediment, route the sediment load downstream and update the size distribution of the channel bed material. These constituent parts of the sub-component are described below.

5.2 SEDIMENT TRANSPORT CAPACITY

A large number of equations have been formulated to predict the sediment transport capacity from various combinations of hydraulic and sediment properties. All contain some empirical element and none of the equations yield accurate results for all hydraulic and sediment conditions. Currently two equations are available in SHESED for calculating sediment transport capacity in channels, these being the Engelund and Hansen (1967) and Ackers and White (1973) equations (see Appendix B). These two equations were chosen because: (1) both are total load equations and are therefore in keeping with the total load approach taken in SHESED (the sub-component does not distinguish between bed and suspended bed material loads); (2) both equations have performed well in tests which have compared sediment transport rates predicted by various equations with measured transport rates (e.g. Vanoni, 1975; White et al., 1975; Alonso, 1980; Bathurst et al., 1987); and (3) neither of the equations has excessive computational requirements. The Day (1980) modification to the Ackers-White equation is also included in SHESED (see Appendix B). This seeks to account for the effects of particle exposure and shielding on the initiation of movement of nonuniform bed material. It is also very easy to introduce extra equations into the program if a more suitable transport capacity equation is available.

For any particular application of SHESED the selection of the sediment transport capacity equation from the multitude of documented equations will depend on such factors as: (1) whether any of the equations were derived using concepts and data for situations similar to those to be modelled; and (2) whether the equation performed well in independent comparative tests, preferably with data sets for conditions similar to those to be modelled. Also, the data used to derive and test the equations should be checked to make sure that supply effects are not present - this will be difficult to achieve with field data. An alternative approach is to use the transport capacity equations to calibrate the model. This may involve trying various equations in the model and choosing the equation which gives the best fit of measured to simulated response. Alternatively, the empirical factor in a equation may be adjusted until the best fit is obtained. If the sediment transport capacity equation is used to calibrate a SHESED model, then the calibration period should be for conditions where an excess of sediment supply exists. This is so that the possible errors in simulating supply effects do not influence the choice of transport capacity equation.

5.3 SEDIMENT SOURCES

The sediment transport equations discussed in the previous section calculate the transport capacity of the flow, that is they determine the sediment transport rate assuming a plentiful supply of sediment. In many situations this assumption is not justified, and therefore the supply of sediment to the channel needs to be considered. Also, the transport capacity equations do not predict the wash load transport rates. In the SHESED channel sub-component, the sediment sources are the channel bed material, sediment eroded from the hillslopes and transported into the channel by overland flow and sediment transported into the study reach at an upstream boundary of the channel system model.

Bank erosion can make a significant contribution to the sediment yield, for example Newson and Leeks (1987) suggest that bank erosion is the major factor with regard to the magnitude of suspended load yields in Mid-Wales. However, as described in Section 2.3.2, the mechanics of bank erosion are complex and physically-based modelling of bank erosion would probably require a more detailed description of the channel geometry and hydraulic conditions than is available within the one-dimensional framework of the SHE channel component. Bank erosion is therefore not included in SHESED. Where good estimates of the bank erosion rate are available, these could in the future be included in

SHESED using a similar approach to that used in IALLUVIAL (see Section 2.3.2).

5.4 CHANNEL ROUTING

5.4.1 Sediment Continuity Equation

Sediment routing in channels is based on the partial differential equation for conservation of sediment mass

$$\frac{\partial(AC)}{\partial t} + (1 - \lambda)W\frac{\partial z}{\partial t} + \frac{\partial(ACV_s)}{\partial x} = \frac{\partial}{\partial x}\left[A\epsilon\frac{\partial C}{\partial x}\right] + g_s \tag{5.1}$$

where A = cross-sectional flow area (m^2); C = sediment concentration (m^3 m^{-3}); λ = bed porosity; W = active bed width (m); z = channel bed elevation (m); V_s = longitudinal sediment velocity (m s^{-1}); ϵ = longitudinal dispersion coefficient (m^2 s^{-1}); g_s = overland flow sediment input to the channel (m^3 s^{-1} m^{-1}); t = time (s); x = distance along the channel (m).

The dispersion coefficient is a function of turbulent diffusion and differential convection due to the variation of velocity in the cross section and it has to be determined by experiment for the site-specific conditions. However, the dispersion term is neglected here owing to the difficulty in determining ϵ values for each particle size and to its negligible magnitude when compared with the other terms in equation 5.1.

5.4.2 Finite Difference Scheme

The solution of equation 5.1 is based on the same four-point finite difference scheme used for hillslope sediment routing (Fig. 4.3). In the interest of clarity, the method of solution presented below is for the simplest case of one particle size and for a node where only two links join. The extension of the method to multiple size fractions and a complex river network is described subsequently.

In equation 5.1, the sediment concentration, C, can be replaced by

$$C = \frac{G}{V_s A} \tag{5.2}$$

where G = sediment transport rate ($m^3\ s^{-1}$). If equation 5.2 is substituted into equation 5.1 and the dispersion term is neglected the following expression is obtained

$$\frac{\partial(G/V_s)}{\partial t} + (1 - \lambda)W\frac{\partial z}{\partial t} + \frac{\partial G}{\partial x} = g_s \tag{5.3}$$

Using the scheme shown in Fig. 4.3, the finite difference approximation of equation 5.3 is

$$\frac{1}{\Delta t}\left[\phi\left[\left(\frac{G}{V_s}\right)_{k+1}^{n+1} - \left(\frac{G}{V_s}\right)_{k+1}^{n}\right] + (1 - \phi)\left[\left(\frac{G}{V_s}\right)_{k}^{n+1} - \left(\frac{G}{V_s}\right)_{k}^{n}\right]\right]$$

$$+ \quad (1 - \lambda_i)W_i\frac{\Delta z_i}{\Delta t}$$

$$+ \quad \frac{1}{\Delta x}\left[\theta\left[G_{k+1}^{n+1} - G_{k}^{n+1}\right] + (1 - \theta)\left[G_{k+1}^{n} - G_{k}^{n}\right]\right]$$

$$= g_{si} \tag{5.4}$$

where Δt = computational time step (s); ϕ = space weighting factor; Δz = change in bed surface elevation over Δt (m), which is the depth of scour (if negative) or deposition (if positive); θ = time weighting factor; Δx = river length associated with the node (m) and given by $\Delta x = 0.5\ (\Delta x_{k+1} + \Delta x_k)$; n and n+1 refer to the start and end of the time step respectively; k and k+1 refer to the upstream and downstream links of the node i respectively.

5.4.3 Longitudinal Sediment Velocity

For silt and clay size particles the longitudinal sediment velocity is approximated by the flow velocity but for larger sediment sizes the following expression for sediment velocity is used (Phillips and Sutherland, 1985)

$$V_s = 8.5\ V_* \left[1 - \frac{V_{*c}}{V_*} \right]^{\frac{1}{2}} \tag{5.5}$$

where V_* = bed shear velocity given by $\sqrt{(ghS)}$; g = acceleration due to gravity; h = water depth (calculated as the mean of adjacent node values); S = water surface slope (calculated from water surface elevations at adjacent nodes); V_{*c} = critical bed shear velocity from the Shields curve (see Appendix B).

The Phillips and Sutherland sediment velocity equation is based on the sediment velocity equation of Engelund and Fredsøe (1976). Engelund and Fredsøe derived their equation from a simplified consideration of forces acting on a sediment particle with empirical factors derived from a limited data set. Thus equation 5.5 cannot be relied on to yield accurate values of sediment velocities for conditions different from those in the experiments used to determine the empirical factors. However, it is expected to yield better results than the more common alternative of assuming that the sediment velocity equals the flow velocity, irrespective of the sediment size. In the SHESED program the function is constrained to give sediment velocities less than or equal to the flow velocity.

5.4.4 Overland Flow Sediment Input

The overland flow sediment input to node i, g_{si}, will be a known quantity as the hillslope transport calculations precede the channel calculations for the current time step. As the overland flow grid rectangles are aligned with channel links (not nodes), the overland flow sediment input to a node region will consist of half the sediment input from adjacent grid rectangles, i.e.

$$g_{si} = 0.25\ \Delta x_k \left[(gr_k^{n+1} + gr_k^n) + (gl_k^{n+1} + gl_k^n) \right]$$

$$+\ 0.25\ \Delta x_{k+1} \left[(gr_{k+1}^{n+1} + gr_{k+1}^n) + (gl_{k+1}^{n+1} + gl_{k+1}^n) \right] \qquad (5.6)$$

where gr and gl = overland flow sediment inputs from the right and left hand side banks respectively.

5.4.5 Solution Procedure for the Simple Case

Downstream sediment behaviour has no influence on upstream sediment behaviour other than through the effect on hydraulic variables, which is not in any case accounted for in SHESED (see

Section 5.6). Therefore, if calculations start at the top of the fluvial system (usually the node with the highest elevation) and proceed in a downstream direction, the four-point finite difference scheme can be solved explicitly. With reference to equation 5.4 and with known initial and boundary conditions, there remain two unknowns: G_{k+1}^{n+1} and Δz_i. The final stage of the solution is based on the concept that the water will transport all available sediment up to the point where the sediment load equals the transport capacity for the particular sediment size fraction. One of two approaches is used, depending on the size of the sediment particles.

For silt and clay size particles the flow can usually transport all available sediment and therefore the sediment transport capacity is assumed to be infinite. Equation 5.4 can be rearranged to obtain G_{k+1}^{n+1} directly

$$G_{k+1}^{n+1} = \left[g_{si} - \frac{1}{\Delta t} \left[-\phi \left(\frac{G}{V_s}\right)_{k+1}^{n} + (1 - \phi) \left[\left(\frac{G}{V_s}\right)_{k}^{n+1} - \left(\frac{G}{V_s}\right)_{k}^{n} \right] \right] \right.$$

$$\left. - (1 - \lambda_i) W_i \frac{\Delta z_i}{\Delta t} - \frac{1}{\Delta x} \left[-\theta G_k^{n+1} + (1 - \theta) (G_{k+1}^{n} - G_k^{n}) \right] \right]$$

$$/ \left[\frac{\theta}{\Delta x} + \frac{\phi}{\Delta t \ V_{s\,k+1}^{n+1}} \right] \qquad (5.7)$$

where Δz_i = depth of available sediment in the channel bed. The only occasion when equation 5.7 does not apply for silt and clay size particles is when there is no water flowing out of the node region (i.e. $Q_{k+1}^{n+1} = 0$). In this case the sediment input to the node region is deposited at the node (the value of Δz_i is calculated by equation 5.8 with G_{k+1}^{n+1} set to zero).

For sediment particles larger than 0.062 mm the transport capacity of the flow is calculated using one of the sediment transport capacity equations introduced earlier (see Section 5.2). The hydraulic variables defined at k+1,n+1 are used in its determination. The solution technique then involves rearranging equation 5.4 to calculate the potential Δz_i value if transport is at capacity

$$\Delta z_i = \left[g_{si} - \frac{1}{\Delta t} \left[\phi\left[\left(\frac{G}{V_s}\right)_{k+1}^{n+1} - \left(\frac{G}{V_s}\right)_{k+1}^{n}\right] + (1 - \phi)\left[\left(\frac{G}{V_s}\right)_{k}^{n+1} - \left(\frac{G}{V_s}\right)_{k}^{n}\right]\right] \right.$$

$$\left. - \frac{1}{\Delta x} \left[\theta \left(G_{k+1}^{n+1} - G_{k}^{n+1}\right) + (1 - \theta)\left(G_{k+1}^{n} - G_{k}^{n}\right) \right] \right]$$

$$/ \left[\frac{(1 - \lambda_i)\, W_i}{\Delta t} \right] \tag{5.8}$$

with G_{k+1}^{n+1} set equal to the sediment transport capacity. If deposition is predicted (Δz_i positive) or a depth of scour is predicted which is less than the depth of available sediment in the channel bed (i.e. excess of sediment supply), then the sediment transport rate G_{k+1}^{n+1} is equal to the sediment transport capacity and the predicted Δz_i is as calculated from equation 5.8. However, if equation 5.8 predicts more scour than there is available sediment in the channel bed (i.e. supply limited), then equation 5.7 is used to calculate the transport rate, G_{k+1}^{n+1}, with Δz_i set equal to the depth of available sediment in the channel bed. Thus the unknowns G_{k+1}^{n+1} and Δz_i are determined and calculations are then repeated for the next node downstream.

5.4.6 Extension of the Method to Routing by Size Fraction

The extension of the method to routing by size fraction involves dividing the sediment size distribution into a number of size fractions and then writing the sediment continuity equation for each size fraction

$$\frac{\partial(G_m/V_{s,m})}{\partial t} + (1 - \lambda)\, W\, \frac{\partial z_m}{\partial t} + \frac{\partial G_m}{\partial x} = g_{sm} \tag{5.9}$$

where m = size fraction index.

The calculation procedure described in Section 5.4.5 for uniform sediment is simply repeated for each size fraction in turn, before moving to the next link downstream. Note that if the transport capacity equation is not formulated for calculations by size fraction (e.g. the Engelund-Hansen equation), then the transport capacity is calculated from the transport equation using the current size fraction diameter and density and multiplied by the proportion of the size fraction in the potential sediment load. The potential sediment load consists of sediment entering the node region from overland flow and upstream inflow, in addition to available sediment in the channel bed, but excludes sediment of silt and clay sizes.

This procedure relies on the sediment transport capacity equation to account for interparticle effects on the initiation of motion and transport rate of a given size fraction in a sediment mixture.

5.4.7 Extension of the Method to Complex River Systems

The extension of the above procedure to a complete river system involves allowing for two, three or four river links to join at a node. However, as SHESED is restricted to non-bifurcating systems, water and therefore sediment can move away from the node in only one of these links. The changes made to the procedure described above involved redefining the terms with the subscript k (denoting the upstream link) to refer to the summation of the effects of all inflows to the node. For example, for a node with four links joining: $G_k = G_{k1} + G_{k2} + G_{k3}$, where G_{k1}, G_{k2} and G_{k3} are the sediment transport rates for the three sediment inflows to the node. Also, the calculation sequence is adjusted so that before starting calculations for a specific node, calculations for all nodes upstream from this node (including branches) have already been carried out.

5.4.8 Initial and Boundary Conditions

The solution of the sediment continuity equation requires that initial sediment transport rates are given for all links and that upstream boundary data are given. The specification of the initial and boundary conditions depend on the application and on the availability of data. For an event-based simulation in a small catchment, the initial sediment transport rates in all channel links may well be zero and the upstream inflows to the channel system (the boundary conditions) will also be zero. By contrast, for analysis of a river reach, measured data on the initial sediment transport rates may be necessary, along with the time series of sediment inflows at the upstream boundary. For initial and boundary data the size distribution of the sediment load also has to be given.

5.4.9 Numerical Behaviour

The behaviour of the numerical solution depends on the particle size, the relative importance of the processes occurring, the values of the time and space weighting factors and the value of the Courant number ($V_s\Delta t/\Delta x$). The solution is well-behaved for routing particles of sand size and larger. However, when silt and clay particles are being routed with no bed interaction, then equation 5.3 reduces to a pure convection equation and numerical diffusion can become significant if the time and space weighting factors are not equal to 0.5. To restrict this numerical diffusion, the time step should then be selected so as to produce a Courant number near to unity. The space and time weighting factors are set to values between 0.5 and 0.75 to introduce some light damping to eliminate long term instability; both factors were set to 0.55 for the examples presented herein. As for overland transport, near the start and end of an event, the numerical solution of the sediment continuity equation may produce physically meaningless negative concentrations, the cause of which are discussed in Appendix D. These negative concentrations are of minor significance in terms of the mass of sediment involved, and are a characteristic common to a number of finite difference schemes (e.g. see Holly and Preissmann, 1977). However they cannot be accommodated within the explicit solution technique used in SHESED. To overcome this problem the weighting factors are temporarily increased to 1.0 and the calculations repeated for the offending size fraction. Alternatives to this approach were discussed in Section 4.5.5.

5.5 BED ARMOURING

5.5.1 Active and Parent Layer Concept

The particle size distribution of the bed material is important for modelling selective entrainment and the development of armour layers. It is possible to model these effects if sediment is routed by size fraction and if a variation in particle size distribution is allowed for in the vertical within the bed material layer. To keep complexity and computational cost down, SHESED considers only two bed material layers in the vertical. The thickness of the upper or active layer is set equal to the D_{99} size of the lower or parent layer particle size distribution (D_{99} = sediment diameter for which 99% of the material is finer). The choice of the D_{99} size as the active layer thickness is somewhat arbitrary, although similar upper layer thicknesses are used in other models, and field and laboratory studies have reported armour layer thicknesses of about the maximum particle size present. In the current version of SHESED, the active depth is not adjusted if the D_{99} size of the parent layer changes during the simulation. The SHESED program offers the possibility of adjusting the depth of the active layer through a calibration factor; however, this has not been used in any simulations to date. If the depth of bed material is less than the D_{99} size, then the active depth is set equal to the bed material depth and the parent layer ceases to exist.

The active layer can be thought of as the depth of bed material that the water acts upon and treats as a potential source of transportable material. As the smaller particles are selectively entrained from the active layer, they are replaced from below by particles with the parent layer size distribution. Those sizes too large to move eventually dominate the surface layer distribution, protecting the lower layer from further erosion. Over time, this leads to a reduction in sediment transport rate for a constant flow depth and velocity. In SHESED the bed is assumed to be fully armoured (i.e. no more scour can occur for the current hydraulic and sediment conditions) when more than 99.9% of the sediment in the active layer have diameters which are bigger than the critical diameter calculated from the Shields curve (Appendix B).

The concept of the active and parent layers is introduced into the sediment routing scheme, as described in Section 5.4.5, by defining the depth of available sediment for size fraction m as equal to the product of the active layer depth and the proportion of size fraction m in the active layer. The active and parent layer sediment size distributions are updated at the end of each time step using the algorithms presented in Appendix C.

5.5.2 Test of the Armouring Algorithms

Data from an experiment by Mosconi (1988) were used to verify the ability of SHESED to simulate the trend of decreasing sediment transport rates with time caused by the armouring process. Mosconi used a 27.4 m long by 0.91 m wide recirculating flume to study the evolution of armour layers for steady uniform flow. The bed material was in the size range 0.06 mm to 8 mm, with D_{16} = 0.34 mm, D_{50} = 0.77 mm, and D_{84} = 3.90 mm. Figure 5.1 shows a comparison of the variation of simulated and measured sediment transport rates over a 31-day period for a run with water discharge = 0.0482 $m^3 s^{-1}$, depth = 0.1 m, velocity = 0.53 m s^{-1}, and slope = 0.00164. The only calibration in this simulation involved choosing the Ackers-White-Day equation to calculate sediment transport capacity; it produced a closer match of simulated to measured transport rates than did the Engelund-Hansen equation or the Ackers-White equation without the Day modification. (Neither the transport equation's parameters nor the active layer depth were adjusted.) As the initial simulated transport rate calculated by the Ackers-White-Day equation was nearly twice the initial measured rate, dimensionless transport rates (defined here as transport rate divided by maximum transport rate) are used in the figure.

5.6 DISCUSSION

While it is recognised that the SHESED channel sub-component does not contain all the advanced features of current river sediment routing models, SHESED does represent a significant improvement, in terms of processes modelled, on most sediment yield models. Because of the enhanced consideration of channel processes, it is hoped that SHESED will be used in studies which look at the within channel effects of eroded soil, in addition to studies which require only predictions of sediment yield.

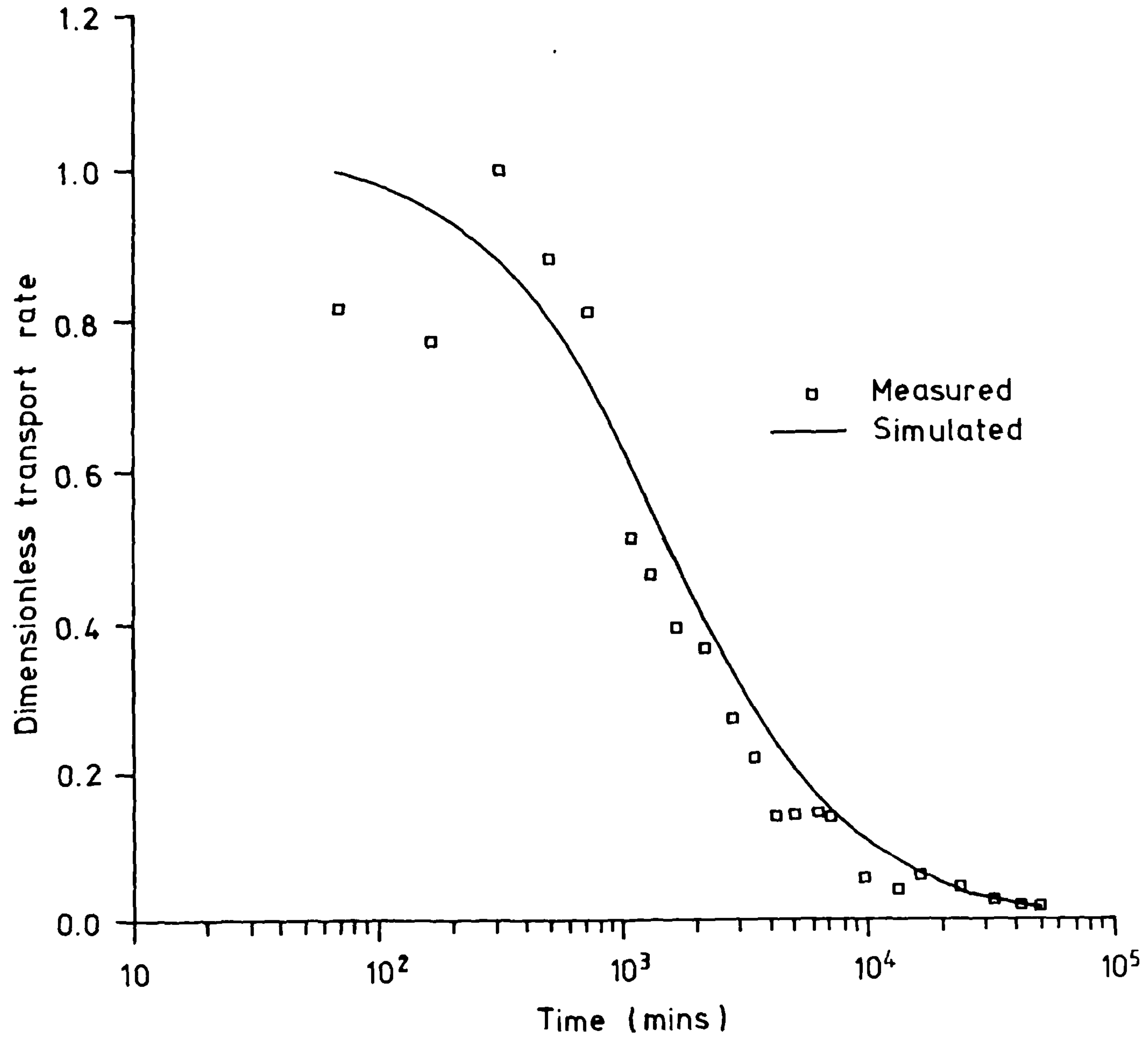

Fig. 5.1 Simulated and measured dimensionless sediment transport rates for run 3-4, reach 3 of Mosconi (1988).

However, it is important to recognise the limitations of the sub-component and therefore, in the remainder of this section, the simplifications and areas of uncertainty in the SHESED channel sub-component are discussed.

Perhaps the main simplification is the neglect of feedback from the sediment model to the water routing model; changes in river bed elevation calculated by SHESED have no effect on the hydraulic variables as calculated by the channel flow component of the SHE. Therefore poor results may occur when severe scour or deposition have a significant effect on the hydraulic conditions. The reasons for neglecting the feedback from SHESED to the SHE are that its inclusion would greatly increase the complexity of the calibration process for both the SHE and SHESED and, more importantly, that the spatial extent of severe erosion and deposition may well be too localised to be significant at the scale of the SHE's grid network. (SHESED was not designed as a detailed alluvial channel model and, for example, should not be used for predicting localised scour and deposition around river structures.)

The SHESED armouring procedure, as presented in Section 5.5, has a number of problems associated with it. Perhaps the most serious is that, in certain circumstances, the erosion rate will be a function of the computational time step. For example, consider the case when clear water flowing into an alluvial river reach has a very high transport capacity and can transport all the grain sizes present in the river bed. During one time step the maximum depth of erosion is equal to the active depth (which, in SHESED, is equal to the D_{99} size of the parent bed material layer). During a time step Δt the depth of erosion will equal the active depth, AD. If the time step is now reduced to $0.1\Delta t$, the depth of erosion over the same length of time, Δt, will be 10AD. This suggests that the active depth should be related to the time step, e.g. $AD \propto D_{99}\Delta t$. The physical significance of this is that over a large time period the flow can sort through a greater depth of bed material. This second approach fails to work, however, when the case of a fully armoured bed is considered. Here, the simulated armour layer depth will be a function of the time step, whereas the armour layer depth has been frequently reported to be of a thickness comparable to the largest sediment particle present. Further, it seems reasonable to make the active depth also a function of flow conditions, as a more aggressive flow should be able to sort through a greater depth of bed material (although to some extent the dependence of the transport capacity on the flow conditions will account for this). The armouring procedure of SHESED, and that of most other models, can also be criticised on the grounds that the bed material properties (e.g. the size distribution in the active layer) used during a time step are those determined at the end of the previous time step - a kind of backward difference approach. The influence of the possible numerical errors from this approximation have not been investigated.

From the above discussion of modelling armouring, it is clear that, although improvements on the procedure used in SHESED are available, the active layer concept still requires much development. Recent additions to the literature on modelling armour layers include Lee and Odgaard (1986), Park and Jain (1987) and Willetts et al. (1987); all three papers report different variations on the active layer concept but none of the proposed methods can successfully deal with all the possible armouring/sorting situations occurring in alluvial rivers.

Deposition of sediment in the channel is dealt with in a similar way as deposition on the hillslope (Section 4.6.2), that is deposition is predicted only when the transport capacity is less than the sediment load for a particular size fraction. This corresponds to a positive value of Δz in equation 5.8. No account is taken of the finite time it takes for a particle to fall out of suspension. Deposited sediment is added to the active bed layer, and the active and parent layer size distributions updated using the procedure presented in Appendix C.

Chapters 4 and 5 have provided a detailed description of the process equations used in SHESED, and have described the tests of the process equations. More complete test applications of SHESED are described in the next three chapters. Chapter 6 describes the applications in the Reynolds Creek catchment, Idaho, which form the major test of SHESED. Transfer of parameter values between different spatial scales and the effects of a range of surface conditions on the sediment response are investigated. Chapter 7 describes the testing of the hillslope sub-component for the ISU catchments, Iowa, while Chapter 8 describes the application of the channel sub-component to the East Fork River, Wyoming. These last two applications provide the opportunity for comparing SHESED results with those obtained by existing models.

CHAPTER 6 - APPLICATION OF SHESED TO REYNOLDS CREEK RAINFALL SIMULATOR PLOTS AND SUB-CATCHMENT

6.1 INTRODUCTION

A major problem in the application of physically-based soil erosion and sediment yield models is the representation of the soil's ability to withstand erosion. In SHESED the soil's resistance to detachment is quantified by two detachment coefficients: K_R for raindrop soil detachment and K_F for overland flow soil detachment. At present these coefficients cannot be calculated from soil properties and therefore their evaluation must depend on calibration with measured detachment or net erosion data. In the absence of other effects, this is best done at a small spatial scale since data collection is then easiest and the influences of other processes are at their least. However, it has yet to be shown that detachment coefficients thus determined remain representative at significantly larger scales. For example, it is possible that at the larger scale the detachment coefficient will be used, not only as an expression of the soil's resistance to detachment, but also to represent the effects of processes that are either poorly represented by the process equations in SHESED, or not included in the model at all. In order to examine the problem of parameter transferability between different spatial scales, SHESED was calibrated at a rainfall simulator plot scale (32.54 m^2) and then applied at a sub-catchment scale of 1 ha, using data from the semi-arid Reynolds Creek rangeland research catchment. The rainfall simulator plot data also allowed an evaluation of the effects of different land management options on the detachment coefficients.

6.2 DESCRIPTION OF THE STUDY AREA

The 234-km^2 Reynolds Creek catchment (Fig. 6.1) is located near Boise, in south west Idaho, USA, and is operated by the Northwest Watershed Research Center (NWWRC) of the US Department of Agriculture's Agricultural Research Service. In the catchment the elevation ranges between 1100 and 2250 m with average annual precipitation from 250 to 1100 mm. Vegetation varies from sparse sagebrush and desert-type plants at low elevations to dense sagebrush associated with grass, forb, and forest species at high elevations. Land use is primarily cattle grazing, with some irrigated farming close to the main channel.

From a number of instrumented sub-catchments within the main basin, the Flats area was chosen for an application of the SHESED model as suitable data were available for the 1-ha Flats sub-catchment (Fig. 6.2), and for rainfall simulator plots (32.54 m^2) lying adjacent to the sub-catchment. At these sites, elevation is about 1190 m, average annual precipitation is about 250 mm, the predominant vegetation is Shadscale (*Atriplex confertifolia*), Cheatgrass (*Bromus tectorum*) and Bottlebrush squirreltail (*Sitanion hystrix*), the soil is Nannyton Loam (fine, loamy, mixed, mesic typic haplargids) and the land use is cattle grazing. Phreatic surface levels are deep and surface runoff occurs by excess of rainfall over infiltration.

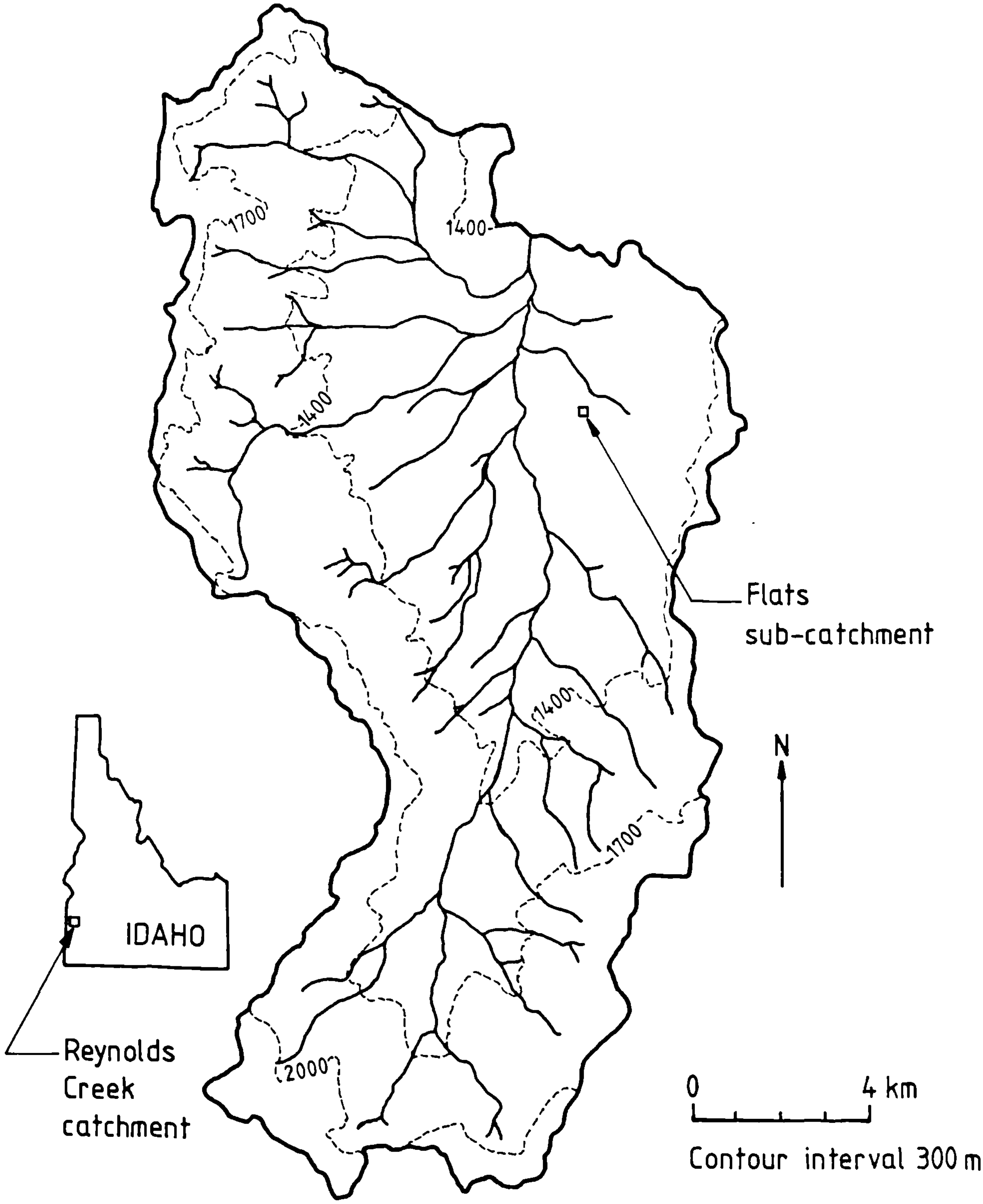

Fig. 6.1 Map of Reynolds Creek catchment. (After Johnson and Hansen, 1976.)

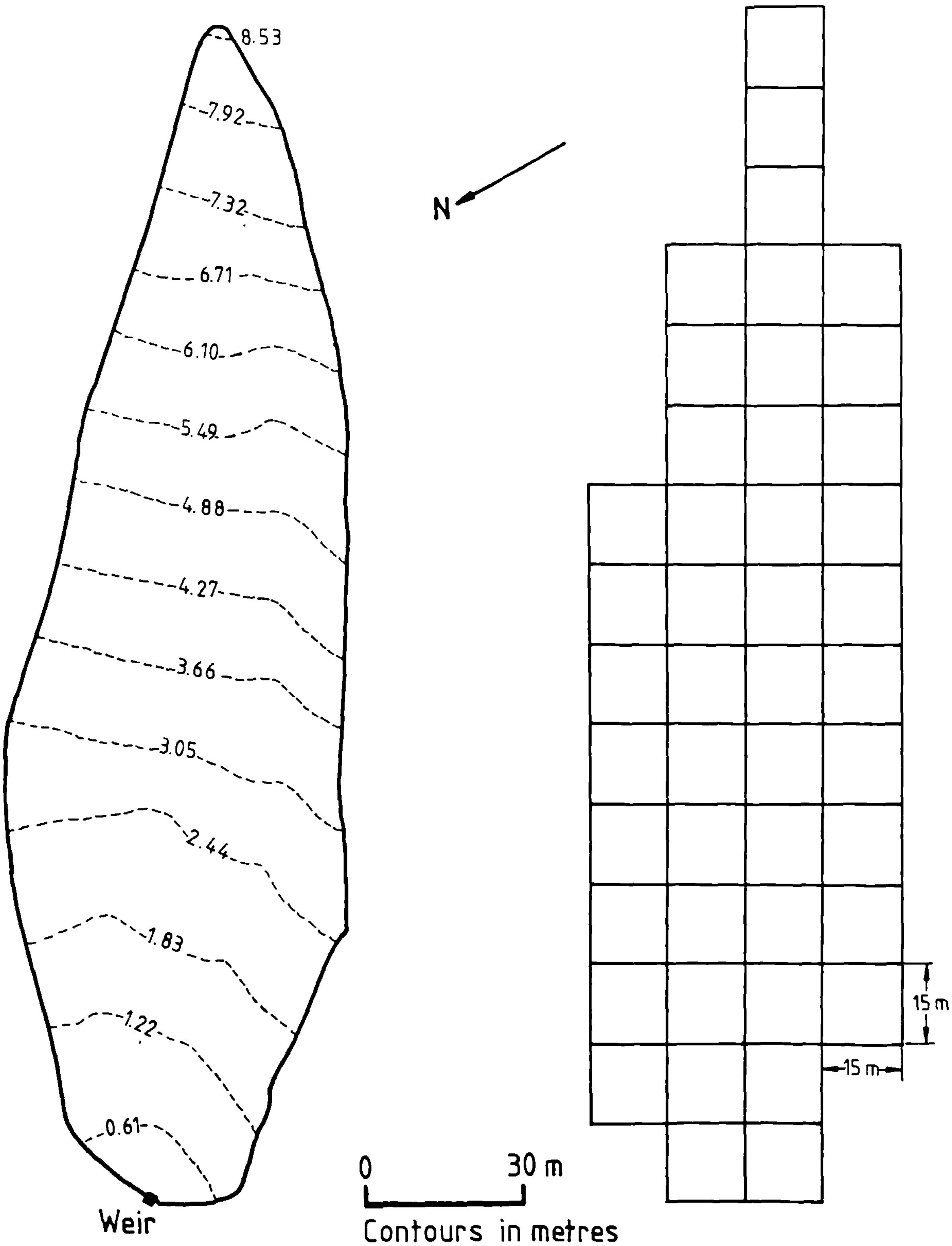

(a) Flats sub-catchment (b) SHE segmentation

Fig. 6.2 Map of the Flats sub-catchment with the SHE model segmentation.

Data sets were assembled during a two week period at Boise, Idaho, in August 1987. Data were obtained from computer files, chart recordings, scientific papers, reports and maps. A qualitative understanding of the hydrological and sediment yield responses, important in calibrating the SHE and SHESED and for interpreting simulation results, was gained from detailed discussions with NWWRC staff and from a visit to the catchment. Some of the data are available in: "Reynolds Creek cooperative watershed study. Volumes I (summary report), II (comprehensive report), and III (data and bibliography)", available from the Northwest Watershed Research Center, USDA-ARS, 270 S. Orchard, Boise, Idaho, USA.

6.3 RAINFALL SIMULATOR EXPERIMENTAL PROCEDURE

The rainfall simulator plot experiments were designed to study the applicability of the Universal Soil Loss Equation, USLE, to rangeland conditions. The following details of the experimental procedure are based on the published report of these experiments (Johnson et al., 1984).

Seven pairs of plots, 3.05 m wide and 10.67 m long, were set up in 1982 in the Flats area just outside the Flats sub-catchment. Each pair of plots had a different combination of slope and surface treatment as shown in Table 6.1.

Table 6.1 Summary of the rainfall simulator runs

Plot [1]	Date 1982	Slope (%)	Rain (mm)	Cover (%) [2]	Soil moisture % [3]	Runoff (mm)	Soil loss (t ha^{-1})
FTR3	19/7	3.356	114	0	14	99	11.96
FTL3	19/7	3.908	113	0	14	93	10.40
FTR9	8/7	8.492	113	0	16	98	22.18
FTL9	8/7	9.116	115	0	16	103	30.37
FKR3	12/8	3.356	119	0	12	99	15.36
FKL3	12/8	3.908	113	0	12	96	15.65
FBR3	11/8	4.091	121	75	12	38	0.54
FBL3	11/8	4.272	117	76	12	35	0.49
FBR9	12/7	8.492	118	94	15	26	0.41
FBL9	12/7	8.761	118	81	15	45	1.71
FGR3	14/7	3.085	109	86	15	27	0.26
FGL3	14/7	3.360	113	87	15	32	0.46
FUR3	15/7	3.085	101	94	15	4.4	0.03
FUL3	15/7	3.360	106	92	15	3.2	0.04

Notes: [1] 'F' denotes Flats, 'T' tilled plot, 'K' tilled twice, 'B' clipped bare, 'G' grazed, 'U' ungrazed, 'R' right plot, 'L' left plot, '3'% nominal slope and '9'% nominal slope. [2] Cover consists of shrubs, grass, rocks, moss and litter. [3] Initial soil moisture content by volume.

The following treatments were applied to the plots:

(1) Tilled - At least two weeks before simulator runs, all vegetation was cut off and dug out, and the plots were rototilled, raked and levelled in about 3 cm deep stages until the soil was well pulverized and free of root clumps and all litter except fine organic material. The soils were then restored to their original bulk densities by either natural settling or light foot trampling.

(2) Clipped - All vegetation was cut off at the ground surface and the plot was lightly raked to remove plant fragments without seriously disturbing the soil and surface rocks.

(3) Grazed - Moderate seasonal cattle grazing, consistent with the past 20 years of use, was allowed before simulator runs were made.

(4) Ungrazed - Areas were fenced and not grazed by livestock for about 10 years.

A rotating-boom rainfall simulator (Swanson, 1965) was used to apply water on two plots simultaneously at approximately 60 mm h^{-1}. The following sequence of simulated rainfall was applied to all the plots: (1) dry run - initial 60-minute run under initially dry soil conditions; (2) wet run - 30-minute run about 24 hours after completion of the dry run; (3) very wet run - 30-minute run 30 minutes after completion of the wet run. Owing to wind and operational problems the rate at which rain reached the plots was less than stated above, and the total amounts are as shown in Table 6.1.

6.4 AVAILABILITY OF DATA

6.4.1 Rainfall Simulator Plots

The high quality data available for the controlled conditions of the plot experiments included percentage cover, surface slope, initial soil moisture content, rainfall input, potential evaporation, some soil property data and water and sediment outlet discharges. The water discharge was obtained from weighing samples of water collected over a known time period (10 to 20 s) and pint bottles were used to collect sediment samples for laboratory analysis. Table 6.1 shows the measured total rainfall input, surface slope, percentage cover and initial soil moisture contents for the 14 plots. The D_{50} size of the soil was 0.075 mm. The potential evaporation ranged from 0.06 to 0.80 mm h^{-1}. The most important missing data were the soil's saturated hydraulic conductivity and data to determine the Averjanov coefficient (that is the coefficient n in the equation $K(\theta)/K_{sat} = [(\theta - \theta_r)/(\theta_s - \theta_r)]^n$, where $K(\theta)$ = hydraulic conductivity at a soil moisture content of θ; K_{sat} = saturated hydraulic conductivity; θ, θ_r and θ_s = actual, residual and saturated moisture contents respectively). However, infiltration experiments, as reported by Devaurs and Gifford (1984), had been carried out in the Flats area one year previous to the soil erosion studies. The mean final 30-minute infiltration rates from these experiments were therefore assumed to be approximations to the saturated hydraulic conductivity (see Table 6.2).

Table 6.2 Final infiltration rates from Devaurs and Gifford (1984)

Site condition	Slope (%)	Rainfall (mm h^{-1})	Mean final 30-minute infiltration (m day^{-1}) (± standard deviation)
Flats grazed	3	63.5	0.60 ± 0.24
Flats ungrazed	3	63.5	0.96 ± 0.24
Flats tilled	9	63.5	0.41 ± 0.05
Flats tilled	3	63.5	0.31 ± 0.07
Flats tilled	3	127.0	0.31 ± 0.14

6.4.2 Flats Sub-catchment

For the Flats sub-catchment, a data base collected over some 20 years yielded only four summer natural rainfall events with good sediment yield records, indicative of the problems of sampling sediment yield in an area of low and spatially varying rainfall. Two of the events are isolated (1984 and 1985) while two (in 1983) form a sequence over three days. Data quality is poorer than for the simulator plots and in particular the correlation in timing and rate between rainfall and runoff is not always apparent (see Figs. 6.11 to 6.14). It is uncertain whether this reflects the actual rainfall/runoff relationship, problems with the runoff recorder or the distance of about 180 m separating the sub-catchment from the rain gauge (used to supply the rainfall record). The problems in timing are most likely caused by the use of different charts (with different clocks) for runoff and rainfall and by the fact that the ink lines on the runoff charts are up to 20 minutes wide (personal communication from K.R. Cooley, NWWRC, Boise, Idaho).

The sediment record for the storms consists of concentrations from three stage samplers (activated early on the rising limb of the hydrograph) and deposits collected from a sediment detention tank. Thus the time-varying sediment discharge is not available, only the bulk yield. The total sediment yield for an event was estimated by multiplying the total water yield by the geometric mean of the three sediment concentration measurements, and then adding this to the deposited load from the detention tank. For the two 1983 events, though, the stage sampling bottles and detention tank were not emptied between the events, and therefore the yield for each event had to be estimated based on the ratios of water yields for each event. It is clear from the above discussion that there is much uncertainty in the calculated sediment yield values.

6.5 APPLICATION OF THE SHE TO THE RAINFALL SIMULATOR PLOTS

The calibration procedure involves first calibrating the SHE model for the runoff response and then calibrating the SHESED model for the sediment response (the SHESED applications to the plots are described in Section 6.6).

Each plot was modelled by a single grid rectangle with the three-event sequence simulated on a continuous basis over 26.5 hours. Antecedent soil moisture conditions were therefore required for the dry runs only, with the model determining the conditions for the wet and very wet runs. (No moisture measurements were made between the runs.) A computational time step of 0.6 minutes was used during the events, with this increased to 6 minutes between events. The simulations were found to be sensitive to the vertical distance step in the root zone and a small value of 1 cm was required.

The approach taken to calibrating a SHE model is not that of a 'blind' optimisation of parameters to produce the 'best fit', but of trying to find one set of physically realistic parameter values which can be used for a number of events which have similar conditions. A large volume of event data is available (14 plots each with three rainfall applications) and, if considered concurrently, would lead to a very complex calibration procedure. As the two grazed plots were to be used in the study of scale effects, it was decided to concentrate effort initially on the calibration for grazed conditions.

6.5.1 Calibration for Grazed Plots

Following a non-rigorous sensitivity analysis of the SHE hydrology model parameters which had not been measured, the most influential were found to be the saturated hydraulic conductivity, the Averjanov coefficient and the Strickler overland flow roughness coefficient. With the saturated hydraulic conductivity set to the value of 0.6 m day^{-1} as determined by Devaurs and Gifford (Table 6.2), the Averjanov coefficient was calibrated by minimising the total percentage error in simulated water yield for the two grazed plots combined. The resulting value of 15 is within the range given by Mualem (1978) for soil types comparable with that at Flats. The calibrated value of the Strickler coefficient was obtained by visually matching the shapes of the simulated and measured hydrographs. The resulting value of 10 (Manning's n value of 0.1), compares well with the value of 7.7 recommended by Engman (1986) for rangeland. Observed and simulated hydrographs are compared in Fig. 6.3, the percentage errors in water yield for the six individual hydrographs varying between -26.9% and +42.7% with a total error of -0.9%. Generally the hydrograph shapes are well simulated especially for the wet and very wet runs, indicating the ability of the model to simulate antecedent soil moisture conditions correctly. For the dry runs, simulated start of runoff is typically 10 minutes late and the hydrograph shape is less well simulated.

6.5.2 Calibration for Clipped Bare Plots

The values of the calibration parameters determined for the grazed plots were found to be equally applicable to the four plots clipped bare of vegetation. Observed and simulated hydrographs are compared in Figs. 6.4 and 6.5. The percentage errors in water yields for the twelve individual hydrographs vary between +218.9% and -37.3%, with total percentage error in water yield for the plots at 3% slope of -8.3% and that for the 9%

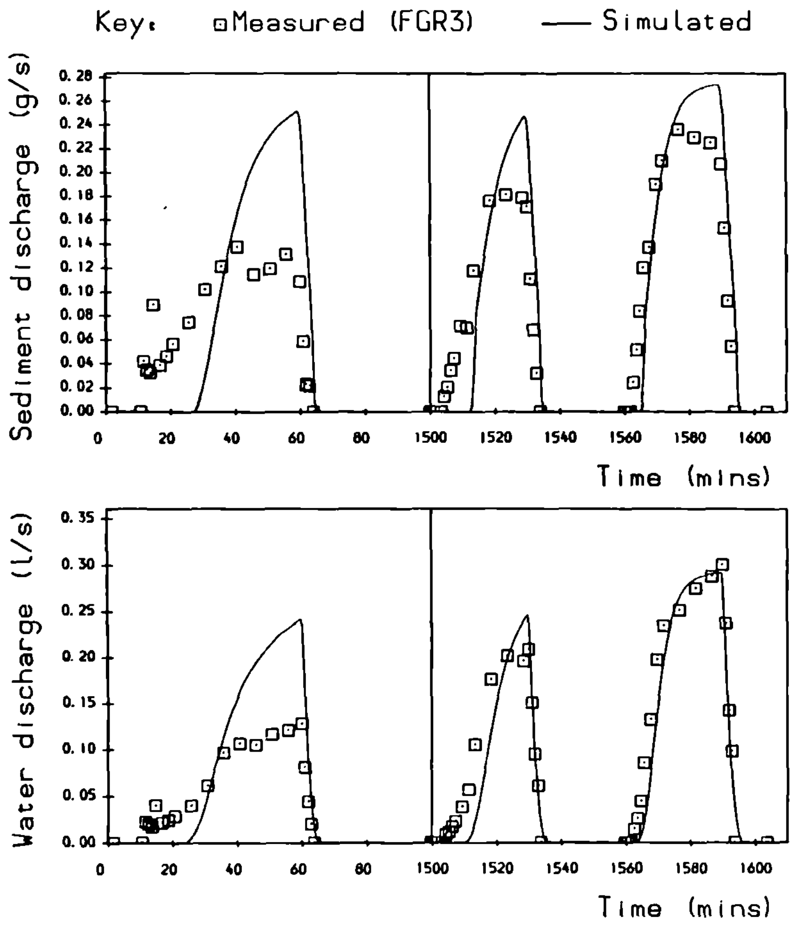

(a) Right hand plot

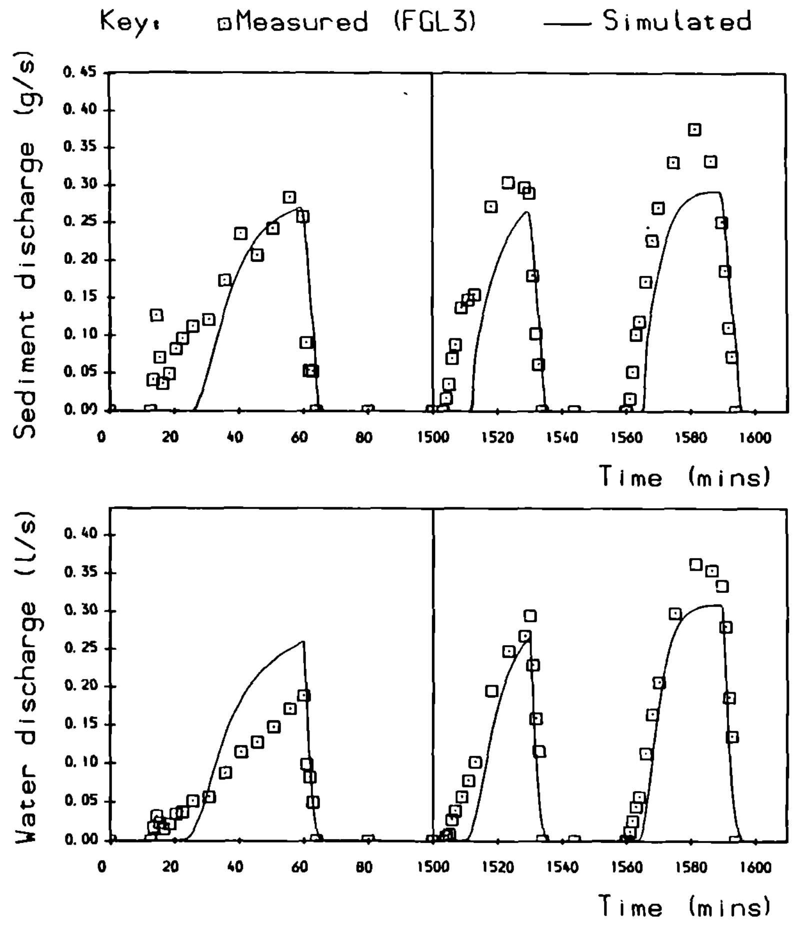

(b) Left hand plot

Fig. 6.3 Simulated and measured water and sediment discharges for the grazed rainfall simulator plots.

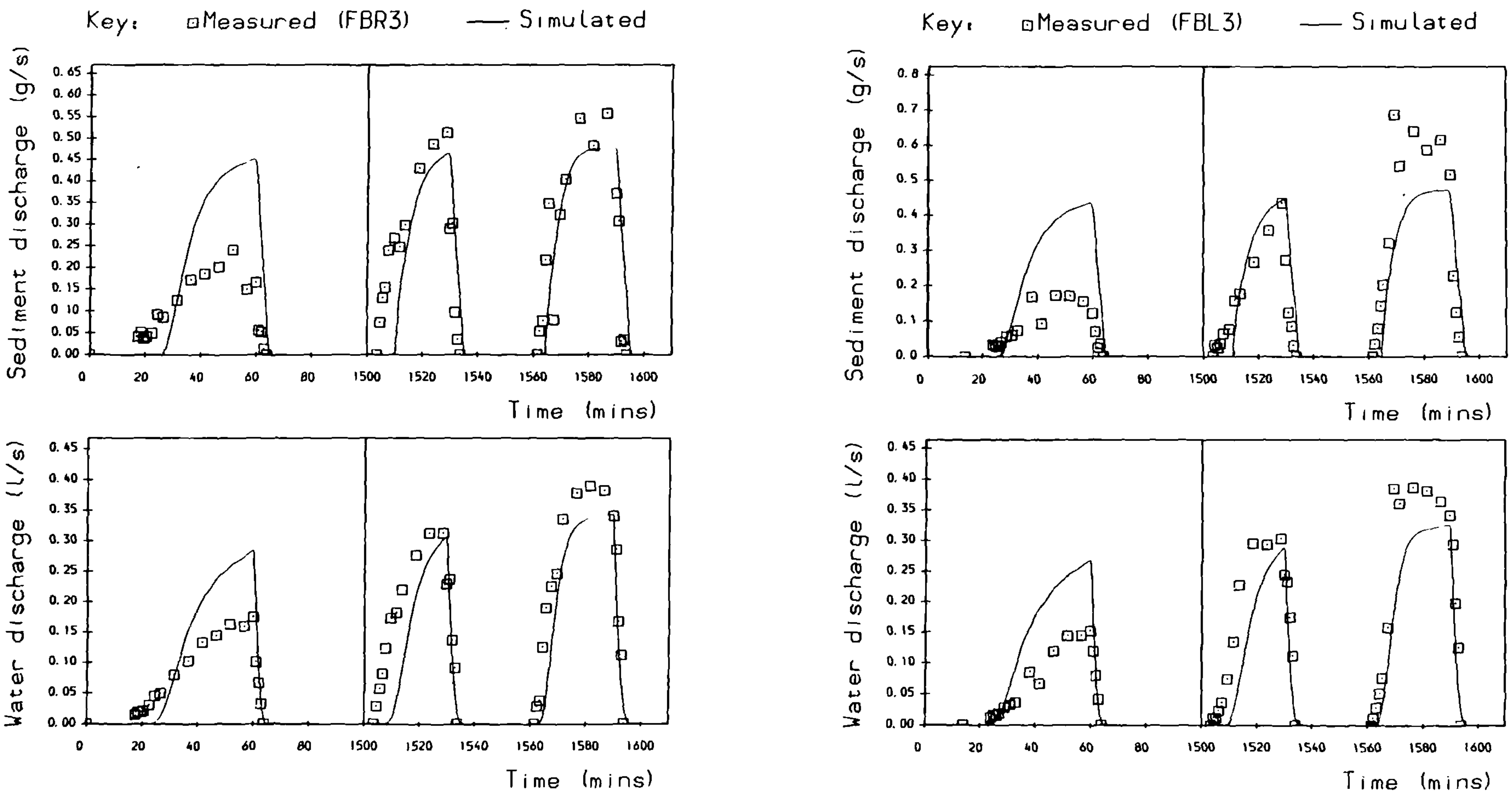

(a) Right hand plot

(b) Left hand plot

Fig. 6.4 Simulated and measured water and sediment discharges for the 3% slope clipped rainfall simulator plots.

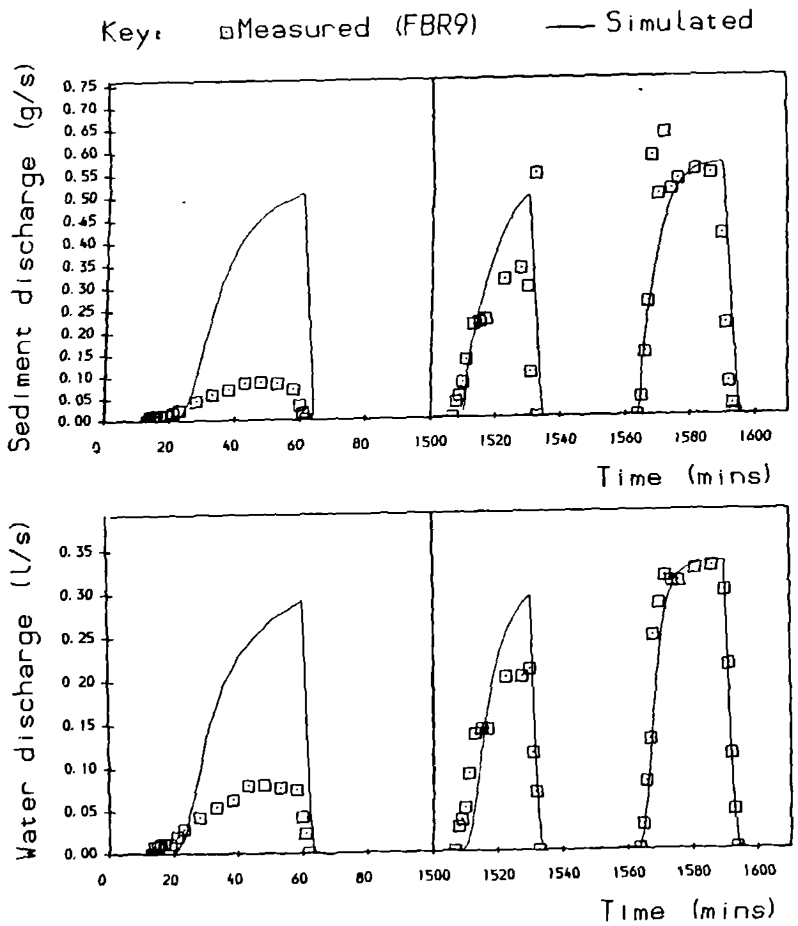

(a) Right hand plot

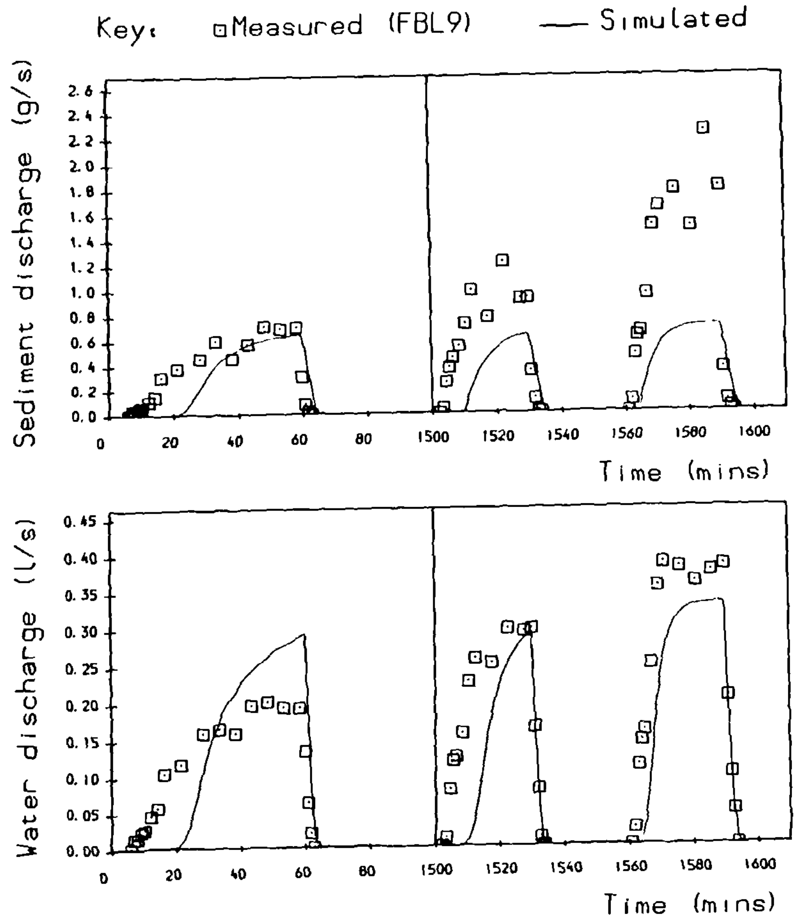

(b) Left hand plot

Fig. 6.5 Simulated and measured water and sediment discharges for the 9% slope clipped rainfall simulator plots.

slope of 3.4%. The very large overprediction of 218.9% is for the initial (dry) run on the FBR9 plot and contrasts with the very good fit of simulated and measured hydrographs for the final run in that sequence (-3.2% error) (see Fig. 6.5).

6.5.3 Calibration for Ungrazed Plots

For the ungrazed plots the Averjanov coefficient and the Strickler coefficient were kept at the values of 15 and 10 respectively, as determined for the grazed plots. The saturated hydraulic conductivity was adjusted by trial and error to minimise the total percentage error in the simulated water yield for the two plots combined; a value of 1.1 m day^{-1} was obtained. The higher saturated hydraulic conductivity value corresponds to the loose surface soil layer which had not been trampled by cattle. This value is slightly higher than the mean final infiltration rate determined by Devaurs and Gifford for ungrazed land at Flats, but is within the range of the mean ± standard deviation (see Table 6.2). The individual hydrographs are on the whole poorly simulated, with the SHE predicting runoff where none was measured while underestimating the runoff for other hydrographs (maximum underestimation of -60%, which represents an absolute error of 5 litres) (see Fig. 6.6). The total percentage error for all six individual hydrographs combined is -8.8%.

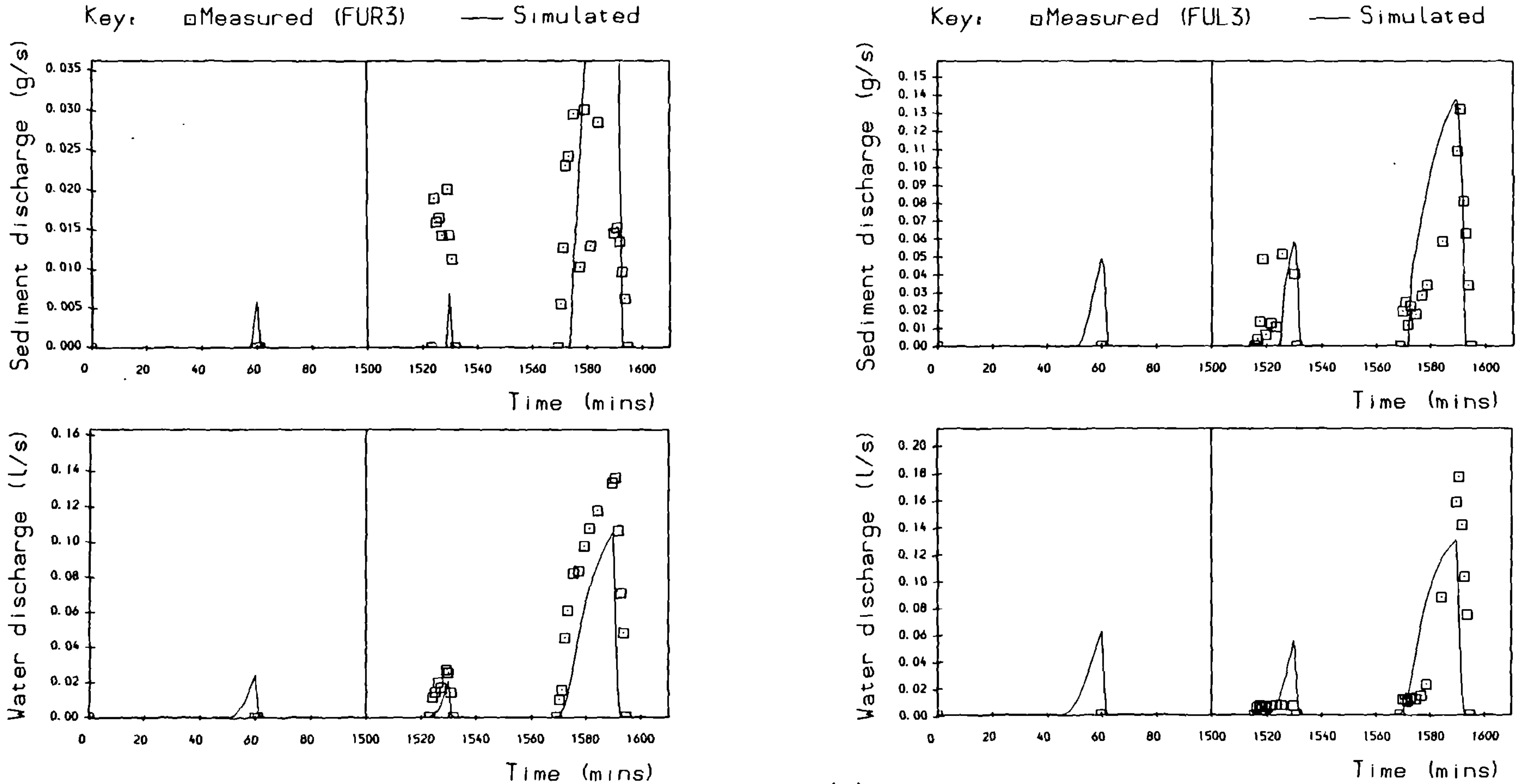

(a) Right hand plot (b) Left hand plot

Fig. 6.6 Simulated and measured water and sediment discharges for the ungrazed rainfall simulator plots.

6.5.4 Calibration for Tilled Plots

The trial and error based calibration for the tilled plots resulted in a saturated hydraulic conductivity of 0.01 m day^{-1} and a Strickler coefficient of 50 (Manning's coefficient 0.02). These values correspond to the pulverised and smooth conditions of the surface soil. The saturated hydraulic conductivity value is much less than that determined by Devaurs and Gifford (0.31 - 0.41 m day^{-1}, see Table 6.2) for tilled conditions; the reasons for this are not known although differences in tillage procedure may be the main cause. In an attempt to use higher saturated hydraulic conductivity values, the Averjanov coefficient was allowed to vary; however, the resulting simulated hydrographs matched poorly with the observed and therefore the Averjanov coefficient was kept at 15. The value of the Strickler coefficient is slightly higher than the values recommended for similar surface conditions by Engman (1986), but is within the range of values he presents. Observed and simulated hydrographs are compared in Figs. 6.7, 6.8 and 6.9. The percentage errors in water yield for the 18 individual hydrographs vary between -9.4% and 10.4%, with the total percentage errors of -0.4%, 1.8% and 1.2% for the tilled 3% slope, tilled twice 3% slope and tilled 9% slope plot pairs respectively.

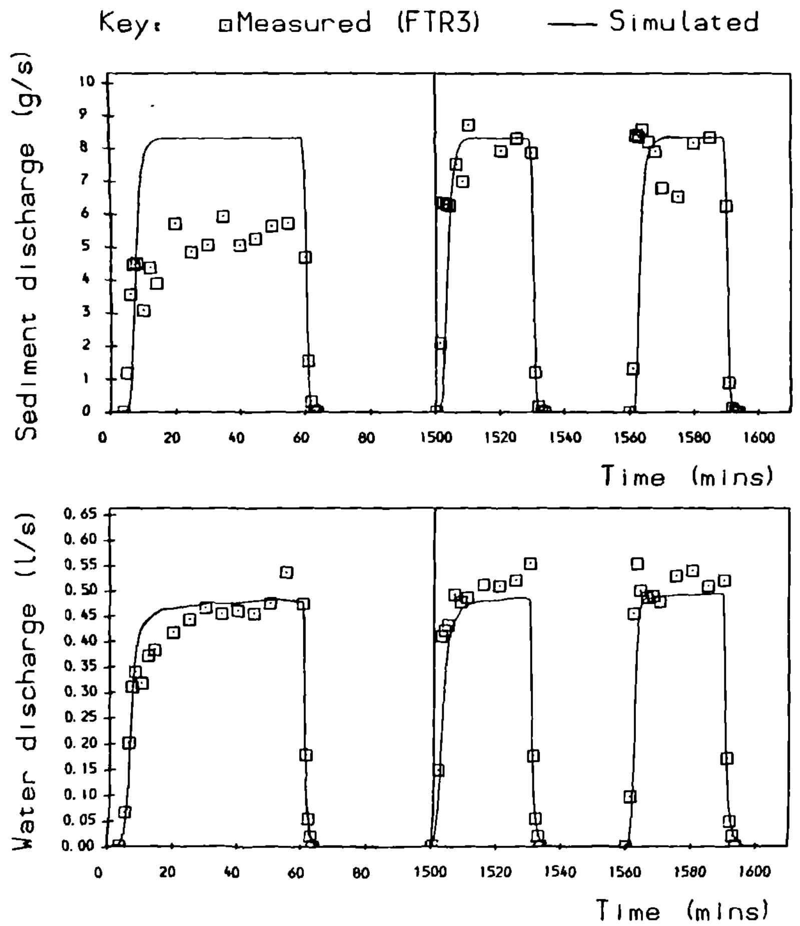

(a) Right hand plot

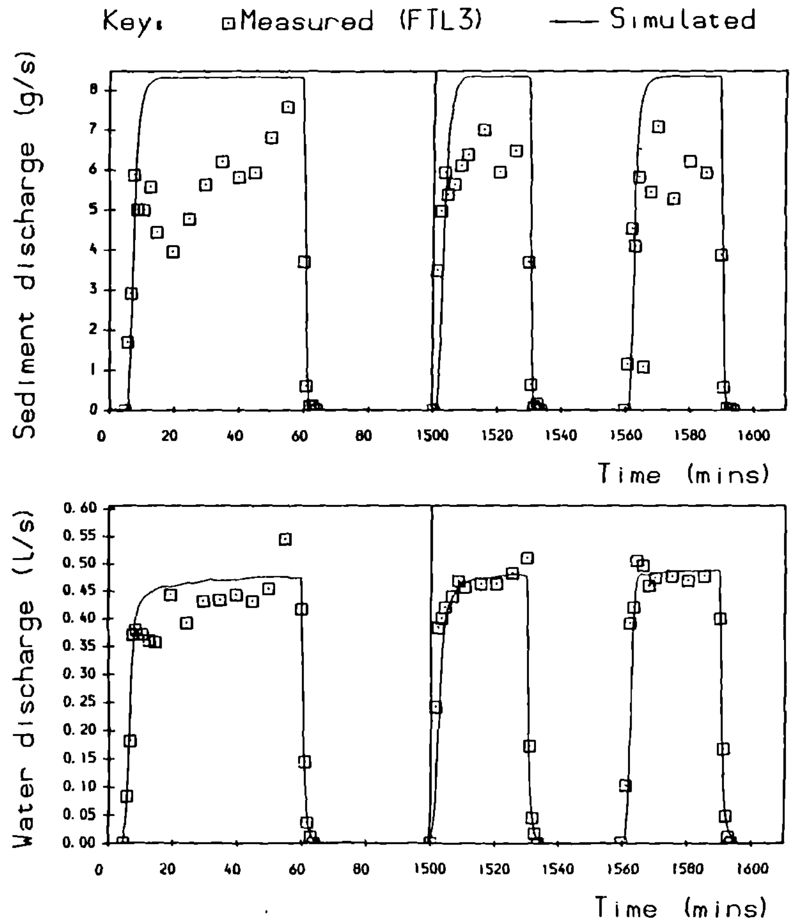

(b) Left hand plot

Fig. 6.7 Simulated and measured water and sediment discharges for the 3% slope tilled rainfall simulator plots.

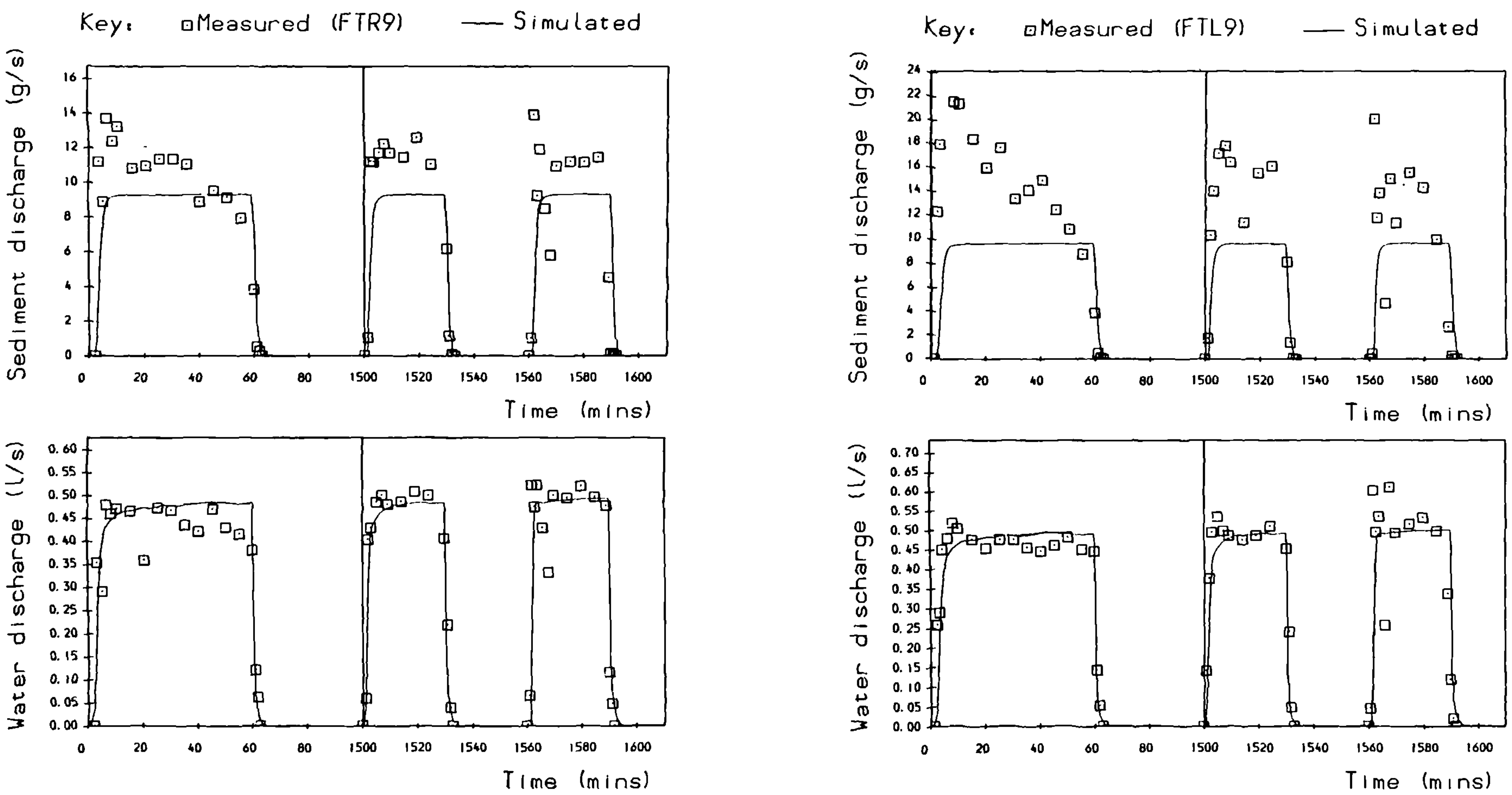

(a) Right hand plot

(b) Left hand plot

Fig. 6.8 Simulated and measured water and sediment discharges for the 9% slope tilled rainfall simulator plots.

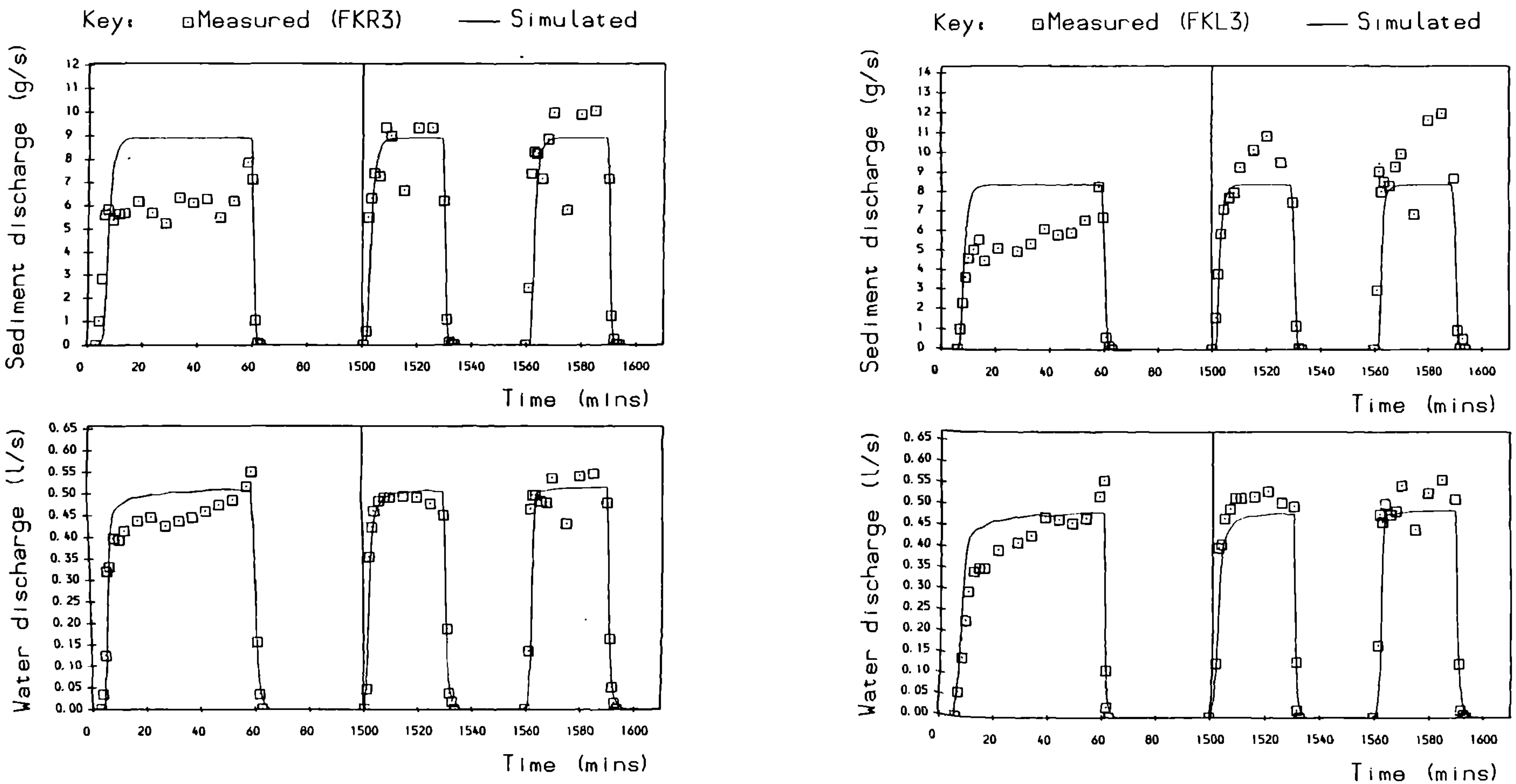

(a) Right hand plot

(b) Left hand plot

Fig. 6.9 Simulated and measured water and sediment discharges for the tilled twice rainfall simulator plots.

6.6 APPLICATION OF SHESED TO THE RAINFALL SIMULATOR PLOTS

As for the hydrology, each plot was modelled by a single grid rectangle with the three-event sequence simulated on a continuous basis over 26.5 hours. The computational time step used was 0.6 minutes during the events and 6 minutes between events.

The possible effects of leaf drip were ignored in this application of SHESED as the vegetation was of a limited height (<1 m) and because of the presence of localised ground cover underneath the canopy. As no data were available on the storm drop size distributions the default Marshall-Palmer distribution was used. Note, however, that the rainfall simulator had been designed to produce simulated rain with drop size and energy characteristics near those of natural rainfall (Swanson, 1965).

In order to minimise the influence of differences between the observed and SHE simulated hydrological responses, the SHESED model was calibrated using the measured water discharge (but with the calibrated roughness coefficient to determine the overland flow depths). After considering the findings of the SHE calibration and the likely effects of the various surface treatments on soil erosion, it was decided to calibrate the grazed and clipped plots as a group and then deal with the tilled plots separately. The ungrazed plots are also included in the first group, but owing to the inconsistency of the measured sediment discharge, and the small mass of sediment involved (the six rainfall applications combined produced only 136 g), there was limited confidence in the representativeness of the measured response.

6.6.1 Calibration for Grazed, Ungrazed and Clipped Plots

The calibration procedure for SHESED involves choosing a sediment transport capacity equation and determining the values of the raindrop detachment coefficient, K_R, and the flow detachment coefficient, K_F. The Engelund-Hansen and Yalin equations were tested to see which best described the transport capacity for the plot conditions. With the supply set to a high value (high K_R and K_F values), the Engelund-Hansen equation always underpredicted the transport (therefore no amount of calibration of detachment coefficients could improve the simulations) while the Yalin equation could overpredict (indicating that calibrating K_R and K_F would improve the simulations). The Yalin equation was therefore selected to calculate the transport capacity.

As the functions defining sediment detachment by raindrop impact and overland flow have different behaviours (equations 4.6 and 4.7), it was possible to establish a correlation between the two detachment coefficients within the functions by comparing volumes and shapes of sediment graphs. The establishment of this correlation effectively reduces the number of calibration parameters to one, and thus greatly facilitates the calibration. Fig. 6.10 shows an example of the method for establishing the correlation between K_R and K_F for the right side, grazed plot. The figure shows that the sediment discharge from flow detachment only, responds in a similar way to the runoff (i.e. the sediment graph in Fig. 6.10(a) for flow detachment only, has a similar shape as the hydrograph in Fig. 6.10(c)), whereas the sediment discharge from raindrop detachment only, tends to reach a maximum before the runoff peaks. Also, as a constant rainfall rate was used, the peak sediment discharge from raindrop detachment only,

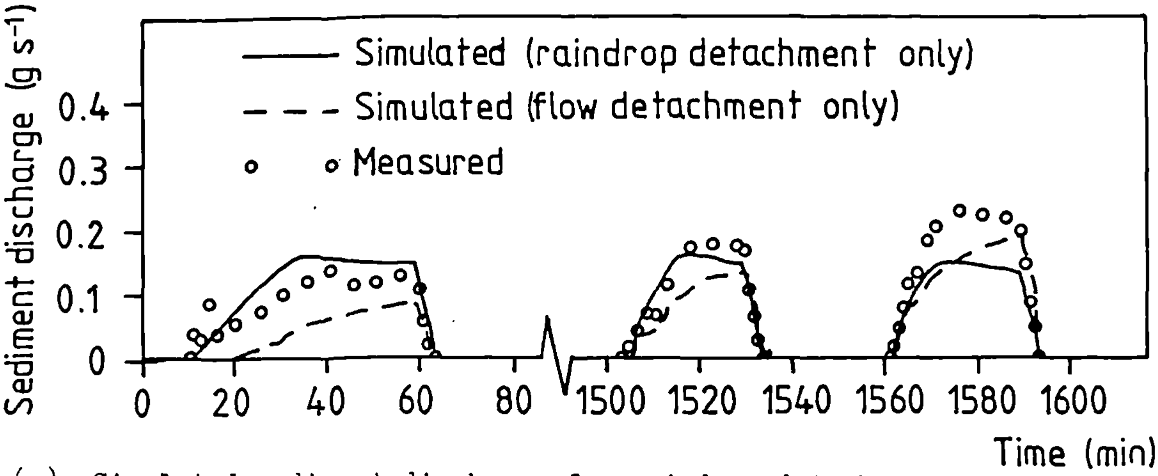

(a) Simulated sediment discharge for raindrop detachment or overland flow detachment only

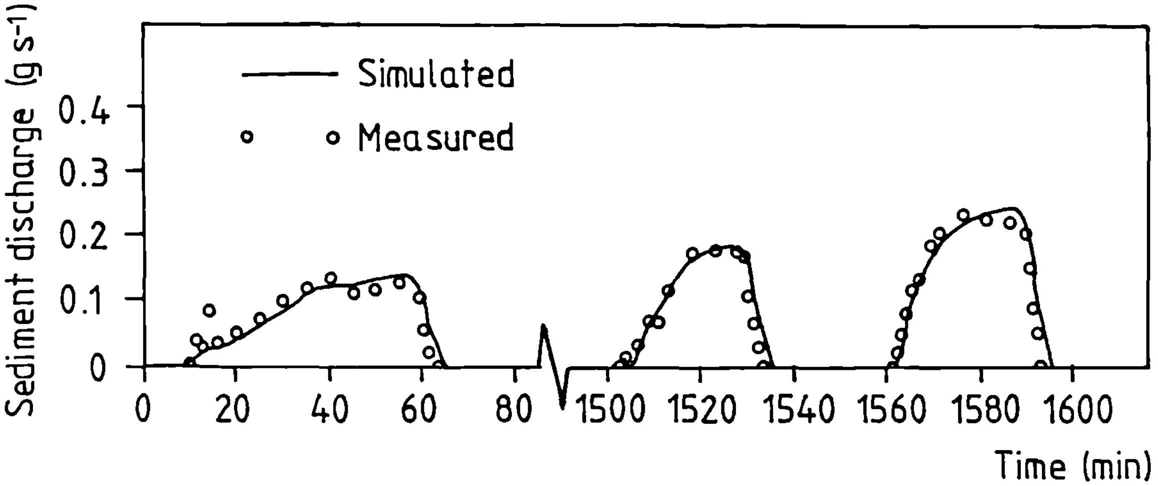

(b) Simulated sediment discharge for a combination of raindrop and overland flow detachment

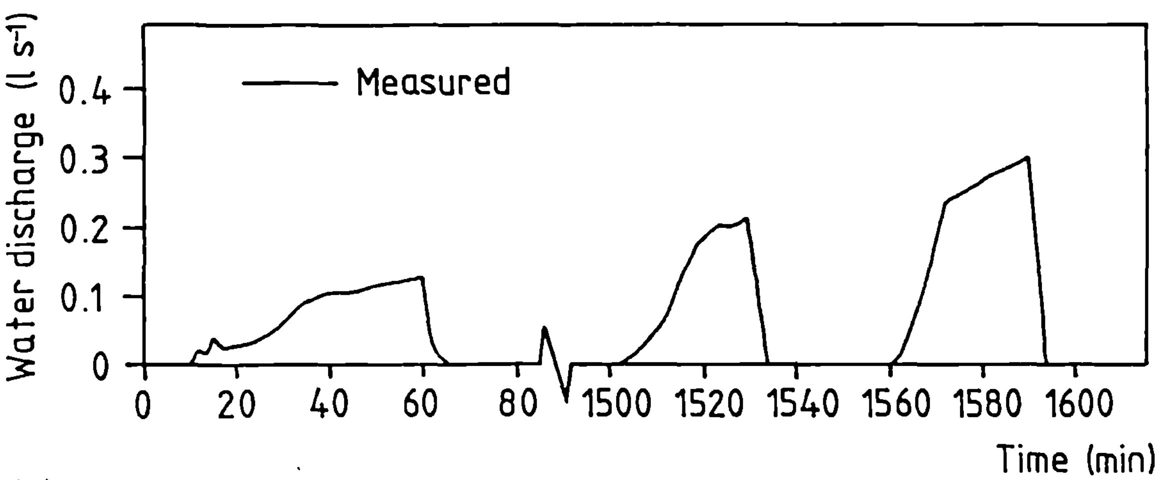

(c) Measured water discharge as used in the above simulations

Fig. 6.10 Example of the procedure used to determine the detachment coefficients.

does not increase further into the three-event sequence (as does runoff). As shown by Fig. 6.10(b), a combination of flow and raindrop detachment is able to produce a very good match to the measured response. A ratio of K_R to K_F of 2:1 (with K_R in J^{-1} and K_F in mg m^{-2} s^{-1}) was found to be appropriate for the four clipped and two grazed plots. The ungrazed plot data were too inconsistent to allow the use of the above procedure, and therefore it was assumed that the same ratio applied.

With the ratio of flow to raindrop detachment coefficients held constant at the determined value, the magnitudes of the coefficients were varied until the total simulated sediment yield (i.e. dry, wet and very wet events combined) for each plot was within 1% of the total measured yield. Thus eight pairs of K_R and K_F values were obtained and are shown in Table 6.3.

Table 6.3 Raindrop and flow detachment coefficient values for each plot calibrated separately

Plot (1)	Raindrop detachment coefficient (J^{-1})	Overland flow detachment coefficient (mg m^{-2} s^{-1})
FTR3	9.85	4.93
FTL3	8.3	4.15
FTR9	13.6	6.80
FTL9	17.8	8.90
FKR3	10.1	5.05
FKL3	11.3	5.65
FBR3	1.04	0.52
FBL3	1.07	0.44
FBR9	1.09	0.55
FBL9	2.1	1.05
FGR3	1.05	0.53
FGL3	1.53	0.77
FUR3	0.45	0.23
FUL3	2.4	1.20

Note: (1) For an explanation of the notation see Table 6.1.

The table shows that for the clipped, grazed and ungrazed plots the variation in detachment coefficients was greater between the supposedly near-identical plot pairs than between the different surface treatments and slopes. In view of this, and because the soil conditions are basically the same for the eight plots, it was decided to use just one pair of detachment coefficients for all these plots; this was determined as the mean of the eight values, giving $K_R = 1.3\ J^{-1}$ and $K_F = 0.65\ mg\ m^{-2}\ s^{-1}$. The simulated sediment discharges shown in Figs. 6.3, 6.4, 6.5 and 6.6 were then calculated using the SHE simulated water discharge and the detachment coefficient values of $K_R = 1.3\ J^{-1}$ and $K_F = 0.65\ mg\ m^{-2}\ s^{-1}$. The accuracy of the individual sediment graphs corresponds to a large extent to the accuracy with which the water discharge was simulated. For example, the dry run on the clipped 9% slope right plot is very poorly simulated for both water and sediment (219% and 434% errors respectively) but for the very wet run on the same plot a good water simulation (-3% error) produced a good sediment simulation (1% error) (Fig. 6.5). The total yield percentage errors for the clipped 3%, clipped 9%, grazed and ungrazed plots are 12%, -29%, -10% and 50% respectively.

6.6.2 Calibration for Tilled Plots

For the tilled plots it was not possible to establish a correlation between the raindrop and flow detachment coefficients as a variation in either coefficient tended to produce the same response (in terms of the sediment discharge graph). This was probably caused by the rapid rise in measured water discharge to near equilibrium levels and therefore all three driving parameters in the flow and raindrop detachment equations (water depth, flow velocity and rainfall rate) were constant for most of the time during the individual events. It was therefore assumed that the ratio of K_R to K_F determined for the grazed and clipped plots was also applicable to the tilled plots. With this ratio held constant, the magnitudes of the coefficients were varied until the total simulated yield for each plot was within 1% of the total measured yield (again using the measured water discharge). The six pairs of values obtained are shown in Table 6.3. Although the variation in detachment coefficients is greater between the different surface treatments and slopes than between the plot pairs, the soil surface condition for the six plots were basically the same, and therefore it should be possible to represent the soil's detachability by single values (neglecting spatial variability and assuming SHESED is an adequate model for the Flats area). The representative detachment coefficients for tilled conditions were determined as the mean of the six pairs of values shown in Table 6.3, giving $K_R = 11.8\ J^{-1}$ and $K_F = 5.9$ mg $m^{-2}\ s^{-1}$. Using these values and the SHE simulated water discharge, the simulated and observed sediment discharges were obtained as shown in Figs. 6.7, 6.8 and 6.9. The percentage errors in sediment yields for the 18 individual sediment graphs vary between 55% and -39%, with total yield percentage errors of 29%, -24% and 11% for the tilled 3% slope, tilled 9% slope and tilled twice plots respectively.

6.7 APPLICATION OF THE SHE TO THE FLATS SUB-CATCHMENT

Forty-five grid squares of 15 m by 15 m were used to simulate the sub-catchment. Given the land use, the parameter values determined for the grazed rainfall simulator plots were used for the Flats sub-catchment. Soil moisture measurements were taken in the Flats area between two and eleven days previous to the storms, and these values were used as the initial soil moisture contents for the simulations. As the SHE model was run between the two August 1983 events, no initial soil moisture data were necessary for the second of these events (23/8/83) (no data are available to check the SHE soil moisture predictions).

Runoff simulations based on the plot-calibrated parameters were generally poor, except for the second of the paired events (indicating again the ability of the SHE to simulate antecedent soil moisture conditions) (Table 6.4).

Simulated and measured water yields for the events of 20/8/83, 23/8/83 and 24/5/85 could be matched on the basis of reasonable variations in antecedent soil moisture contents from the measured (or SHE calculated for 23/8/83) values (-14%, -3% and +8% change in value, respectively) with no other changes in the model parameters. For the event of 30/8/84, though, an unrealistic increase of 125% of the measured value was needed to give a good fit. The simulated (with the adjusted antecedent moisture contents) and measured hydrographs are shown in Figs. 6.11, 6.12, 6.13 and 6.14, with the water yields presented in Table 6.4. The match between measured and simulated hydrograph shapes is very poor.

Table 6.4 Measured and simulated values of water and sediment yield for all events simulated at the Flats sub-catchment

Event	Water yield (m^3)			Sediment yield (kg)		
	Measured	Simulated with parameters fitted for		Measured	Simulated with parameters fitted for	
		plots	Flats		plots	Flats water
20/8/83	4.41	55.1 (1150)	3.41 (-23)	24	422 (1673)	24.5 (2.9)
23/8/83	1.24	1.9 (53)	1.17 (-5.6)	7	9.6 (43)	6.2 (-7.5)
30/8/84	1.35	0 (-)	1.56 (16)	83	0 (-)	10.0 (-88)
24/5/85	3.28	0.26 (-92)	3.59 (9.5)	191	0.82 (-100)	29.2 (-85)

Note: the value in brackets below each calculated yield is the percentage error in that yield, i.e. 100x(simulated - measured)/measured.

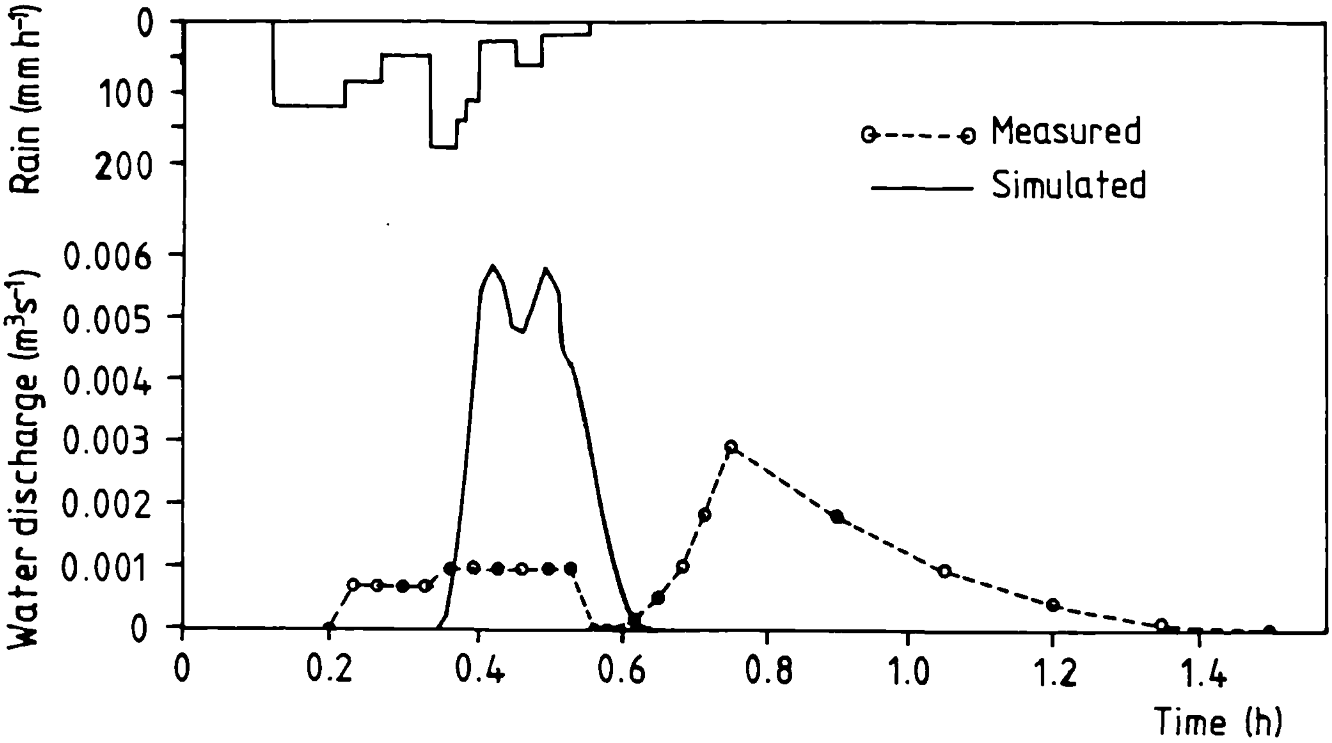

Fig. 6.11 Simulated and measured water discharges for the 20/8/83 event at the Flats sub-catchment.

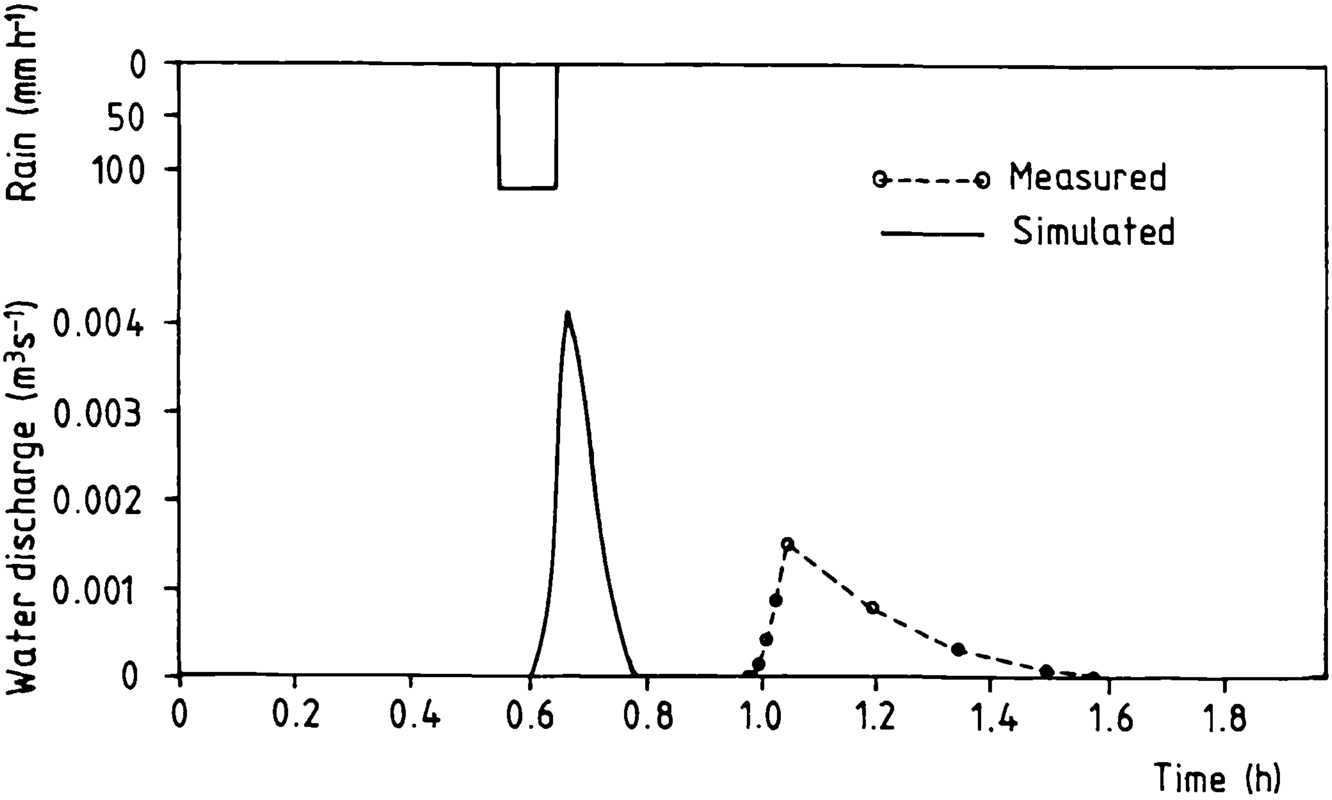

Fig. 6.12 Simulated and measured water discharges for the 23/8/83 event at the Flats sub-catchment.

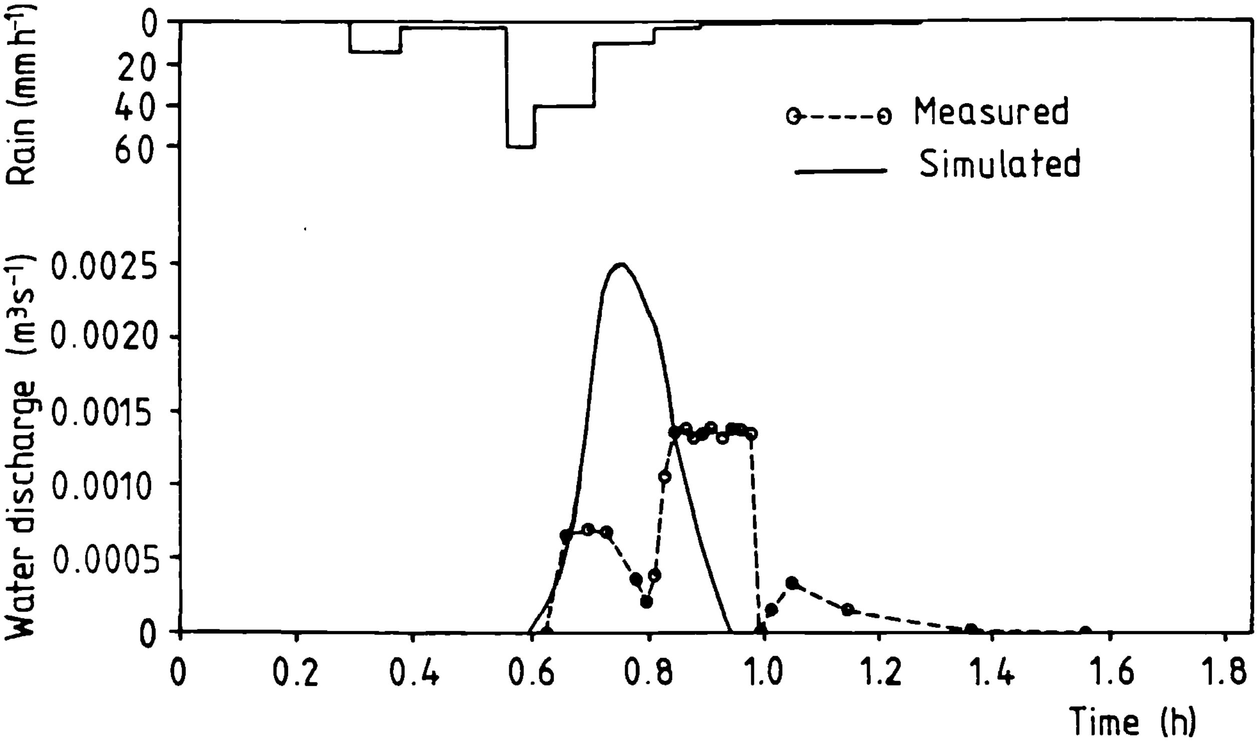

Fig. 6.13 Simulated and measured water discharges for the 30/8/84 event at the Flats sub-catchment.

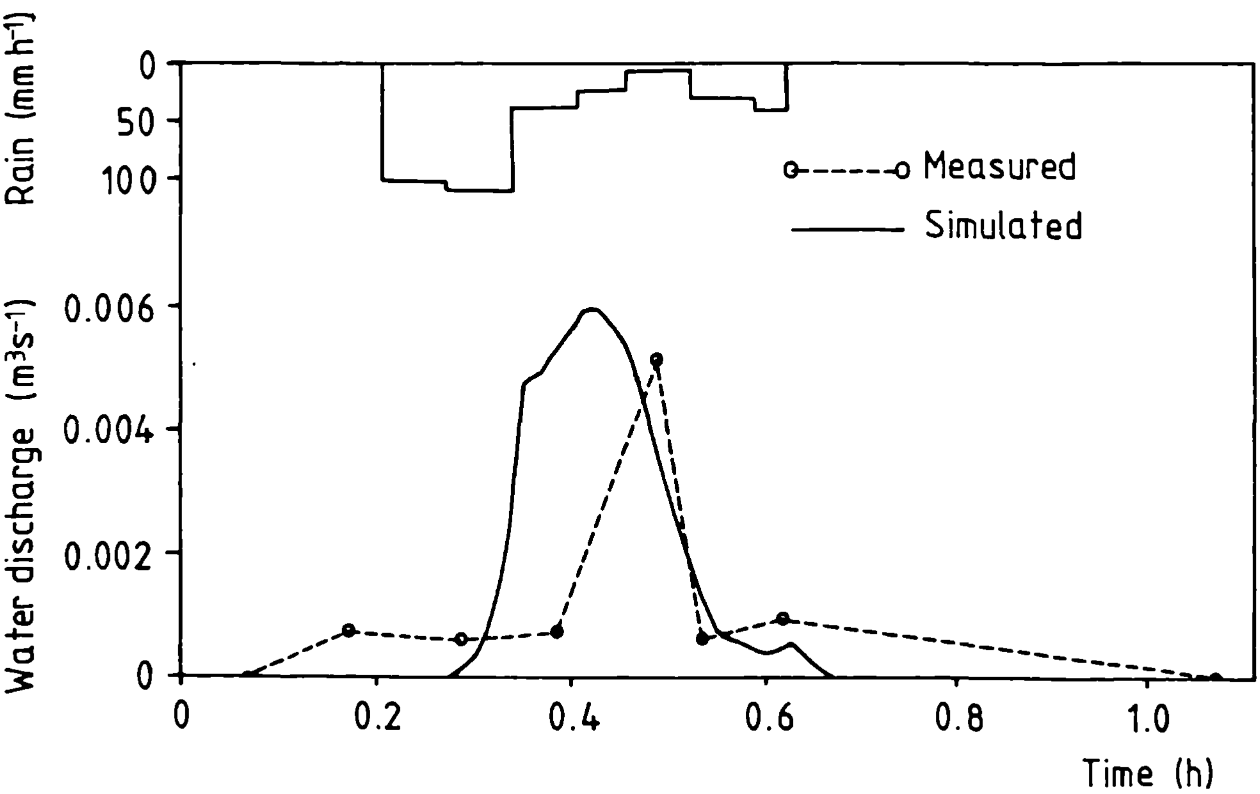

Fig. 6.14 Simulated and measured water discharges for the 24/5/85 event at the Flats sub-catchment.

6.8 APPLICATION OF SHESED TO THE FLATS SUB-CATCHMENT

Using the SHE and SHESED parameters as calibrated for the rainfall simulator plots, the simulated sediment yields were in error by an amount similar to the error in the simulated water yields (Table 6.4). When the simulated water discharges calculated using adjusted initial soil moisture contents were used (but still with sediment parameters for the plots calibration), good sediment yield simulations were possible for the paired August 1983 events, but the other two events show significant underestimation (Table 6.4). The simulated and measured sediment discharge graphs cannot be compared because of the lack of measurements (see Section 6.4.2).

6.9 DISCUSSION

6.9.1 Rainfall Simulator Plots

For the rainfall simulator plots, three sets of SHE calibration parameters and two sets of SHESED calibration parameters produced generally good simulation results for the 14 plots (Table 6.5). The sets of calibration parameter values, as summarised in Table 6.6, show trends of variation in values which are as expected from a consideration of the physics of the processes occurring and of the results of previous experimental work. The only persistent error in the results is the inability to simulate the shape of the hydrograph for many of the clipped and grazed plot dry runs; the simulated runoff starts approximately 10 minutes late and the peak runoff is overpredicted

Table 6.5 Summary of Flats rainfall simulator simulations

Plot [1]	Water yield (mm) Measured	Water yield (mm) Simulated	Water yield (mm) %Error [2]	Water yield (mm) %Error [3]	Sediment yield (kg) Measured	Sediment yield (kg) Simulated [4]	Sediment yield (kg) %Error [2]	Sediment yield (kg) %Error [3]
FTR3	99.7	96.8	-3	0	44.7	53.1	19	29
FTL3	93.6	95.7	2		38.0	53.7	41	
FTR9	97.4	100.3	3	1	71.4	62.9	-12	-24
FTL9	102.8	102.2	-1		98.5	65.4	-34	
FKR3	98.5	102.6	4	2	48.9	57.1	16	11
FKL3	96.1	95.6	-1		50.3	53.4	6	
FBR3	38.3	34.7	-9	-8	1.70	1.87	10	12
FBL3	34.8	32.2	-7		1.55	1.78	15	
FBR9	25.7	36.2	41	3	1.30	2.09	61	-29
FBL9	44.6	36.4	-18		5.50	2.76	-50	
FGR3	26.3	27.5	4	-1	0.86	0.95	11	-10
FGL3	32.2	30.5	-5		1.37	1.06	-23	
FUR3	4.4	2.6	-41	-9	0.04	0.06	63	51
FUL3	3.3	4.4	34		0.10	0.15	47	

Notes: [1] Notation is explained in Table 6.1; [2] %Error = 100(simulated-measured)/measured; [3] %Error for left and right plots combined; [4] Simulated sediment yield using the SHE simulated water discharge with the soil detachment coefficients shown in Table 6.6.

(Figs. 6.3, 6.4 and 6.5). This may be caused by poorly defined model soil hydraulic functions (relating moisture content, tension and conductivity) for dry conditions, which form an important element in the SHE.

Table 6.6 Final values of the calibration parameters

Plot (1)	Saturated hydraulic conductivity (m day^{-1})	Strickler roughness coefficient	Raindrop detachment coefficient (J^{-1})	Flow detachment coefficient (mg m^{-2} s^{-1})
FT3	0.01	50	11.8	5.90
FT9	0.01	50	11.8	5.90
FK3	0.01	50	11.8	5.90
FB3	0.60	10	1.3	0.65
FB9	0.60	10	1.3	0.65
FG3	0.60	10	1.3	0.65
FU3	1.10	10	1.3	0.65

Note: (1) Notation is explained in Table 6.1.

A raindrop detachment coefficient of 1.3 J^{-1} was used for the clipped, grazed and ungrazed plots. This is significantly smaller than the detachment coefficients determined from experimental data, which are in the range 20 to 40 J^{-1} for similar soil types (Table 4.3). The most probable reason for this discrepancy is that, for the majority of the experimental data, highly disturbed soil samples were used, whereas the soil in the clipped, grazed and ungrazed plots was undisturbed. For the tilled plots a raindrop detachment coefficient of 11.8 J^{-1} was used, which is again less than the values for loams shown in Table 4.3. However, a discrepancy of this magnitude may be expected considering the uncertainties in the model and data (e.g. lack of data on the raindrop size distribution and the influence of soil consolidation and moisture content).

6.9.2 Transfer of Parameter Values to the Flats Sub-catchment

The SHE and SHESED models were successfully calibrated for the rainfall simulator plots, suggesting that they are valid representations of the infiltration, runoff and erosion processes for the study area. However, the SHE simulations for Flats, based on calibrated parameters transferred from the grazed rainfall simulator plots, were poor, with the most accurately simulated event having a percentage error in water yield of 53%. Sediment yield predictions calculated with these simulated water discharges were correspondingly in error, although this does not itself suggest that either SHESED is a poor representation of the processes at Flats or that the calibration parameters determined for the rainfall simulator plots are not appropriate for the Flats sub-catchment. In fact when the initial soil moisture contents were adjusted to produce good water yields, two of the four events were simulated well using the SHESED parameters as calculated for the plots. Also the rainfall simulator plot applications were successful and three of the four Flats events could be successfully simulated for water yield with only minor variations in initial soil moisture contents. In view of this it may be suggested that the situations when the models performed poorly are attributable to either data problems or scale effects, rather than model deficiencies. The results indicate that, in this case, any scale effects are obscured by data problems.

First, it is apparent from both the plots and sub-catchment results that there are difficulties in simulating the hydrograph for an initial or isolated event with low antecedent moisture content. At both scales the results improve for subsequent events in a sequence, for which antecedent moisture contents are higher. As discussed earlier, the poor results for water yield may have arisen from inadequately quantified model soil hydraulic functions for dry conditions.

Second, the soil detachment coefficients were calibrated for only one rainfall rate (60 mm h^{-1}) which gave ratios of total sediment yield to water yield of 1.0 kg m^{-3} and 1.3 kg m^{-3} for the right and left grazed plots respectively. For the Flats sub-catchment, the sediment/water yield ratios for the paired 1983 events (for which good sediment yields could be predicted based on fitted water yields) were not dissimilar at 5.4 kg m^{-3}. For the events of 30/8/84 and 24/8/85, though, the sediment/water yield ratios were significantly higher at 61.7 kg m^{-3} and 58.2 kg m^{-3} respectively. Also, the rainfall energy from the rainfall simulator is less than that experienced in a natural event. Therefore, the poor soil erosion simulations may well reflect the use of detachment coefficients well outside the range of conditions used for their calibration. In this particular case, the range of calibration conditions was limited to that available from the rainfall simulator study, which was designed to evaluate the Universal Soil Loss Equation parameters rather than to reproduce natural events at the Flats sub-catchment. More generally, though, if small-scale field calibration is to be used, it is important that the experimental conditions reflect the type of events that need to be simulated at the larger scale.

The results illustrate the importance of obtaining good water yield simulations as the prelude to simulating sediment yield. A particular problem at the Flats sub-catchment is that measured runoff is only about 1% of the rainfall input. Thus a small absolute error in simulated runoff translates into a large percentage error in simulated runoff and thence in sediment yield.

Concurrent with the application of SHESED, a second model, MULTSED (Li et al., 1979; Ward, 1987), was also calibrated for the grazed rainfall simulator plots and then the parameters transferred for simulations at the Flats sub-catchment. The MULTSED model is based on the CSU model discussed in Section 2.4.3, and the application was carried out by Professor T.J. Ward, New Mexico State University. Both the MULTSED and SHESED applications are reported in Wicks et al. (1988). Although designed differently and using different calibration parameters, the MULTSED model yielded results which were of similar accuracy to those presented in this chapter. This can be interpreted as further evidence to support the conclusion that data problems were a major cause of the poor simulations and also that SHESED is at least as good as existing models.

The applications to Reynolds Creek suggest that transfer of calibrated parameter values from the scale of the rainfall simulator plots to the 1-ha scale is feasible, provided the calibration has a suitable data base. For the future, therefore, to allow full calibration and validation of physically-based sediment yield models, the data should ideally include detailed field measurements of such quantities as soil moisture profiles and soil erosion and transport patterns, as well as the outlet hydrograph and sediment graph which traditionally provide the basis for calibration.

CHAPTER 7 - APPLICATION TO THE ISU CATCHMENTS

7.1 INTRODUCTION

The Iowa State University (ISU) data were used to test the SHESED hillslope sub-component for agricultural conditions, data from two field-sized catchments, ISU1 and ISU2, being available. The main attraction of the ISU data is that precipitation, runoff and sediment concentration data are available at a temporal scale sufficiently small to allow characterisation of the catchment response for short, high intensity storms. The spatial scale is such that homogeneity can be assumed within the catchment, thus aiding the calibration process. Also, the data have been used previously to test the models of Park et al. (1982) and Nielsen et al. (1986), and should therefore allow a comparison of results from different models.

Interpretive reports on the data have been published (Hamlett et al., 1984; Hamlett et al., 1987), with some of the data base published in Johnson and Baker (1982), although the simulations reported in this chapter used the data as provided by C.L. Armstrong, Department of Agricultural Engineering, University of Illinois at Urbana-Champaign.

7.2 DESCRIPTION OF STUDY AREA

The two catchments, ISU1 (5.1 ha) and ISU2 (6.4 ha) (Fig. 7.1), form part of the Four Mile Creek catchment (50.5 km^2) located in eastern-central Iowa, USA. The 18-year mean annual precipitation is 820 mm. ISU1 and ISU2 are adjacent, field-sized

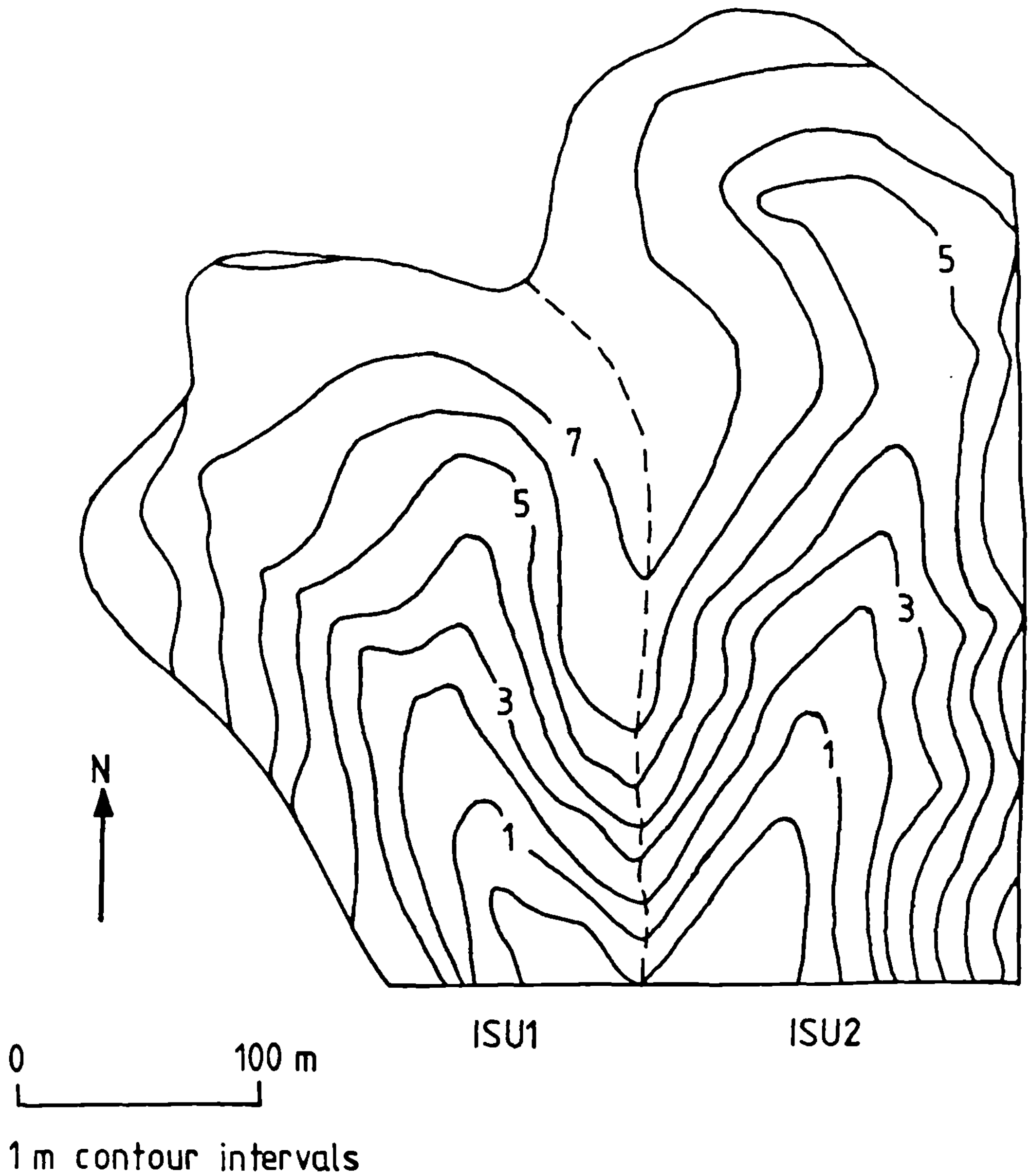

Fig. 7.1 Map of the ISU1 and ISU2 catchments. (After Johnson and Baker, 1982.)

catchments having single cover conditions and crop management practices. The catchments were planted with soybeans and maize in rotation; in 1977 ISU1 was in maize and ISU2 was in soybeans. Both catchments have silt loam soils with slopes ranging between 2 and 9%.

7.3 AVAILABILITY OF DATA

A recording rain gauge was located at ISU2 and breakpoint readings from the charts were used to determine rainfall intensities which were used as the rainfall input for both catchments. A 1.22-m H-L flume was used at the outlet of ISU1 and ISU2 to record the water discharge. Pump samplers (PS-69), single-stage samplers and hand-grab sampling were used to collect sediment concentration samples. Percentage canopy cover was determined from photographs taken from 3.3 m above the ground level at weekly intervals. The rainfall and water and sediment discharge data are available at about one minute intervals. A detailed analysis of the particle size distribution of the sediment load is available in Hamlett et al. (1987) from which the model representative particle size of 0.0068 mm (the average D_{50} size) is taken.

The most important data which are missing from the ISU data base are details of the soils hydraulic properties, for example saturated hydraulic conductivity and the soil moisture tension/content relationship. These soil variables had to be estimated from values for other silt loam soils. Leaf drip fall heights, drip diameters and percentage drainage falling as leaf drip were also not available and values of fall height of 0.5 m, drip diameter of 5 mm and percentage drainage as leaf drip of 50% were assumed, based on values given in Section 4.2.4.

Data are available for five events at ISU1 and three at ISU2. Three of these events are short duration (less than 30 minutes) high intensity (greater than 160 mm h^{-1}) storms with the remainder having lower intensities.

7.4 APPLICATION OF THE SHE

Both catchments were simulated using 25 m by 25 m grid squares and a computational time step of 0.3 minutes. The computational distance step in the root zone was set to 0.5 cm. As no information was available about the phreatic surface level, it was set to 4 m below the ground surface, which resulted in all simulated runoff occurring through excess of rainfall over infiltration. Antecedent soil moisture values were not available, although the values used in the previous modelling attempt of Park et al. (1982) were known. Park (1981) states that these values were based on measured moisture contents adjusted by a water balance model for the period between the measurements and the event. Park's values are also used in this application; the accuracy of these values is not known.

The SHE model was calibrated by adjusting the saturated hydraulic conductivity and the overland flow roughness to match simulated and observed hydrographs. With reasonable adjustments to the calibration parameters for different soil-plant conditions, good agreement between observed and measured water discharges for the three largest events could be achieved (Table 7.1, Figs. 7.2, 7.3, 7.4). Data for four minor events were also available. However, a set of physically realistic infiltration and surface roughness parameters which would give an adequate match of hydrograph shapes for these events could not be found. To match the measured runoff volumes for the small events required saturated hydraulic conductivity values ranging from 0.132 to 0.077 m day^{-1} and Strickler coefficients ranging from 5 to 40. Hydrograph shapes were, however, generally poor and there was no pattern in the variation of the calibration parameters. For example, the saturated hydraulic conductivity had to be changed from 0.132 to 0.077 m day^{-1} and the Strickler coefficient changed from 5 to 30 between the 17/4/78 and 18/4/78 events on the ISU2 catchment despite no apparent change in soil-plant conditions. It is therefore concluded that the SHE model is only calibrated for the larger events.

7.5 APPLICATION OF SHESED

The same time and distance steps were used for the SHESED simulations as for the SHE simulations. The proportion of the ground covered by mulch was used in the SHESED data files as the ground cover, with the canopy cover of soybeans or maize used as the vegetation cover in the SHE. No data were available on the raindrop size distribution and therefore the default Marshall-Palmer distribution was used in the simulations.

The SHESED hillslope component is calibrated by choosing a sediment transport capacity equation and by adjusting the raindrop soil detachment coefficient, K_R, and the overland flow soil detachment coefficient, K_F. The calibration process should

Table 7.1 The SHE calibration parameters and summary of results for the ISU catchments

Event date	Catchment	Soil-plant condition	Total rainfall (m^3)	Saturated hydraulic conductivity (m day^{-1})	Strickler coefficient	Total runoff (m^3)		Peak runoff (m^3s^{-1})	
						Measured	Simulated	Measured	Simulated
19/4/77	ISU1	Following tillage	1155	0.350	35	266	367 (38)	0.568	0.587 (3)
15/8/77	ISU1	Soybean	1058	0.255	20	268	263 (-2)	0.327	0.344 (5)
15/8/77	ISU2	Maize	1115	0.315	20	46	48 (3)	0.055	0.054 (-2)

Note: values in brackets are the percentage errors in the simulated values relative to the measured

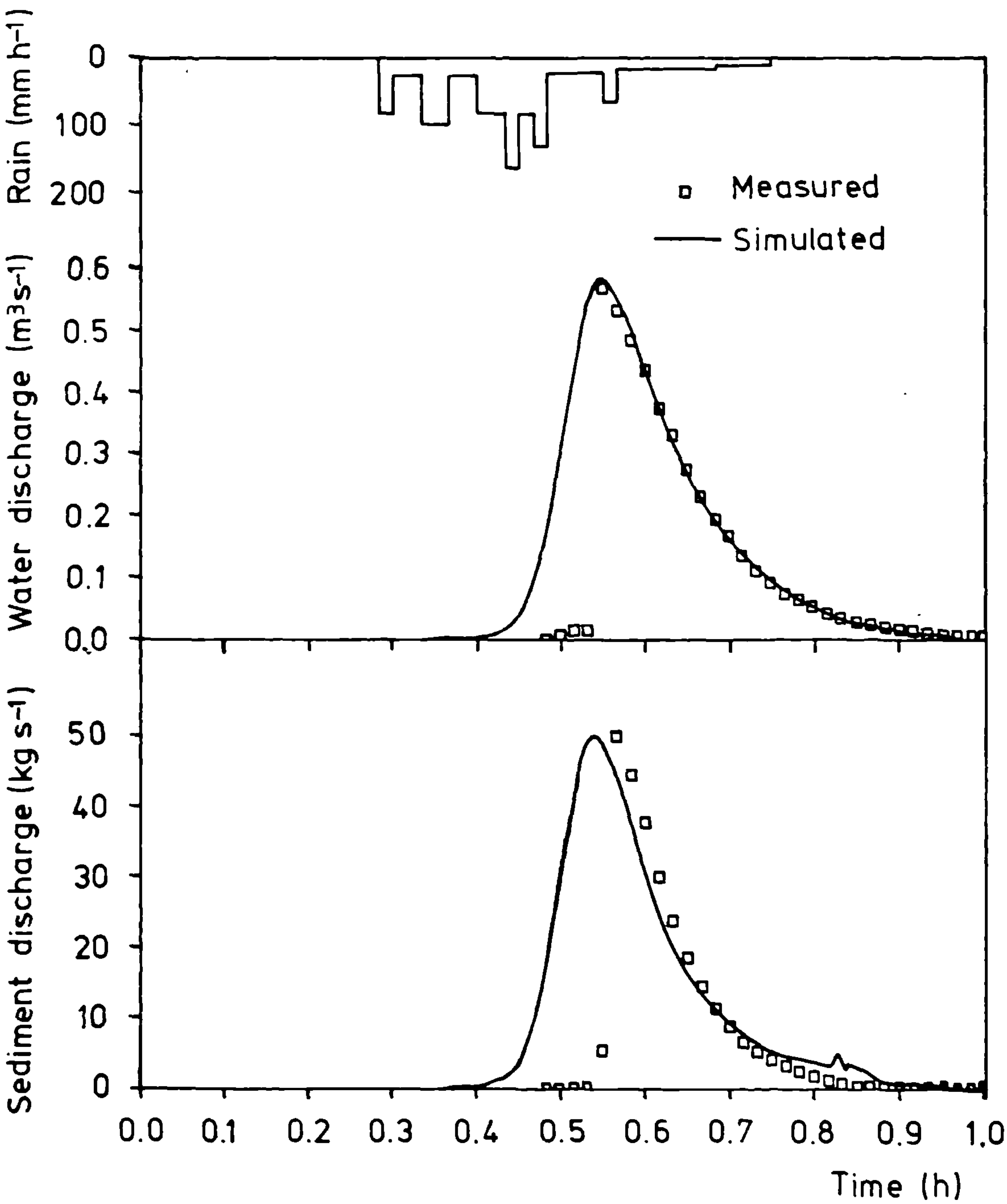

Fig. 7.2 Simulated and measured water and sediment discharges for the 19/4/77 event at the ISU1 catchment.

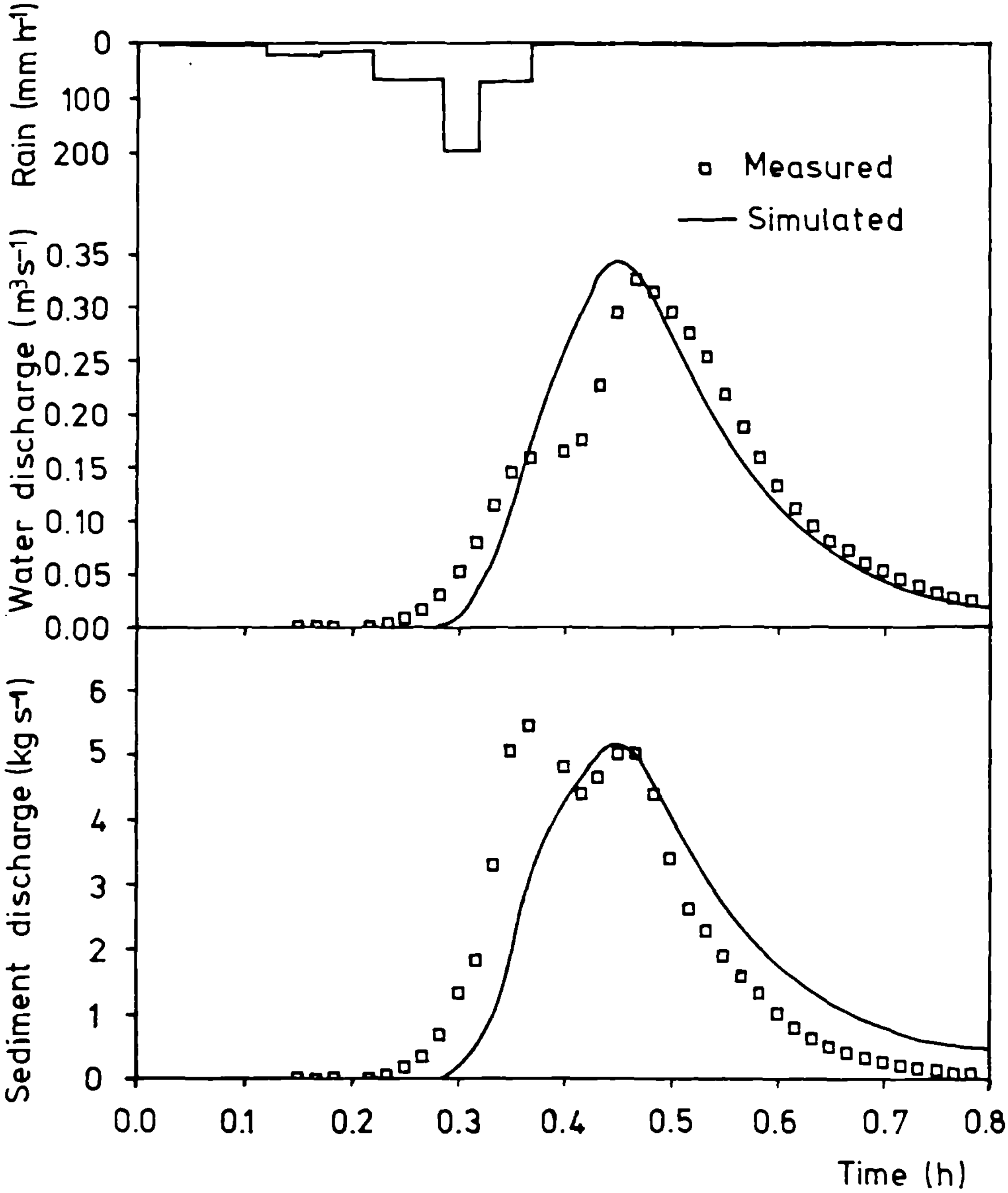

Fig. 7.3 Simulated and measured water and sediment discharges for the 15/8/77 event at the ISU1 catchment.

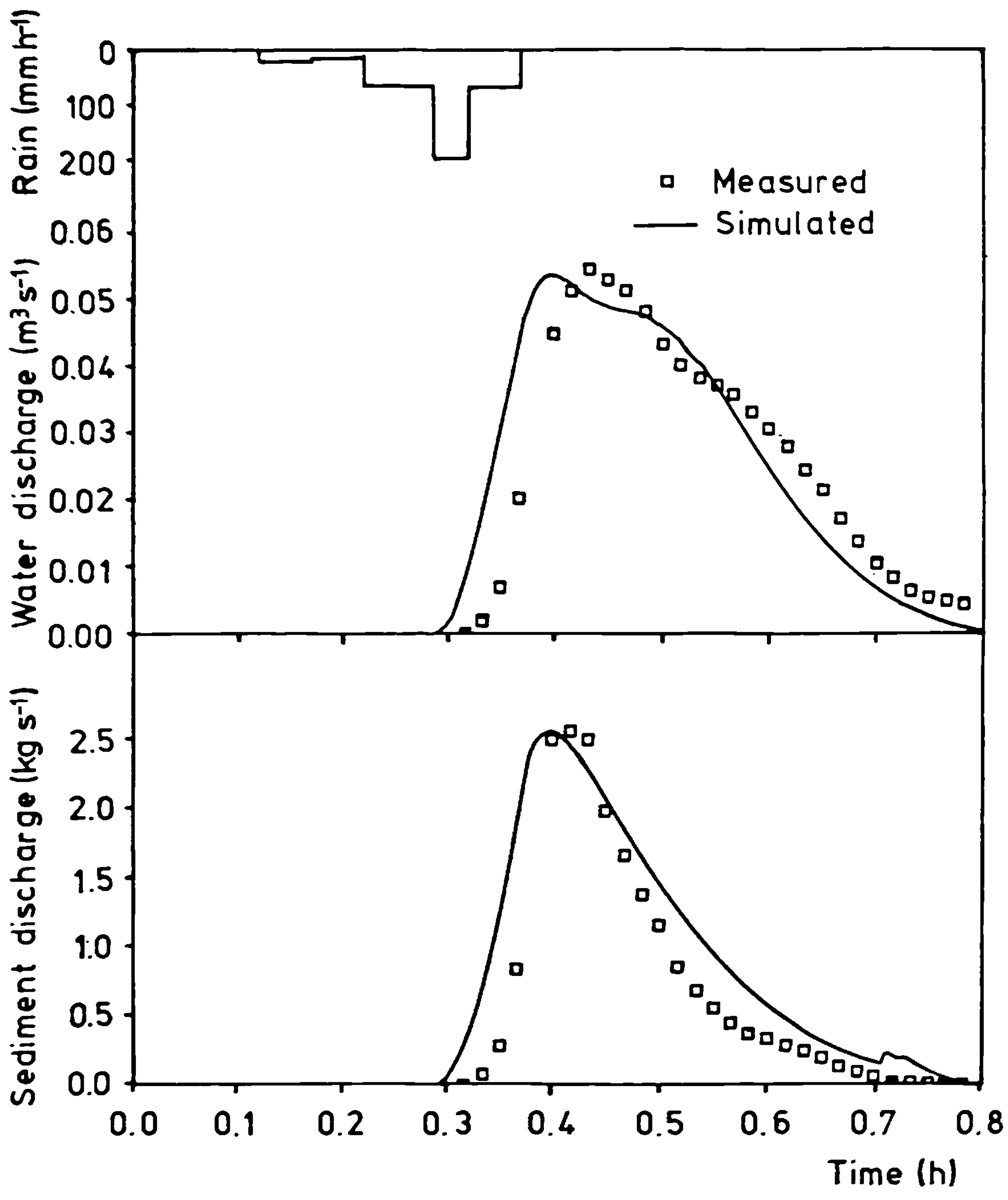

Fig. 7.4 Simulated and measured water and sediment discharges for the 15/8/77 event at the ISU2 catchment.

lead to K_R and K_F values which can be used for all events with the same soil-plant conditions. However, for the three events which were successfully simulated by the SHE, no two events had the same soil-plant conditions and therefore the calibrated detachment coefficients for the specific soil-plant conditions could not be verified, although their relative values should reflect the soil-plant conditions.

The first step in the SHESED calibration involved choosing the Engelund-Hansen equation, in preference to the Yalin equation, to predict sediment transport capacity, as it gave a better match of simulated and observed sediment graphs over a range of K_R and K_F values. Then different ratios of K_R to K_F were tested with the three events until a single ratio was found which produced good sediment graph shapes for all events. With this ratio of K_R to K_F held constant, the magnitudes of the coefficients were then varied until the final calibrations were achieved (Table 7.2, Figs. 7.2, 7.3, 7.4).

Tentative calibrations for the small events (which were generally poorly simulated by the SHE) showed that, using the same ratio of K_R to K_F as for the larger events, the K_R values should be in the range 1 to 8 J^{-1} to reproduce the measured sediment yields.

7.6 DISCUSSION

The successful applications of SHESED to the two Iowa catchments show that the hillslope sub-component can simulate the soil erosion and sediment transfer behaviour for the agricultural conditions. The variation in the SHE and SHESED calibration

Table 7.2 The SHESED calibration parameters and summary of results for the ISU catchments

Event date	Catchment	Soil-plant condition	Raindrop detachment coefficient (J^{-1})	Overland flow detachment coefficient ($mg\ m^{-2}\ s^{-1}$)	Sediment yield (kg)		Peak sediment discharge ($kg\ s^{-1}$)	
					Measured	Simulated	Measured	Simulated
19/4/77	ISU1	Following tillage	82	0.41	16604	28230 (70)	50.06	50.02 (0)
15/8/77	ISU1	Soybean	28	0.14	4199	4183 (0)	5.47	5.17 (-6)
15/8/77	ISU2	Maize	66	0.33	1256	1718 (37)	2.56	2.55 (0)

Note: values in brackets are the percentage errors in the simulated values relative to the measured parameters between the three large events is expected as soil-plant conditions varied. Hamlett et al. (1984) detail the effects of different crops and tillage practices on the runoff and sediment transport from ISU1 and ISU2.

Table 7.2 shows the calibrated raindrop detachment coefficients to be in the range 28 to 82 J^{-1} which compares well with values for silt loam soils calculated from independent experimental data, which are in the range 25 to 40 J^{-1} (Table 4.3). However, note that the variation in calibrated K_R values is large in comparison with the variation in K_R between different soil types as shown in Table 4.3. The K_R value of 82 J^{-1} is for conditions immediately following tillage (discing) and therefore is expected to be larger than values for crop conditions. The closeness of experimentally derived and calibrated K_R values is encouraging for the transfer of experimentally derived K_R values to simulations in ungauged catchments.

For the smaller events, generally poor SHE simulations were achieved. The difficulties with these events may be caused by the lack of site specific soil hydraulic property data. The calibration of all the assumed parameters was not attempted as this would have been too time consuming. In any case these small events are of minor significance for annual sediment yield calculations, the average sediment yield for the five events being only 220 kg. Tentative SHESED simulations for these events required K_R values an order of magnitude smaller than the K_R values for the larger events. It is not clear whether the low values are caused by the incorrect simulation of the water, deficiencies in the SHESED model, or data problems. Hamlett et al. (1984) report that small dykes were constructed to direct flow into the flumes at ISU1 and ISU2. These resulted in temporary impoundment of runoff which caused appreciable deposition of sediment upslope of the dykes. (This localised effect is not modelled by the SHE.) It may be that a greater proportion of the eroded soil was deposited in this area for the smaller storms than the larger storms. If so, this may be a contributing factor in the large variation in detachability values between the large and small events. The hypothesis that a larger proportion of the eroded soil was deposited upslope for the smaller events cannot be verified as data is lacking for the study period. However, for 1979 the data are available in Hamlett et al. (1984) and show that the three events with the smallest total sediment yield had the largest proportion of eroded sediment deposited in front of the flumes (46 to 51% compared with 23 to 43% for the remaining, larger sediment events).

The SHESED results compare favourably with the previous studies of the ISU catchments by Park et al. (1982) and Nielsen et al. (1986). In both of these studies, the surface roughness, soil hydraulic and soil erosion calibration parameters had to be varied in order to simulate a range of events. The simulated sediment graphs for the Park et al. and Nielsen et al. models are reproduced in Figs. 7.5 to 7.8. (These are the only sediment graphs shown by Park et al., Park (1981) and Nielsen et al. which correspond to the events presented in this chapter.) It is inappropriate to comment on which is the more suitable model for the ISU catchments owing to differences in calibration criteria, method of reporting results and choice of events to simulate.

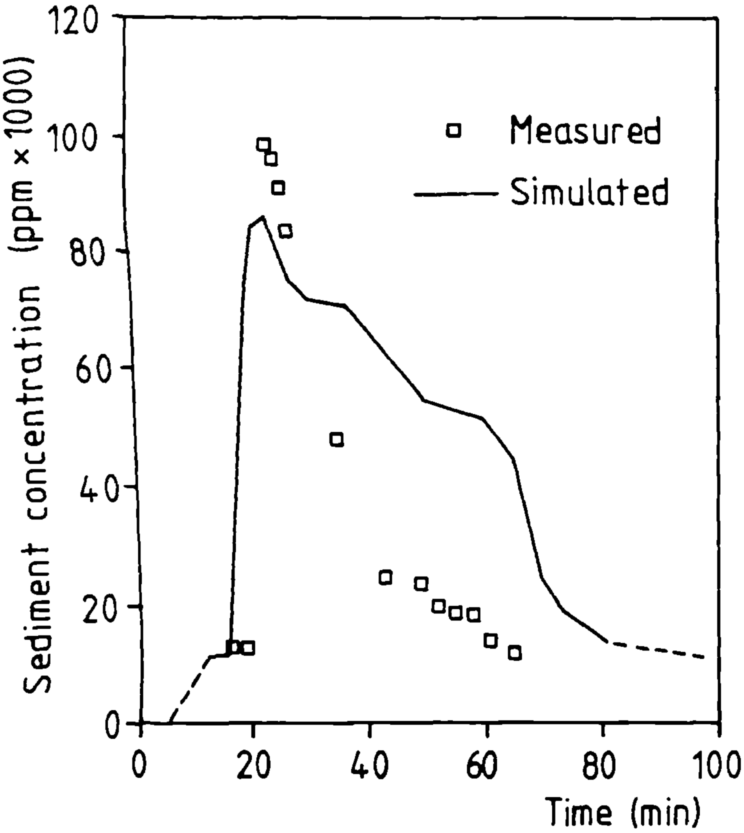

Fig. 7.5 Simulated and measured sediment concentrations for the 19/4/77 event at the ISU1 catchment using the Park et al. model. (After Park, 1981.)

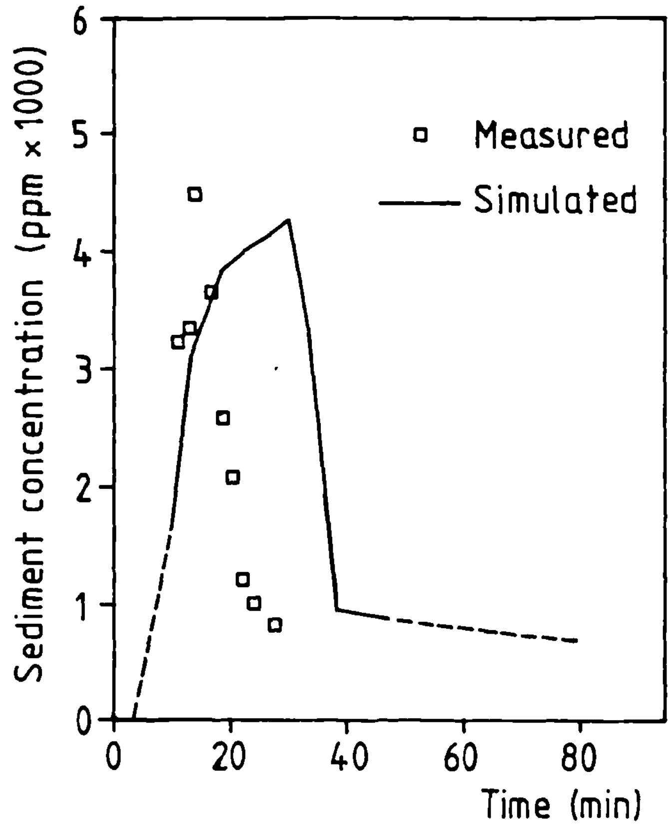

Fig. 7.6 Simulated and measured sediment concentrations for the 15/8/77 event at the ISU2 catchment using the Park et al. model. (After Park, 1981.)

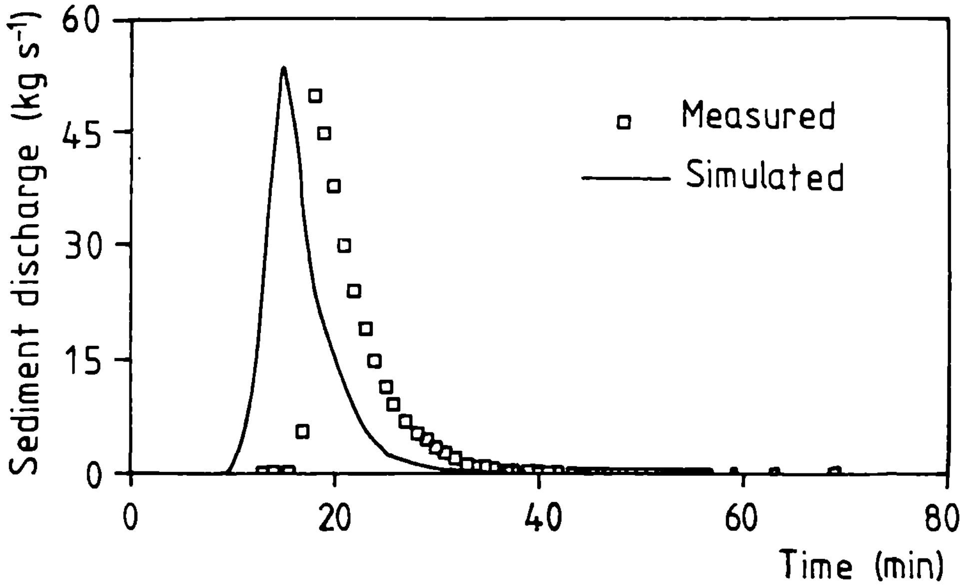

Fig. 7.7 Simulated and measured sediment discharges for the 19/4/77 event at the ISU1 catchment using the Nielsen et al. model. (After Nielsen et al., 1986.)

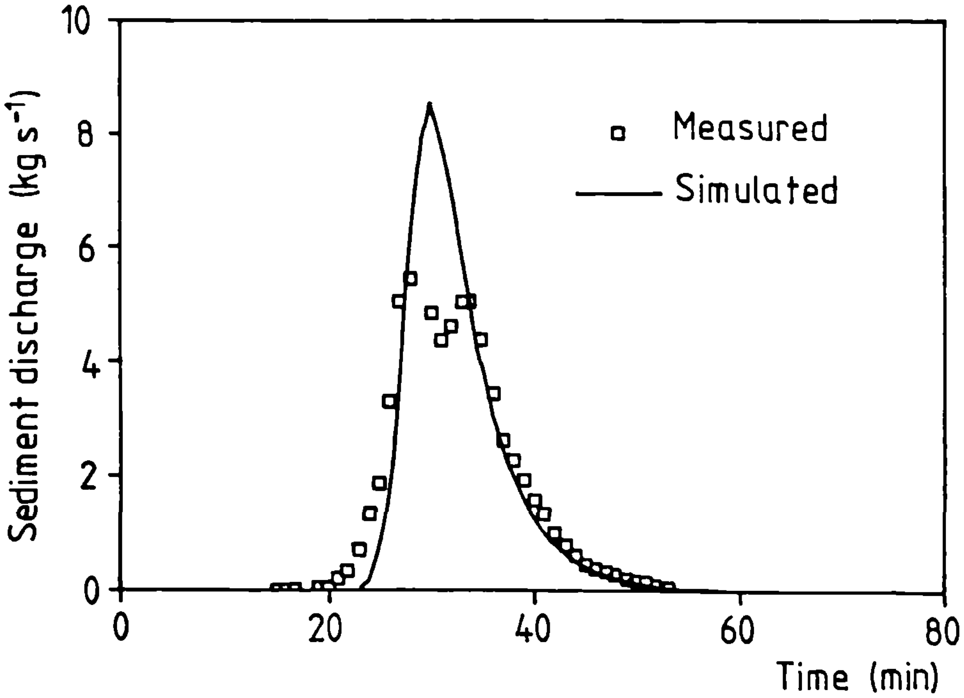

Fig. 7.8 Simulated and measured sediment discharges for the 15/8/77 event at the ISU1 catchment using the Nielsen et al. model. (After Nielsen et al., 1986.)

CHAPTER 8 - APPLICATION TO THE EAST FORK RIVER

8.1 INTRODUCTION

The main aim of the applications of SHESED presented in this thesis is to assess the performance of the model for a range of sediment yield situations. The applications of SHESED described in the two preceding chapters were hillslope based (i.e. source areas) and did not warrant the inclusion of channel links in the model built from the SHE. It was hoped to apply the full model to a reasonably sized catchment so that the performance of the model in a situation with both hillslope and channel processes could be assessed with field data. Unfortunately a sufficiently detailed data set could not be found for a catchment with hill-slope supply areas feeding a channel system which transports both bed material and wash loads. Hence a thorough combined testing of the hillslope and channel sub-components could not be achieved (apart from testing using hypothetical data, which was done to test the Fortran77 code and numerical methods). The separate testing of the channel sub-component with data from the East Fork River, Wyoming, is the subject of this chapter.

The East Fork River was chosen for an application of the SHESED channel sub-component because an extensive data base is available and because a number of interpretive reports on the sediment response have been published. A particular attraction of the East Fork River is that a bed load trap was constructed across the river to measure the bed load discharge at the down-stream end of the study reach.

8.2 DESCRIPTION OF THE STUDY AREA

The 3.3-km study reach of the East Fork River is situated near Boulder in western Wyoming, USA (Fig. 8.1). The drainage area of the East Fork River above the study reach is 470 km^2, with about half of this within the Wind River Mountains (granitic and metamorphic rocks) and the other half in an area of rolling hills (sandstone and shale) drained by Muddy Creek, which joins the East Fork River just upstream of the study reach.

For the study reach, the average river width is about 20 m, the water surface slope averages 0.0007, the bankfull discharge and average depth are about 20 $m^3 s^{-1}$ and 1.2 m respectively. High flows at the bed load trap are the result of snowmelt in the Wind River Mountains. The snowmelt season hydrograph typically shows strong diurnal fluctuations with multiple seasonal peaks (e.g. see Fig. 8.3).

Most of the sediment that moves as bed load through the study reach is coarse sand and fine gravel (D_{50} = 0.5 to 1.5 mm) that comes from Muddy Creek. This moves over bed rock or a virtually immobile layer of coarse gravel (D_{50} = 1.6 to 64 mm). During the low flow periods the movable bed material is stored in distinct regions of the channel which are centred on average 500 to 600 m apart. Each storage area contains an average of 2500 to 3000 tonnes of material - equivalent to the annual bed load discharge. Meade (1985) shows that the bed material is moving down the river in distinct wavelike pulses; during a typical snowmelt season the material from one storage area is moved to the next storage area downstream.

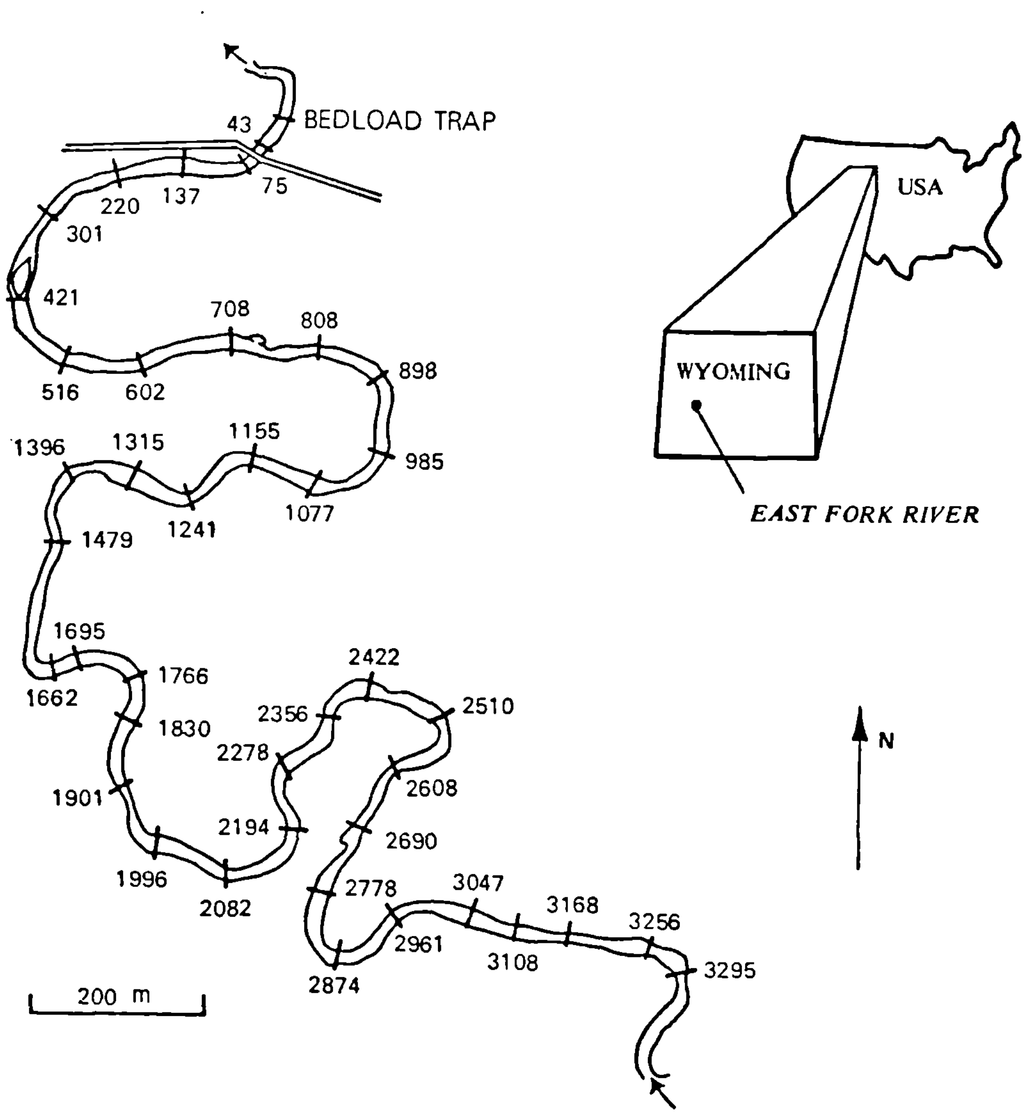

Fig. 8.1 Map of the 3.3-km study reach of the East Fork River showing the distance, in metres, of the measurement sections upstream from the bed load trap. (From Emmett et al., 1980.)

The above description of the study area is based on information in Andrews (1979), Emmett et al. (1980), Meade et al. (1981) and Meade (1985). Further details of the bed load trap are available in Leopold and Emmett (1976).

8.3 AVAILABILITY OF DATA

Data from the 1979 snowmelt runoff season were used to test the SHESED channel sub-component. The main sources of data are Emmett et al. (1980) for river hydraulics and sediment transport data, and Meade et al. (1980) for bed elevation data. Forty-one sections were established in the 3.3-km study reach (Fig. 8.1). At each of the 39 internal sections the bed material size distribution was sampled at the start of the snowmelt runoff season and cross-section measurements were taken every day during the study period. Hourly values of water discharge were available for the upstream and downstream sections. Near-synoptic measurements of water surface elevations for all sections were made on numerous occasions. Daily bed load measurements at the upstream section were made with a Helley-Smith sampler and at the downstream section with a Helley-Smith sampler and the bed load trap. The size distribution of the bed load measurements is available. Suspended load concentrations were also measured daily at the two sections.

8.4 APPLICATION OF THE SHE

The 41 measurement sections were used as computational nodes, giving distance steps varying between 32 and 183 m. A trapezoidal channel cross section was used, based on the cross section elevations at the start of the snowmelt runoff season. A 20 m wide flood plain at a transverse slope of 0.05 was added to both sides of the channel. A computational time step of 0.5 h was used for the 37.5-day (900 h) simulation period from 17 May to 24 June 1979. The measured inflow to the reach was used as the upstream boundary condition with the measured water surface elevations at the bed load trap as the downstream boundary condition - both time series were given as breakpoint values at intervals of about 6 h.

The SHE channel component was calibrated by adjusting the Strickler roughness coefficient to match simulated and observed water surface elevations at a discharge about equal to the bankfull rate (at the simulation time of 203.5 h). This resulted in a Strickler coefficient of 30 (Manning's n of 0.033) for all sections. This value of Manning's n compares well with the range quoted in Chow (1959) of 0.033 to 0.045 for "clean, winding, some pools and shoals, top width < 100 feet", the nearest description to the conditions in the East Fork River. The simulated and measured water surface elevations for the calibration are compared in Fig. 8.2. Good agreement was obtained between simulated and observed water discharges at the downstream end of the reach (Fig. 8.3). (Note, however, that this agreement reflects more the minimal translation of the upstream inflow, than the accuracy of the model.)

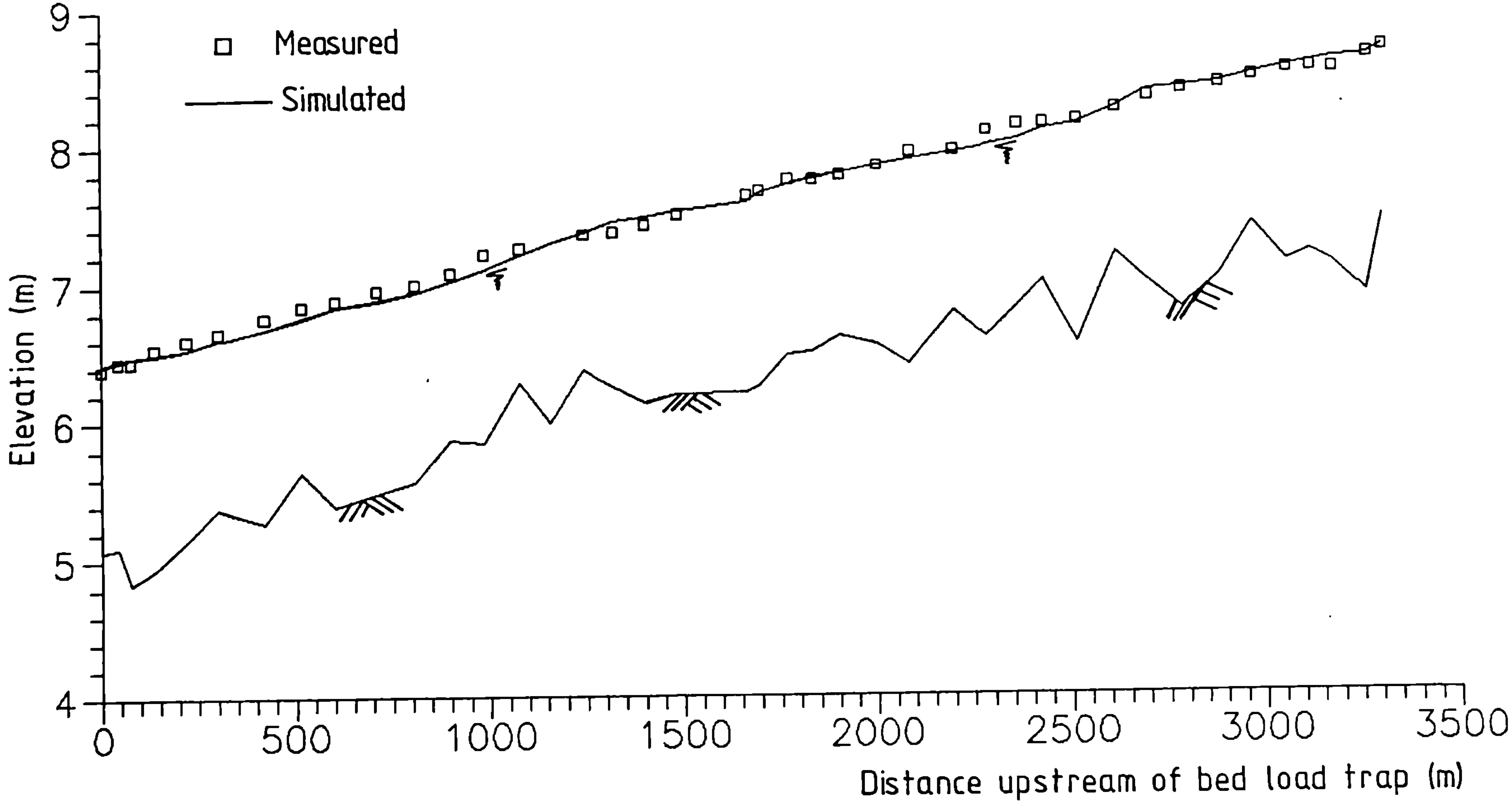

Fig. 8.2 Simulated and measured water surface elevations for the East Fork River study reach at a simulation time of 203.5 h.

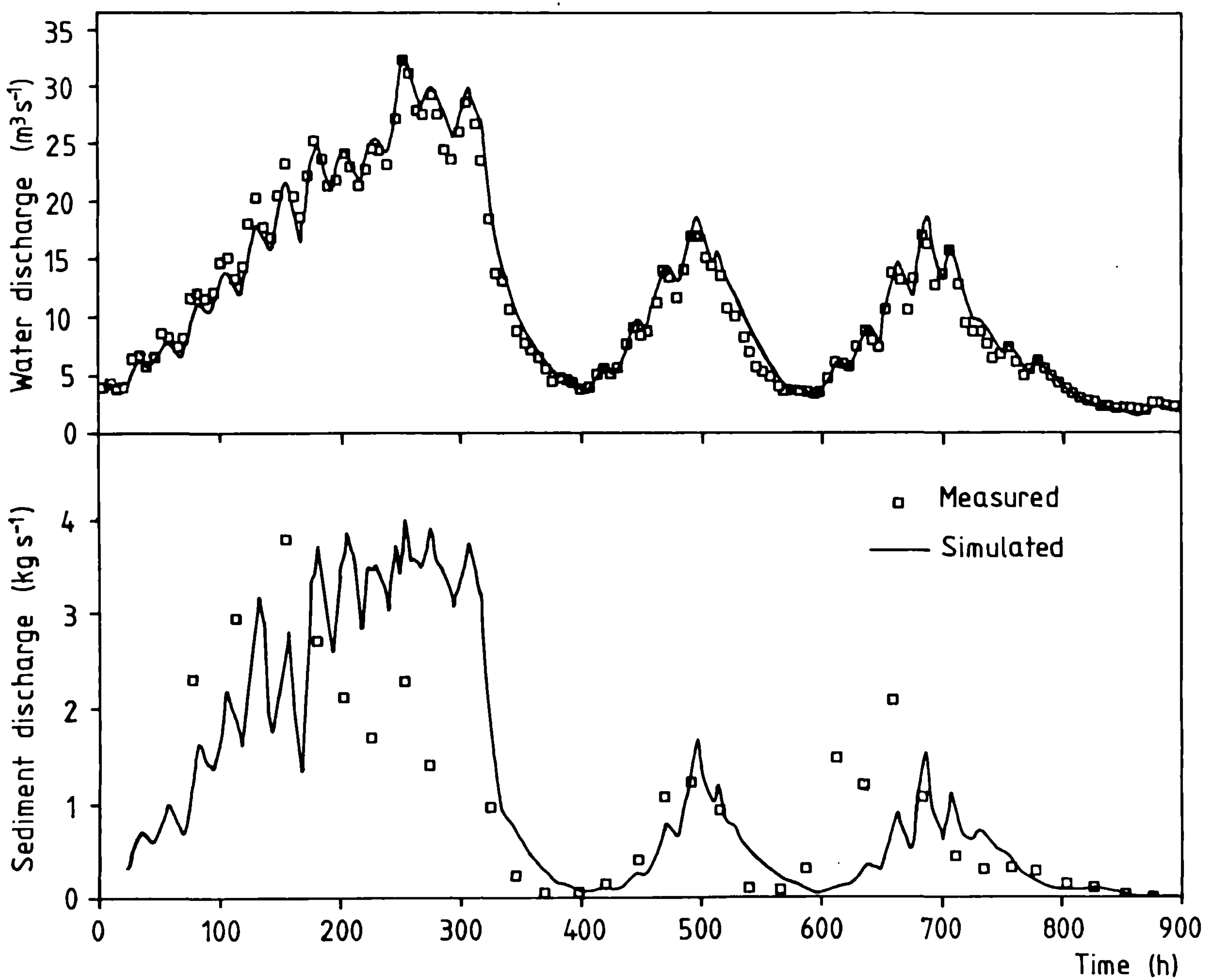

Fig. 8.3 Simulated and measured water and sediment discharges at the bed load trap in the East Fork River.

8.5 APPLICATION OF SHESED

For the SHESED simulations the same distance step was used as for the SHE simulations but the time step was increased to 1 h (this reduced the computational time without affecting the accuracy). Eleven particle size classes were used with size fraction boundaries at 0.062, 0.125, 0.25, 0.5, 1, 2, 4, 8, 16, 32 and 64 mm. Bed material size distributions, as measured at the start of the study period, were input for each computational node. The daily measurements of the sediment inflow to the reach were used as the upstream boundary condition. The sediment inflow was determined by adding the bed load and the product of the suspended load concentration and water discharge. However, the particle size distribution of the inflow could not be calculated without making assumptions, as the suspended load size distribution was not available. Nevertheless, the proportion of the suspended load less than 0.062 mm was known and Emmett (1981) states that for the East Fork River there is no significant quantity of suspended sediment larger that 0.5 mm. With the assumption that the suspended load larger that 0.062 mm is distributed evenly between the three size classes 0.062 - 0.125 mm, 0.125 - 0.25 mm, and 0.25 - 0.5 mm, the particle size distribution could be determined. This assumption should have a minor effect on the downstream sediment discharge and on changes in bed elevations other than at the upstream part of the reach. The initial sediment transport rates throughout the study reach were assumed to be zero; an alternative assumption of initial transport rates of 0.01 kg s^{-1} had an insignificant effect on the response. The bed porosity was taken as 0.4. The active width of the channel at the 41 computational nodes was set equal to that given in Meade et al. (1980) and ranged between 11.5 and 30.5 m. The depth of loose bed material at every section is needed as input data and for the East Fork River should probably correspond to the depths of the storage areas described in Section 8.2. However, the position and depth of these storage areas was not easy to establish from the numerical data; for example, the position of the storage areas is not clear from Fig. 8.2 which shows the mean bed elevations for the start of the study period. This is probably an instance where first hand knowledge of the river would have been very useful. The representation of these storage areas in the model was made more difficult because the variation with depth of the bed material size distribution was not available. The depths of loose bed material used in the model were calculated as the difference between the mean bed elevations for each section at the start of the study period and the mean channel floor elevations calculated from data in Meade et al. (1980). The floor elevation is defined by Meade et al. as

> "...the elevation of the 'floor' below the more movable material on the bed of the river. In most places, this floor was determined by probing the bed with a steel rod and measuring the thickness of material above the level of resistance where the rod could no longer be forced into the bed. This level of resistance usually consisted of coarse gravel or bedrock."

The only calibration a SHESED channel model needs involves choosing between the Engelund-Hansen equation and the Ackers-White equation (with or without the Day modification) for predicting sediment transport capacity. For this application the Engelund-Hansen equation gave the best results. The observed and simulated sediment discharges at the downstream section over the 37.5-day simulation period are shown in Fig. 8.3. Both simulated and measured values comprise bed load and suspended load (including material smaller than 0.062 mm). The figure shows that the sediment discharge is simulated well for parts of the simulation period but with a large discrepancy occurring around the peak water discharge. The simulated changes in bed elevations along the study reach are compared with the measured values in Fig. 8.4. The model simulates the general trend of erosion and deposition for part of the reach and the simulated and measured depths of erosion and deposition are of the same order of magnitude throughout the reach, except at the upstream boundary. However, at a number of sections the model predicts significant depths of erosion where deposition was measured (and vice versa). The large depths of simulated deposition at the upstream end of the reach represent the inability of the model to simulate transport of all the sediment influx given as the upstream boundary condition. This may have been aggravated by the assumption made for distributing the suspended load among the particle size classes.

8.6 DISCUSSION

The application of the SHESED channel sub-component to the East Fork River has indicated that the model is able to predict much of the observed transport behaviour of a complex alluvial river. However, Figs. 8.3 and 8.4 show that within the overall

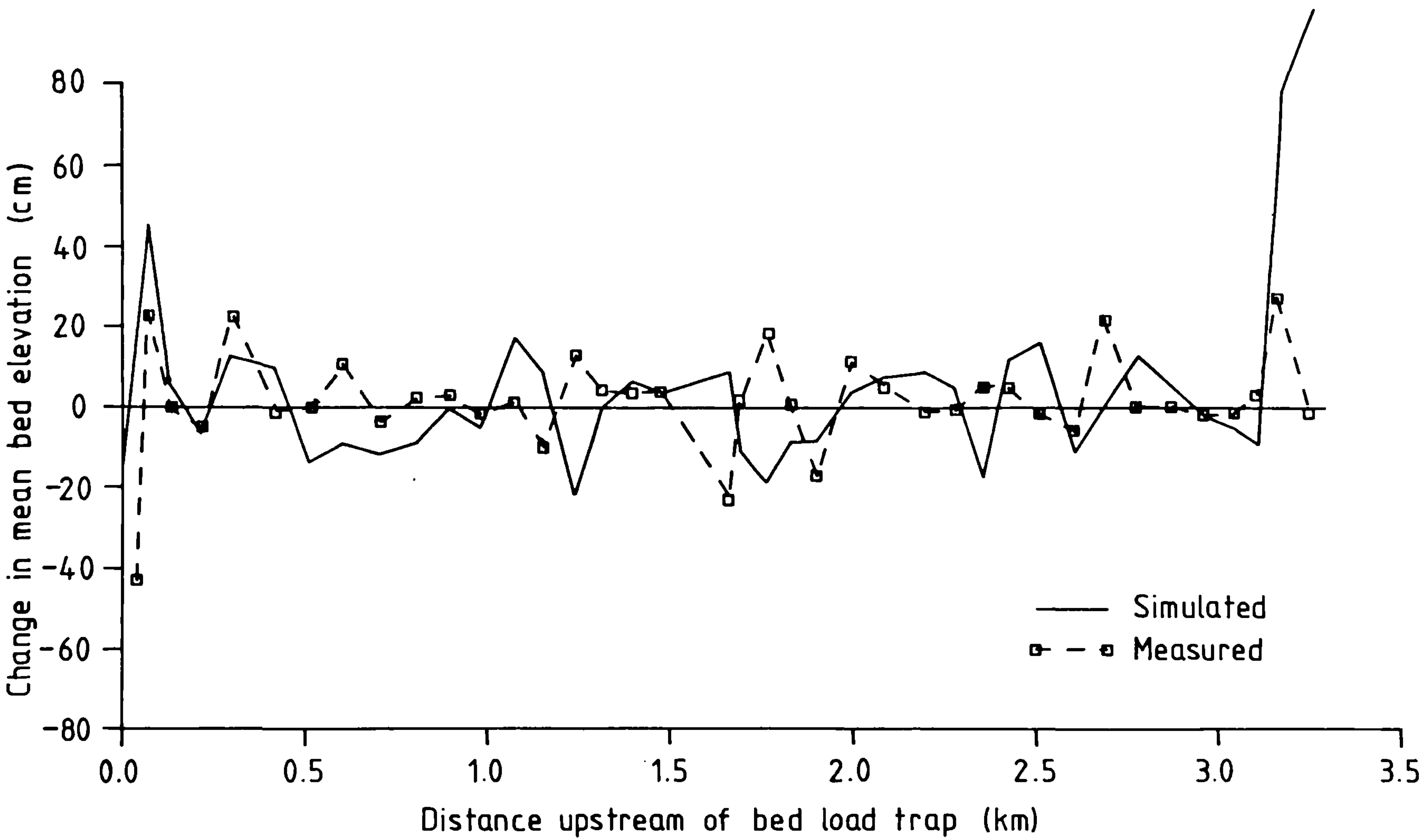

Fig. 8.4 Simulated and measured changes in mean bed elevation over the 37.5-day simulation period for the 3.3-km study reach of the East Fork River.

good simulation, large local errors in the simulated response occurred. The possible reasons for these discrepancies are discussed below in terms of model and data deficiencies.

8.6.1 Model Deficiencies

Figure 8.3 shows that the measured sediment discharge at the bed load trap peaked four days prior to the peak water discharge. The simulated sediment discharge, however, peaked about the same time as the peak water discharge, although simulated sediment transport rates of magnitudes about the same as the peak measured value had occurred for two days following the peak measured sediment discharge. The sediment supply effects which lead to the wavelike motion of bed material (see Section 8.2) may explain why the measured water and sediment discharges did not peak at the same time. SHESED should be able to model the wavelike motion of bed material if the water is simulated well, if the transport capacity for the individual particle size classes is correctly calculated and if there is sufficient spatial detail in the model. Figures 8.2 and 8.3 suggest that the water discharges and depths are correctly modelled. The accuracy of the sediment transport capacity equation can be assessed if it is applied to a reach with suspended and bed load measurements where there is an excess of sediment supply for all size fractions. This was not done for this study and therefore an evaluation independent of supply effects of the transport equation for the East Fork River is not available. The spatial detail in the East Fork River model depended on the availability of data and is therefore discussed in Section 8.6.2. Other deficiencies in the model which may account for the errors in the simulation include the one-dimensional representation of the river with the idealised trapezoidal cross section, the simplified active depth procedure (discussed in Section 5.6), and the lack of feedback from the sediment model to the hydraulic model (simulated changes in bed elevation have no effect on simulated hydraulic variables).

8.6.2 Data Deficiencies

Although the East Fork River data set is extensive, there appear to be no data concerning the change in bed material size distribution with depth other than through the channel floor measurements (Section 8.5) which concern coarse gravel and bed rock; therefore the effect of any initial bed material layering cannot be included. This may be an important deficiency. Andrews (1979) states:

> "... R. H. Meade (written commun., 1977) systematically measured the thickness of sand size bed material in the East Fork River channel for a distance of nearly 2.5 miles upstream from the bedload trap. The streambed was normally stratified by sediment size. The surface layer, approximately 0.3 foot thick, was significantly finer - median diameter = 0.5 mm - than the underlying material - median diameter = 1 - 2 mm."

If there was a layer of finer sand above a coarse layer at the start of the 1979 snowmelt runoff season, then this finer material may have been transported out of the reach during the rising limb of the hydrograph resulting in an early peak in the sediment discharge. Once all fine material has been entrained and transported out of the reach, the sediment discharge may be reduced, even with an increasing water discharge, because only material from the lower coarse sand and gravel layer is now available to be entrained. This hypothesis ties in with the measured sediment transport rates as shown in Fig. 8.3.

The 1979 measurement sections may have been too far apart to allow simulation of the wavelike movement of sediment. This is illustrated by Fig. 8.4 which shows the observed change in mean bed elevation along the reach over the 37.5-day simulation period. From this figure it can be seen that the variation in the measured change in mean bed elevation between adjacent measurement sections could be very large; for example at the first section upstream of the bed load trap 43 cm of erosion was measured, whereas at the next section the measurements show 23 cm of deposition. Such a large variation suggests that the measurements made at a cross section may not be representative of the associated computational link. Therefore a closer spacing of measurement sections (and therefore computational nodes) may have resulted in an improved simulation.

Measurement errors are unlikely to be the cause of the discrepancies between measured and simulated responses as bed elevations were reported to be accurate to 2 - 3 cm, and the bed load trap is thought to be one of the most accurate measures of bed load transport. However, the infrequency of the sediment transport data (at best once a day) in combination with the large daily variation in water discharge (and therefore presumably sediment discharge) may give a misleading picture of the actual sediment discharge graph. A problem associated with the use of the daily measurements of sediment transport is the specification of the upstream sediment influx. The daily measurements of upstream sediment inflow were taken at the time of the daily peak water discharge, and therefore, as the SHESED model uses linear interpolation between measured values to produce a continuous influx, the total sediment influx to the reach in the model may be greater than the actual influx. This may have contributed to the large predicted depths of deposition just downstream of the upstream boundary.

8.6.3 Previous Attempts at Modelling the East Fork River

Previous attempts at modelling the East Fork River have been reported by Bennett and Nordin (1977) and Borah et al. (1982b). As these were for a different snowmelt season (1975) a direct comparison of results with SHESED is not possible. However, the results from these models are no more accurate than those of SHESED, despite their added complexity and requirement for more calibration. For example, Fig. 8.5 shows a comparison of Borah et al.'s simulated bed load discharge with the measured discharge, and Fig. 8.6 shows a comparison of Bennett and Nordin's simulated change in bed elevation with the measured change.

In conclusion, the sediment response for the 1979 snowmelt runoff season in the East Fork River is in general well simulated but does contain some large errors. These errors are of a magnitude similar to those produced when two existing alluvial channel models were applied to the same river. The application suggests that the SHESED channel component, although containing various simplifications, is appropriate for simulating sediment routing in alluvial channels, but may not yield accurate results where complex supply/storage effects exist.

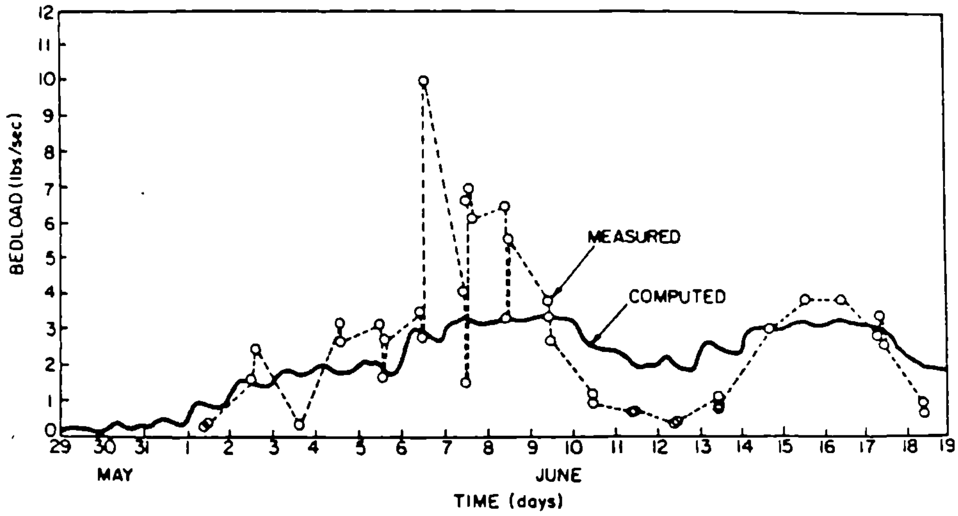

Fig. 8.5 Simulated and measured bed load discharges for the 1975 snowmelt runoff season in the East Fork River using the Borah et al. model. (From Borah et al., 1982b.)

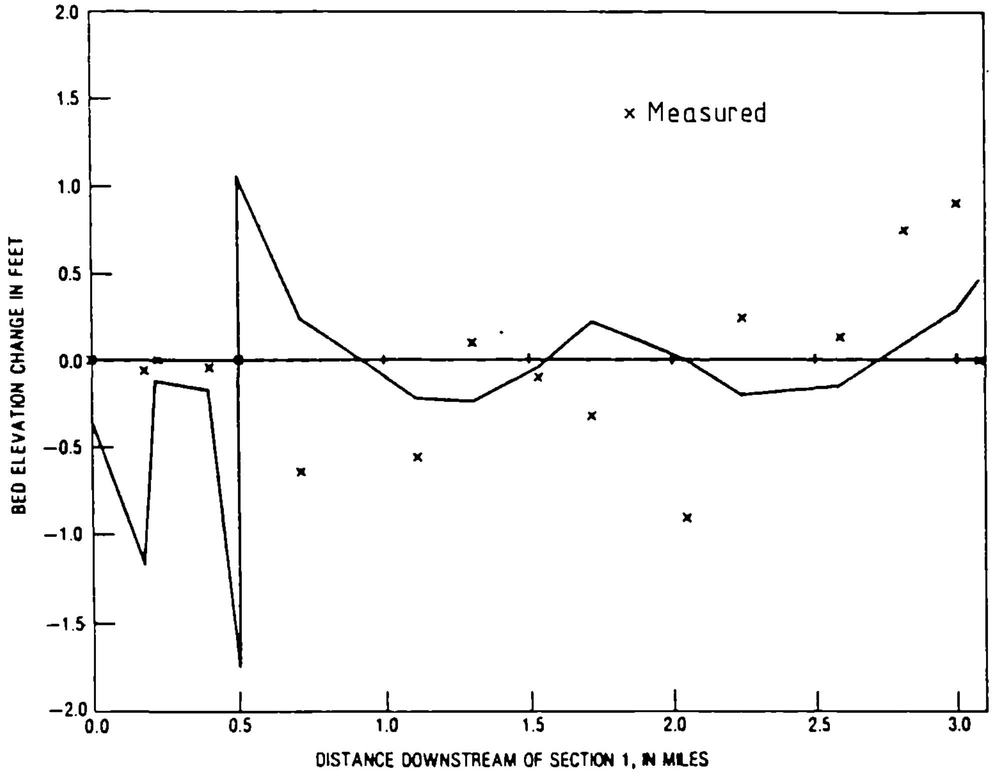

Fig. 8.6 Simulated and measured changes in bed elevation for the 1975 snowmelt runoff season in the East Fork River using the Bennet and Nordin model. (From Bennett and Nordin, 1977.)

CHAPTER 9 - CONCLUSIONS AND RECOMMENDATIONS FOR FURTHER RESEARCH

9.1 SUMMARY

A physically-based, distributed sediment yield component has been developed for the SHE hydrological modelling system. This new component models the hillslope processes of soil detachment by raindrop impact, leaf drip impact and overland flow, and transport by overland flow. If the eroded soil reaches a river system it is routed downstream along with any mobilised river bed material. Deposition on land or in a river is simulated and the river bed material size distribution continuously updated. The component has been tested at the small scale with experimental data from rainfall simulator plots and with laboratory flume data exhibiting armouring. At a larger scale, the component has been applied to a rangeland sub-catchment in Idaho, to two small agricultural catchments in Iowa, and to the East Fork River, Wyoming.

9.2 MAIN ACHIEVEMENTS

(1) Based on the work of Styczen and Høgh-Schmidt (1988), an equation for soil detachment by raindrop and leaf drip impact has been developed (equation 4.6). This has been successfully tested using data for a field plot with a range of soybean canopy covers and rainfall intensities.

(2) The soil detachment coefficient for raindrop impact has been evaluated for a range of soil types (Table 4.3). The variation in value of this coefficient is consistent with that

which may be expected from a consideration of the physics of a soil's resistance to detachment.

(3) A finite difference solution of the sediment continuity equation in two space dimensions has been formulated (Section 4.5).

(4) A computationally inexpensive channel bed armouring algorithm has been developed (Section 5.5). Application of the procedure to data from a laboratory study showed that the algorithm was able to predict the trend of decreasing sediment transport rate with time caused by armouring.

(5) A procedure for routing wash and bed material loads in a channel system was developed (Section 5.4). This is based on a four-point finite difference solution of the sediment continuity equation in one space dimension.

(6) The hillslope sub-component of SHESED was applied to rainfall simulator plots with a variety of surface conditions (Section 6.6). The applications showed that two sets of raindrop and overland flow soil detachment coefficients could be used to simulate a range of soil surface conditions, with the highest coefficient values corresponding to tilled soils.

(7) To investigate scale effects, parameters calibrated at the rainfall simulator plot scale were transferred to a 1-ha rangeland sub-catchment (Section 6.8). With no further calibration, the catchment response for four events was poorly simulated for both water and sediment. However, with reasonable variations in the antecedent soil moisture content but no variation in plot calibrated sediment parameters, the sediment yield for two of the four events could be successfully simulated. The applications suggest that parameter transfer is feasible if the sediment yield

characteristics at the different scales are similar.

(8) Further applications of the hillslope sub-component were carried out for two small agricultural catchments in Iowa (Chapter 7). The water and sediment responses could be simulated well for three short, high intensity storms, although some smaller events could not be simulated. The simulated sediment responses were at least as accurate as those achieved by two existing distributed soil erosion models.

(9) The channel sub-component was applied to the East Fork River, Wyoming (Chapter 8). Although the complex sediment storage/supply effects could not be reproduced completely, the simulated response was nevertheless of similar accuracy to that achieved by two existing alluvial river models.

The new component is considered to be a valuable contribution to sediment yield modelling as a physically-based approach is used for both the hillslope and channel phases of the catchment sediment system, within the framework of an advanced hydrological modelling system.

9.3 MAIN LIMITATIONS OF SHESED

The SHESED component is designed to be generally applicable in the manner of a modelling system component; however, some processes are either not included in the component or are only accounted for indirectly. The sediment component is therefore limited in its applicability to situations where the main processes affecting sediment yield are detachment of soil by raindrop impact and overland flow, and transport in overland and channel flow. It is inappropriate to situations where processes such as gullying, mass movements, wind erosion and bank erosion are significant. In addition, some soil conservation practices may not be able to be explicitly included within a model (e.g. terraces).

The changes in land surface elevation and river bed elevation predicted by SHESED are not fed back into the SHE model. Therefore poor results may occur when severe erosion or deposition has a significant effect on the hydraulic conditions. The reasons for neglecting these effects are that their inclusion would greatly increase the complexity of the calibration process for models built from both the SHE and SHESED, and that the spatial extent of severe erosion and deposition is likely to be too localised to be significant at the scale of the SHE's grid network.

Another limitation of the model arises from the use of the empirical equations which are needed to predict some sub-processes, for example the sediment transport capacity equations, the water depth correction factor (equation 4.5) and the sediment velocity predictor (equation 5.5). These equations should really be used only within the range of conditions used in their formulation; however, for most real-world applications it is currently necessary to extrapolate the functions beyond this range. Problems with the evaluation of parameter values (e.g. lack of field data) will mean that sensitivity analyses for both parameter values and extrapolated empirical formulae are necessary.

The hillslope erosion routines of SHESED require soil detachment coefficients for raindrop impact and overland flow (K_R and K_F respectively). Until sufficient knowledge is acquired concerning variations of these coefficients with soil properties, both coefficients will need to be calibrated. This therefore limits the potential for forecasting soil erosion to situations where K_R and K_F values can be determined from previously recorded events, from small scale experiments or by transfer of calibrated parameters from hydrologically similar gauged catchments.

Further restrictions in the practical application of SHESED arise from the requirements for large computing and data resources; a problem of particular relevance for extended, catchment-scale simulations. This is important as many current design methods require predictions of average annual soil erosion or sediment yield.

9.4 RECOMMENDATIONS FOR FURTHER RESEARCH

(1) With the current SHE framework and available process equations there is limited scope for improvements to SHESED. Perhaps the two most likely modifications are: (a) solving the hillslope sediment continuity equation by size fraction using the available hillslope process equations which account for particle size and density effects; and (b) modifying the model deposition process so that particle fall velocities are taken into consideration.

(2) Further test applications of SHESED are necessary, particularly in the three areas identified below.

(a) The prediction of the spatial distribution of erosion/deposition is often stated as one of the main benefits of using models such as SHESED. However, there appear to have been no verification tests of the predicted spatial distribution of erosion/deposition. Test applications in this area are required but suitable data do not seem to be available.

(b) The applicability of SHESED to catchments with areas greater than a few hectares needs to be verified. This will involve the first test of a SHESED model with both channel and hillslope components.

(c) The applications of SHESED reported in this thesis have not followed the split-sample calibration then validation approach. Suitable data sets need to be identified and applications run.

(3) Research needs to be carried out to try to relate the two soil detachment coefficients to measurable soil properties (e.g. soil shear strength).

(4) Research needs to be done on the calibration procedure for SHESED models. Formal sensitivity analyses need to be performed for a range of conditions, suitable parameter optimisation techniques need to be identified for the soil detachment coefficients with associated research into possible problems in parameter identification (e.g. see Blau et al. (1988) for the first investigation of the parameter identification problem in physically-based soil erosion models).

(5) Further testing is required of the numerical solution of the sediment continuity equation. Analytical solutions to a simplified sediment continuity equation have been presented by Lane et al. (1988) and it is possible that these may be able to be used to test the numerical solution used in SHESED for some simplified cases.

(6) SHESED does not explicitly consider rill processes. A topic worthy of further research is a numerical experiment into the necessity of considering rill geometry for catchment scale

models. The results from a model which uses predetermined rill geometry and density could be compared with those from SHESED for a range of spatial scales. It is possible that above a certain spatial scale the models will predict the same response; if this is not found to be the case, the tests may be useful for determining a correction factor to apply to SHESED overland flow erosion for use where rills are significant.

(7) Sediment storage and the effects of consolidation with time of stored sediment need to be introduced in SHESED. For hillslopes, the SD term in equation 4.12 can be used to 'carry over' loose material from the end of one event to the beginning of the next, although some form of consolidation factor needs to be introduced. For channels the specification of the channel bed material thickness and the active and parent layer size distributions already allows for sediment storage although this may not permit sufficient detail in the model.

(8) Many current design methods require annual average values of soil erosion and sediment yield, whereas models such as SHESED are more suited to predicting the response from single design storms. Although SHESED could be run for extended periods, it may prove more appropriate to develop design methods based on the response from particularly erosive storms and not annual average values.

Most of the above research recommendations will be hampered by the scarcity of data; the major restrictions on the further development of physically-based sediment yield models are the lack of data and the inadequacies in the process equations.

REFERENCES

Abbott, M.B., Bathurst, J.C., Cunge, J.A., O'Connell, P.E., and Rasmussen, J. 1986a. An introduction to the European Hydrological System - Système Hydrologique Européen, "SHE", 1: History and philosophy of a physically-based, distributed modelling system. J. Hydrol., 87, 45-59.

Abbott, M.B., Bathurst, J.C., Cunge, J.A., O'Connell, P.E., and Rasmussen, J. 1986b. An introduction to the European Hydrological System - Système Hydrologique Européen, "SHE", 2: Structure of a physically-based, distributed modelling system. J. Hydrol., 87, 61-77.

Ackers, P. and White, W.R. 1973. Sediment transport: new approach and analysis. J. Hydraul. Div., Am. Soc. Civ. Engrs., 99(HY11), 2041-2060.

Al-Durrah, M.M. and Bradford, J.M. 1982. Parameters for describing soil detachment due to single waterdrop impact. Soil Sci. Soc. Am. J., 46, 836-840.

Alonso, C.V. 1980. Selecting a formula to estimate sediment transport capacity in nonvegetated channels. In: Knisel, W.G. (editor) CREAMS: A field-scale model for chemicals, runoff, and erosion from agricultural management systems. US Dept. Agric., Conservation Research Rep. no. 26, 426-439.

Alonso, C.V. and DeCoursey, D.G. 1985. Small watershed model. In: DeCoursey, D.G. (editor) Proceedings of the natural resources modeling symposium, US Dept. Agric., ARS-30, 40-46.

Alonso, C.V., Neibling, W.H., and Foster, G.R. 1981. Estimating sediment transport capacity in watershed modeling. Trans. Am. Soc. Agric. Engrs., 24(5), 1211-1220, 1226.

Andrews, E.D. 1979. Scour and fill in a stream channel, East Fork River, western Wyoming. US Geol. Surv. Prof. Pap. 1117, 49pp.

Andrews, E.D. 1983. Entrainment of gravel from naturally sorted riverbed material. Geol. Soc. Am. Bull., 94, 1225-1231.

Ariathurai, R. and Arulanandan, K. 1978. Erosion rates of cohesive soils. J. Hydraul. Div., Am. Soc. Civ. Engrs., 104(HY2), 279-283.

Armstrong, C.L. and Mitchell, J.K. 1987. Transformations of rainfall by plant canopy. Trans. Am. Soc. Agric. Engrs., 30(3), 688-696.

Bagnold, R.A. 1966. An approach to the sediment transport problem from general physics. US Geol. Surv. Prof. Pap. 422-I.

Bathurst, J.C. and Wicks, J.M. 1988. Framework for erosion and sediment yield modelling. Proc. NATO Advanced Study

Institute, Recent advances in the modeling of hydrologic systems, Sintra, Portugal, July.

Bathurst, J.C., Graf, W.H., and Cao, H.H. 1987. Bed load discharge equations for steep mountain rivers. In: Thorne, C.R., Bathurst, J.C., and Hey, R.D. (editors) Sediment transport in gravel-bed rivers, Wiley, Chichester, 453-477.

Beasley, D.B. and Huggins, L.F. 1981. ANSWERS users manual. US Environmental Protection Agency Rep. EPA-905/9-82-001, 54pp.

Beasley, D.B., Huggins, L.F., and Monke, E.J. 1980. ANSWERS: a model for watershed planning. Trans. Am. Soc. Agric. Engrs., 23, 938-944.

Bennett, J.P. 1974. Concepts of mathematical modeling of sediment yield. Wat. Resour. Res., 10(3), 485-492.

Bennett, J.P. and Nordin, C.F. 1977. Simulation of sediment transport and armouring. Hydrol. Sci. Bull., 22(4), 555-569.

Bettess, R. and White, W.R. 1981. Mathematical simulation of sediment movement in streams. Proc. Instn. Civ. Engrs., 71(2), 879-892.

Beven, K.J. and O'Connell, P.E. 1982. On the role of physically-based distributed modelling in hydrology. Institute of Hydrology, Wallingford, Rep. no. 81, 36pp.

Bishop, A.A., Simons, D.B., and Richardson, E.V. 1965. Total bed-material transport. J. Hydraul. Div., Am. Soc. Civ. Engrs., 91(HY2), 175-191.

Blau, J.B., Woolhiser, D.A., and Lane, L.J. 1988. Identification of erosion model parameters. Trans. Am. Soc. Agric. Engrs., 31(3), 839-845, 854.

Borah, D.K., Alonso, C.V., and Prasad, S.N. 1982a. Routing graded sediments in streams: formulations. J. Hydraul. Div., Am. Soc. Civ. Engrs., 108(HY12), 1486-1503.

Borah, D.K., Alonso, C.V., and Prasad, S.N. 1982b. Routing graded sediments in streams: applications. J. Hydraul. Div., Am. Soc. Civ. Engrs., 108(HY12), 1504-1517.

Bradford, J.M., Ferris, J.E., and Remley, P.A. 1987a. Interrill soil erosion processes: I. Effect of surface sealing on infiltration, runoff, and soil splash detachment. Soil Sci. Soc. Am. J., 51, 1566-1571.

Bradford, J.M., Ferris, J.E., and Remley, P.A. 1987b. Interrill soil erosion processes: II. Relationship of splash detachment to soil properties. Soil Sci. Soc. Am. J., 51, 1571-1575.

Bubenzer, G.D. 1970. Effect of drop size and impact velocity on the detachment of soils under simulated rainfall. PhD thesis, Univ. of Illinois at Urbana-Champaign, 120pp.

Caine, N. 1980. The rainfall intensity-duration control of shallow landslides and debris flows. Geogr. Ann. 62A(1-2), 23-27.

Carter, C.E., Greer, J.D., Braud, H.J., and Floyd, J.M. 1974. Raindrop characteristics in south central United States. Trans. Am. Soc. Agric. Engrs., 17, 1033-1037.

Chen, Y.H. 1979. Water and sediment routing in rivers. In: Shen, H.W. (editor) Modeling of Rivers, Wiley, New York, 10.1-10.97.

Chow, V.T. 1959. Open-channel hydraulics. McGraw-Hill, New York, 680pp.

Cole, G.W. 1985. Wind erosion modeling. In: DeCoursey, D.G. (editor) Proceedings of the natural resources modeling symposium, US Dept. Agric., ARS-30, 59-63.

Collins, B.D. and Dunne, T. 1986. Erosion of tephra from the 1980 erouption of Mount St. Helens. Geol. Soc. Am. Bull., 97, 896-905.

Cruse, R.M. and Larson, W.E. 1977. Effect of soil shear strength on soil detachment due to raindrop impact. Soil Sci. Soc. Am. J., 41, 777-781.

Davis, S.S. 1978. Deposition of nonuniform sediment by overland flow on concave slopes. MS thesis, Purdue Univ., West Lafayette, 137pp.

Dawdy, D.R. and Vanoni, V.A. 1986. Modeling alluvial channels. Wat. Resour. Res., 22(9), 71S-81S.

Day, T.J. 1980. A study of the transport of graded sediments. Hydraulics Research Station, Wallingford, Rep. no. IT 190.

DeCoursey, D.G. 1982. ARS' small watershed model. Am. Soc. Agric. Engrs. Pap. no. 82-2094.

Devaurs, M. and Gifford, G.F. 1984. Variability of infiltration within large runoff plots on rangelands. J. Range Management, 37(6), 523-528.

Dunne, T. and Leopold, L.B. 1978. Water in environmental planning. Freeman, San Francisco, 818pp.

Einstein, H.A. 1950. The bed-load function for sediment transportation in open channel flows. Technical Bulletin no. 1026, US Dept. Agric., Soil Conservation Service, Reprinted in: Shen, H.W. (editor and publisher) Sedimentation, Fort Collins, Colorado, 1972, Appendix B.

Emmett, W.W. 1981. Measurement of bed load in rivers. In: Erosion and sediment transport measurement, Intl. Ass. Hydrol. Sci. Publ. no. 133, 3-15.

Emmett, W.W., Myrick, R.M., and Meade, R.H. 1980. Field data describing the movement and storage of sediment in the East Fork River, Wyoming. Part 1. River hydraulics and sediment transport, 1979. US Geol. Surv. Open-File Rep. 80-1189.

Engelund, F. and Fredsøe, J. 1976. A sediment transport model for straight alluvial channels. Nordic Hydrology, 7, 293-306.

Engelund, F. and Hansen, E. 1967. A monograph on sediment transport in alluvial streams. Teknisk Forlag, Copenhagen, 65pp.

Engman, E.T. 1986. Roughness coefficients for routing surface runoff. J. Irrig. Drain. Engrg., Am. Soc. Civ. Engrs., 112(1), 39-53.

Epema, G.F. and Riezebos, H.Th. 1983. Fall velocity of waterdrops at different heights as a factor influencing erosivity of simulated rain. In: de Ploey, J. (editor) Rainfall simulation, runoff and soil erosion, Catena Supplement 4, 1-17.

Finney, H.J. 1984. The effect of crop covers on rainfall characteristics and splash detachment. J. Agric. Engrg. Res. 29, 337-343.

Flaxman, E.M. 1972. Predicting sediment yield in western United States. J. Hydraul. Div., Am. Soc. Civ. Engrs., 98(HY12), 2073-2085.

Fleming, G. 1977. The sediment problem. Univ. of Strathclyde, Glasgow.

Fleming, G. 1983/84. River basin model for water and sediment resource assessment. User guide volumes 1 and 2. Univ. of Strathclyde, Glasgow.

Foster, G.R. 1982. Modeling the erosion process. In: Haan, C.T., Johnson, H.P., and Brakensiek, D.L. (editors) Hydrologic modeling of small watersheds, ASAE Monograph no. 5, Am. Soc. Agric. Engrs., St. Joseph, Michigan, 297-380.

Foster, G.R. and Smith, R.E. 1985. A dynamic erosion concept. In: DeCoursey, D.G. (editor) Proceedings of the natural resources modeling symposium, US Dept. Agric., ARS-30, 434-437.

Foster, G.R., Lane, L.J., Nowlin, J.D., Laflen, J.M., and Young, R.A. 1980. A model to estimate sediment yield from field-sized areas: development of model. In: Knisel, W.G. (editor) CREAMS: A field-scale model for chemicals, runoff, and erosion from agricultural management systems. US Dept. Agric., Conservation Research Rep. no. 26, 36-64.

Gessler, J. 1971. Beginning and ceasing of sediment motion. In: Shen, H.W. (editor and publisher) River mechanics, Fort Collins, Colorado, 7.1-7.22.

Gilley, J.E. and Finkner, S.C. 1985. Estimating soil detachment caused by raindrop impact. Trans. Am. Soc. Agric. Engrs., 28(1), 140-146.

Gilley, J.E., Woolhiser, D.A., and McWhorter, D.B. 1985. Interrill soil erosion - Part 1: development of model equations. Trans. Am. Soc. Agric. Engrs., 28(1), 147-153, 159.

Glymph, L.M. 1957. Importance of sheet erosion as a source of sediment. Trans. Am. Geophys. Union, 38, 903-907.

Graf, W.H. 1984. Hydraulics of sediment transport. Water Resources Publ., Littleton, Colorado, 513pp.

Grissinger, E.H., Murphey, J.B., and Coleman, N.L. 1985. Planned gully research at the USDA Sedimentation Laboratory. In: DeCoursey, D.G. (editor) Proceedings of the natural resources modeling symposium, US Dept. Agric., ARS-30, 475-478.

Gunn, R. and Kinzer, G.D. 1949. Terminal velocity of water droplets in stagnant air. J. Meteor., 6(4), 243-248.

Gurnell, A.M. 1987. Suspended sediment. In: Gurnell, A.M. and Clark, M.J. (editors) Glacio-fluvial sediment transfer, Wiley, Chichester, 305-354.

Guy, B.T., Dickinson, W.T., and Rudra, R.P. 1987. The roles of rainfall and runoff in the sediment transport capacity of interrill flow. Trans. Am. Soc. Agric. Engrs., 30(5), 1378-1386.

Hagen, L.J., Lyles, L., and Dickerson, J.D. 1975. Soil detachment from clods by simulated rain and hail. Trans. Am. Soc. Agric. Engrs., 18, 540-543.

Hamlett, J.M., Baker, J.L., and Johnson, H.P. 1987. Size distribution of sediment transported within and from small agricultural watersheds. Trans. Am. Soc. Agric. Engrs., 30(4), 998-1004.

Hamlett, J.M., Baker, J.L., Kimes, S.C., and Johnson, H.P. 1984. Runoff and sediment transport within and from small agricultural watersheds. Trans. Am. Soc. Agric. Engrs., 27, 1355-1363, 1369.

Holly, F.M. and Karim, M.F. 1983. Computer simulation prognosis for the degradation of the Missouri River between Gavins Point Dam and Iowa's southern border. IIHR Rep. no. 267, Iowa Institute of Hydraulic Research, Univ. of Iowa, Iowa City, Iowa.

Holly, F.M. and Preissmann, A. 1977. Accurate calculation of transport in two dimensions. J. Hydraul. Div., Am. Soc. Civ. Engrs., 103(HY11), 1259-1277.

Holtan, H.N. 1961. A concept for infiltration estimates in watershed engineering. ARS-41-51, Agricultural Research Service, US Dept. Agric., 25pp.

Hudson, N. 1981. Soil conservation. Batsford, London, 324pp.

HEC. 1977. HEC-6 Scour and deposition in rivers and reservoirs users manual. Hydrologic Engineering Center, US Army Corps of Engrs.

Johnson, C.W. and Hanson, C.L. 1976. Sediment sources and yields from sagebrush rangeland watersheds. Proc. 3rd Interagency Sedimentation Conf., Denver, Colorado, 1.71-1.80.

Johnson, C.W., Savabi, M.R., and Loomis, S.A. 1984. Rangeland erosion measurements for the USLE. Trans. Am. Soc. Agric. Engrs., 27(5), 1313-1320.

Johnson, H.P. and Baker, J.L. 1982. Field-to-stream transport of agricultural chemicals and sediment in an Iowa watershed. Part I: data base for model testing (1976-1978). Dept. of Agric. Engrg., Iowa State Univ., Ames, Iowa. Rep. prepared for US Environmental Protection Agency, Athens, Georgia (EPA-600/3-82-032), 577pp.

Jones, J.A.A. 1987. The effects of soil piping on contributing areas and erosion patterns. Earth Surf. Process. Landf., 12, 229-248.

Julien, P.Y. and Frenette, M. 1986. Scale effects in predicting soil erosion. In: Drainage basin sediment delivery, Intl. Ass. Hydrol. Sci. Publ. no. 159, 253-259.

Julien, P.Y. and Simons, D.B. 1985. Sediment transport capacity of overland flow. Trans. Am. Soc. Agric. Engrs., 28(3), 755-762.

Karim, M.F. and Kennedy, J.F. 1981. Computer-based predictors for sediment discharge and friction factor of alluvial streams. IIHR Rep. no. 242, Iowa Institute of Hydraulic Research, Univ. of Iowa, Iowa City, Iowa.

Karim, M.F. and Kennedy, J.F. 1982. IALLUVIAL: A computer-based flow- and sediment-routing model for alluvial streams and its application to the Missouri River. IIHR Rep. no. 250, Iowa Institute of Hydraulic Research, Univ. of Iowa, Iowa City, Iowa.

Khanbilvardi, R.M., Rogowski, A.S., and Miller, A.C. 1983. Modeling upland erosion. Wat. Resour. Bull., 19(1), 29-35.

Kirkby, M.J. and Morgan, R.P.C. (editors) 1980. Soil erosion. Wiley, Chichester, 312pp.

Knisel, W.G. (editor) 1980. CREAMS: A field-scale model for chemicals, runoff, and erosion from agricultural management systems. US Dept. Agric., Conservation Research Rep. no. 26, 643pp.

Komura, S. 1976. Hydraulics of slope erosion by overland flow. J. Hydraul. Div., Am. Soc. Civ. Engrs., 102(HY10), 1573-1586.

Laflen, J.M., Thomas, A.W., and Welch, R. 1987. Cropland experiments for the WEPP project. Am. Soc. Agric. Engrs. Pap. no. 87-2544.

Lane, L.J., Shirley, E.D., and Singh, V.P. 1988. Modelling erosion on hillslopes. In: Anderson, M.G. (editor) Modelling geomorphological systems, Wiley, Chichester, 287-308.

Laursen, E.M. 1958. The total sediment load of streams. J. Hydraul. Div., Am. Soc. Civ. Engrs., 84(HY1), Pap. 1530.

Laws, J.O. 1941. Measurements of the fall-velocity of water-drops and raindrops. Trans. Am. Geophys. Union, 22, 709-721.

Laws, J.O. and Parsons, D.A. 1943. The relation of raindrop size to intensity. Trans. Am. Geophys. Union, 24, 452-460.

Lee, H-Y. and Odgaard, A.J. 1986. Simulation of bed armoring in alluvial channels. J. Hydraul. Engrg., Am. Soc. Civ. Engrs., 112(9), 794-801.

Leopold, L.B. and Emmett, W.W. 1976. Bedload measurements, East Fork River, Wyoming. Proc. Nat. Acad. Sci., 73(4), 1000-1004.

Leopold, L.B., Emmett, W.W., and Myrick, R.M. 1966. Channel and hillslope processes in a semiarid area, New Mexico. US Geol. Surv. Prof. Pap. 352-G.

Leopold, L.B., Wolman, M.G., and Miller, J.P. 1964. Fluvial processes in geomorphology. Freeman, San Francisco, 522pp.

Li, R-M. 1979. Water and sediment routing from watersheds. In: Shen, H.W. (editor) Modeling of rivers, Wiley, New York, 9.1-9.88.

Li, R-M., Shen, H.W., and Simons, D.B. 1973. Mechanics of soil erosion by overland flow. Proc. 15th Congress Intl. Ass. Hydraul. Res., Istanbul, Vol. 1, 437-446.

Li, R-M., Simons, D.B., Fullerton, W.T., Eggert, K.G., and Spronk, B.E. 1979. Simulation of water runoff and sediment yield from a system of multiple watersheds. Proc. 18th Congress Intl. Ass. Hydraul. Res., Cagliari, Italy, Vol. 5, 219-226.

Madej, M.A. 1982. Sediment transport and channel changes in an aggrading stream in the Puget Lowland, Washington. In: Swanson, F.J., Janda, R.J., Dunne, T., and Swanston, D.N. (editors) Sediment budgets and routing in forested drainage basins. Rep. PHW-141, US Dept. Agric., Forest Service, Pacific Northwest Forest and Range Experiment Station, 97-108.

Mantz, P.A. 1977. Incipient transport of fine grains and flakes by fluids - extended Shields diagram. J. Hydraul. Div., Am. Soc. Civ. Engrs., 103(HY6), 601-615.

Marshall, J.S. and Palmer, W.M. 1948. The distribution of raindrops with size. J. Meteor. 5, 165-166.

Mason, B.J. and Andrews, J.B. 1960. Drop-size distributions from various types of rain. Q. J. Royal Meteor. Soc., 86, 346-353.

Meade, R.H. 1985. Wavelike movement of bedload sediment, East Fork River, Wyoming. Environ. Geol. Water Sci., 7(4), 215-225.

Meade, R.H., Emmett, W.W., and Myrick, R.M. 1981. Movement and storage of bed material during 1979 in East Fork River, Wyoming, USA. In: Davies, T.R.H. and Pearce, A.J. (editors) Erosion and sediment transport in Pacific Rim steeplands, Intl. Ass. Hydrol. Sci. Publ. no. 132, 225-235.

Meade, R.H., Myrick, R.M., and Emmett, W.W. 1980. Field data describing the movement and storage of sediment in the East Fork River, Wyoming. Part II. Bed elevations, 1979. US Geol. Surv. Open-File Rep. 80-1190.

Megahan, W.F. and King, P.N. 1985. Identification of critical areas on forest lands for control of nonpoint sources of pollution. Environmental Management, 9(1), 7-18.

Meyer, L.D. and Harmon, W.C. 1984. Susceptibility of agricultural soils to interrill erosion. Soil Sci. Soc. Am. J., 48, 1152-1157.

Meyer, L.D. and Wischmeier, W.H. 1969. Mathematical simulation of the process of soil erosion by water. Trans. Am. Soc. Agric. Engrs., 12(6), 754-758, 762.

Meyer-Peter, E. and Müller, R. 1948. Formulas for bed-load transport. Proc. 2nd Meeting Intl. Ass. Hydraul. Structures Res., Stockholm, Sweden, Appendix 1, 39-64.

Misri, R.L., Garde, R.J., and Ranga Raju, K.G. 1984. Bed load transport of coarse nonuniform sediment. J. Hydraul. Engrg., Am. Soc. Civ. Engrs., 110(3), 312-328.

Monteith, J.L. 1965. Evaporation and environment. In: The state and movement of water in living organisms, Proc. 15th Symposium Society for Experimental Biology, Swansea, Cambridge University Press, London, 205-234.

Moore, R.J. 1984. A dynamic model of basin sediment yield. Wat. Resour. Res., 20(1), 89-103.

Morgan, R.P.C. 1978. Field studies of rainsplash erosion. Earth Surf. Process., 3(3), 295-299.

Morgan, R.P.C. 1985. Effect of corn and soybean canopy on soil detachment by rainfall. Trans. Am. Soc. Agric. Engrs., 28(4), 1135-1140.

Morgan, R.P.C. 1986. Soil erosion and conservation. Longman, Harlow, 298pp.

Mosconi, C.E. 1988. River-bed variations and evolution of armor layers. PhD thesis. Dept. of Civil and Environ. Engrg., Univ. of Iowa, Iowa City, Iowa.

Mosley, M.P. 1982. The effect of a New Zealand beech forest canopy on the kinetic energy of water drops and on surface erosion. Earth Surf. Process. Landf., 7, 103-107.

Mualem, Y. 1978. Hydraulic conductivity of unsaturated porous media: generalized macroscopic approach. Wat. Resour. Res., 14(2), 325-334.

Mualem, Y. and Assouline, S. 1986. Mathematical model for rain drop distribution and rainfall kinetic energy. Trans. Am. Soc. Agric. Engrs., 29(2), 494-500.

Musgrave, G.W. 1947. The quantitative evaluation of factors in water erosion: a first approximation. J. Soil Wat. Conserv., 2, 133-138.

Newson, M.D. and Leeks, G.J. 1987. Transport processes at the catchment scale. In: Thorne, C.R., Bathurst, J.C., and Hey, R.D. (editors) Sediment transport in gravel-bed rivers, Wiley, Chichester, 187-218.

Nielsen, S.A., Storm, B., and Styczen, M. 1986. Development of distributed soil erosion component for the SHE hydrological modelling system. Presented at Brit. Hydraul. Res. Ass. Intl. Conf. on Water Quality Modelling in the Inland Natural Environment, Bournemouth.

Novotny, V. 1980. Delivery of suspended sediment and pollutants from nonpoint sources during overland flow. Wat. Resour. Bull., 16(6), 1057-1065.

Onstad, C.A. and Foster, G.R. 1975. Erosion modeling on a watershed. Trans. Am. Soc. Agric. Engrs., 18, 288-292.

Osman, A.M. and Thorne, C.R. 1988. Riverbank stability analysis. I: Theory. J. Hydraul. Engrg., Am. Soc. Civ. Engrs., 114(2), 134-150.

Pall, R., Dickinson, W.T., Green, D., and McGirr, R. 1982. Impacts of soil characteristics on soil erodibility. In: Walling, D.E. (editor) Recent developments in the explanation and prediction of erosion and sediment yield, Intl. Ass. Hydrol. Sci. Publ. no. 137, 39-47.

Palmer, R.S. 1965. Waterdrop impact forces. Trans. Am. Soc. Agric. Engrs., 8(1), 69-70, 72.

Park, I., and Jain, S.C. 1987. Numerical simulation of degradation of alluvial channel beds. J. Hydraul. Engrg., Am. Soc. Civ. Engrs., 113(7), 845-859.

Park, S.W. 1981. Modeling soil erosion and sedimentation on small agricultural watersheds. PhD thesis, Univ. of Illinois at Urbana-Champaign.

Park, S.W., Mitchell, J.K., and Scarborough, J.N. 1982. Soil erosion simulation on small watersheds: a modified ANSWERS model. Trans. Am. Soc. Agric. Engrs., 25, 1581-1588.

Phillips, B.C. and Sutherland, A.J. 1985. Numerical modelling of spatial and temporal lag effects in bed load sediment transport. Proc. 21st Congress Intl. Ass. Hydraul. Res., Melbourne, 571-576.

Pickup, G. 1988. Hydrology and sediment models. In: Anderson, M.G. (editor) Modelling geomorphological systems, Wiley, Chichester, 153-215.

Piest, R.F., Bradford, J.M., and Wyatt, G.M. 1975. Soil erosion and sediment transport from gullies. J. Hydraul. Div., Am. Soc. Civ. Engrs., 101(HY1), 65-80.

Proffitt, G.T. and Sutherland, A.J. 1983. Transport of non-uniform sediments. J. Hydraul. Res., 21(1), 33-43.

Quimpo, R.G. and Brohi, A.B. 1986. On the frequency distribution of raindrop sizes. J. Irrig. Drain. Engrg., Am. Soc. Civ. Engrs., 112(2), 119-129.

Quinn, N.W. and Laflen, J.M. 1983. Characteristics of raindrop throughfall under corn canopy. Trans. Am. Soc. Agric. Engrs., 26, 1445-1450.

Reid, I., Frostick, L.E., and Layman, J.T. 1985. The incidence and nature of bedload transport during flood flows in coarse-grained alluvial channels. Earth Surf. Process. Landf., 10, 33-44.

Reid, L.M. 1982. Evaluating and mapping sources and temporary storage areas of sediment. In: Swanson, F.J., Janda, R.J., Dunne, T., and Swanston, D.N. (editors) Sediment budgets and routing in forested drainage basins. Rep. PHW-141, US Dept. Agric., Forest Service, Pacific Northwest Forest and Range Experiment Station, 138-142.

Rice, R.M. 1982. Sedimentation in the chaparral: how do you handle unusual events? In: Swanson, F.J., Janda, R.J., Dunne, T., and Swanston, D.N. (editors) Sediment budgets and routing in forested drainage basins. Rep. PHW-141, US Dept. Agric., Forest Service, Pacific Northwest Forest and Range Experiment Station, 39-49.

Rice, R.M. and Pillsbury, N.H. 1982. Predicting landslides in clearcut patches. In: Walling, D.E. (editor) Recent developments in the explanation and prediction of erosion and sediment yield, Intl. Ass. Hydrol. Sci. Publ. no. 137, 303-311.

Roose, E.J. 1977. Application of the Universal Soil Loss Equation of Wischmeier and Smith in West Africa. In: Greenland, D.J. and Lal, R. (editors) Soil conservation and management in the humid tropics, Wiley, 177-187.

Rose, C.W. 1985. Developments in soil erosion and deposition models. In: Stewart, B.A. (editor) Advances in soil science, Vol. 2, Springer-Verlag, New York, 1-63.

Ross, B.B., Shanholtz, V.O., and Contractor, D.N. 1980. A spatially responsive hydrologic model to predict erosion and sediment transport. Wat. Resour. Bull., 16(3), 538-545.

Rowlinson, D.L. and Martin, G.L. 1971. Rational model describing slope erosion. J. Irrig. Drain. Div., Am. Soc. Civ. Engrs., 97(IR1), 39-50.

Rowntree, K.M. 1982. Sediment yields from a laboratory catchment and their relationship to rilling and surface armouring. Earth Surf. Process. Landf., 7, 153-170.

Rutter, A.J., Kershaw, K.A., Robins, P.C., and Morton, A.J. 1971/72. A predictive model of rainfall interception in forests, 1. Derivation of the model from observations in a plantation of Corsican pine. Agric. Meteorol., 9, 367-384.

Samaga, B.R., Ranga Raju, K.G., and Garde, R.J. 1986. Bed load transport of sediment mixtures; Suspended load transport of sediment mixtures. J. Hydraul. Engrg., Am. Soc. Civ. Engrs., 112(11), 1003-1035.

Shen, H.W. and Li, R.M. 1976. Watershed sediment yield. In: Shen, H.W. (editor and publisher) Stochastic approaches to water resources. Fort Collins, Colorado, 21.1-21.68.

Simons, D.B. and Li, R-M. 1982. Bank erosion on regulated rivers. In: Hey, R.D., Bathurst, J.C., and Thorne, C.R. (editors) Gravel-bed rivers, Wiley, Chichester, 717-747.

Simons, D.B. and Sentürk, F. 1977. Sediment transport technology. Water Resources Publ., Fort Collins, Colorado, 807pp.

Simons, D.B., Li, R-M., Ward, T.J., and Shiao, L.Y. 1982. Modeling of water and sediment yields from forested drainage basins. In: Swanson, F.J., Janda, R.J., Dunne, T., and Swanston, D.N. (editors) Sediment budgets and routing in forested drainage basins. Rep. PHW-141, US Dept. Agric., Forest Service, Pacific Northwest Forest and Range Experiment Station, 24-38.

Singh, V.P., Krstanovic, P.F., and Lane, L.J. 1988. Stochastic models of sediment yield. In: Anderson, M.G. (editor) Modelling geomorphological systems, Wiley, Chichester, 259-285.

Smerdon, E.T. and Beasley, R.P. 1961. Critical tractive forces in cohesive soils. Agricultural Engineering, 42(1), 26-29.

Smith, D.D. 1958. Factors affecting rainfall erosion and their evaluation. In: Intl. Ass. Sci. Hydrol. Publ. no. 43, 97-107.

Smith, R.E. and Knisel, W.G. 1985. Summary of methodology in the CREAMS2 model. In: DeCoursey, D.G. (editor) Proceedings of the natural resources modeling symposium, US Dept. Agric., ARS-30, 33-36.

Styczen, M. and Høgh-Schmidt, K. 1988. A new description of splash erosion in relation to rain drop sizes and vegetation. In: Morgan, R.P.C. and Rickson, R.J. (editors), Agriculture: erosion assessment and modelling. Commission of the European Communities, Proc. Workshop, Rep. EUR 10860 EN, 147-184.

Sundborg, A. 1983. Sedimentation problems in river basins. Nature and Resources, 19(2), 10-21.

Swanson, N.P. 1965. Rotating-boom rainfall simulator. Trans. Am. Soc. Agric. Engrs., 8(1), 71-72.

Thomas, W.A. 1982. Mathematical modelling of sediment movement. In: Hey, R.D., Bathurst, J.C., and Thorne, C.R. (editors) Gravel-bed rivers, Wiley, Chichester, 487-508.

Thorne, C.R. 1982a. Bank erosion in regulated rivers. In: Hey, R.D., Bathurst, J.C., and Thorne, C.R. (editors) Gravel-bed rivers, Wiley, Chichester, 750-753 (discussion).

Thorne, C.R. 1982b. Processes and mechanisms of river bank erosion. In: Hey, R.D., Bathurst, J.C., and Thorne, C.R. (editors) Gravel-bed rivers, Wiley, Chichester, 227-259.

Toffaleti, F.B. 1969. Definitive computations of sand discharge in rivers. J. Hydraul. Div., Am. Soc. Civ. Engrs., 95(HY1), 225-248.

UNESCO. 1985. Recent developments in erosion and sediment yield studies. Technical documents in hydrology, UNESCO, Paris, 127pp.

USDA. 1987. User requirements. USDA water erosion prediction project (WEPP). US Dept. Agric., Nat. Soil Erosion Res. Lab., Purdue Univ., West Lafayette.

Vanoni, V.A. (editor) 1975. Sedimentation engineering. Am. Soc. Civ. Engrs., Manuals and reports on engineering practice, no. 54, New York, 745pp.

VanSickle, J. and Beschta, R.L. 1983. Supply-based models of suspended sediment transport in streams. Wat. Resour. Res., 19(3), 768-778.

Verhaegen, Th. 1987. The use of small flumes for the determination of soil erodibility. Earth Surf. Process. Landf., 12(2), 185-194.

Vis, M. 1986. Interception, drop size distributions and rainfall kinetic energy in four Colombian forest ecosystems. Earth Surf. Process. Landf., 11(6), 591-603.

Walling, D.E. 1983. The sediment delivery problem. J. Hydrol., 65, 209-237.

Walling, D.E. 1988. Erosion and sediment yield research - some recent perspectives. J. Hydrol., 100, 113-141.

Ward, T.J. 1987. Adaptation and testing of a rainfall-runoff, surface erosion model for army training impact prediction. New Mexico State Univ. Engineering Research Center. Completion Rep. for Contract DACA88-83-M-0854. Prepared for US Army Corps of Engrs., Construction Engineering Research Laboratory, Champaign, Illinois.

Ward, T.J., Li, R-M., and Simons, D.B. 1981. Use of a mathematical model for estimating potential landslide sites in steep forested drainage basins. In: Davies, T.R.H. and Pearce, A.J. (editors) Erosion and sediment transport in Pacific Rim steeplands, Intl. Ass. Hydrol. Sci. Publ. no. 132, 21-41.

White, W.R., Milli, H., and Crabbe, A.D. 1975. Sediment transport theories: a review. Proc. Instn. Civ. Engrs., 59(2), 265-292.

Wicks, J.M., Bathurst, J.C., Johnson, C.W., and Ward, T.J. 1988. Application of two physically-based sediment yield models at plot and field scales. In: Sediment Budgets, Intl. Ass. Hydrol. Sci. Publ. no. 174.

Willetts, B.B., Maizels, J.K., and Florence, J. 1987. The simulation of stream bed armouring and its consequences. Proc. Instn. Civ. Engrs., 82(1), 799-814.

Williams, J.R. and Berndt, H.D. 1972. Sediment yield computed with universal equation. J. Hydraul. Div., Am. Soc. Civ. Engrs., 98(HY12), 2087-2098.

Wischmeier, W.H. and Smith, D.D. 1965. Predicting rainfall-erosion losses from cropland east of the Rocky Mountains. US Dept. Agric. Handbk. no. 282.

Wischmeier, W.H. and Smith, D.D. 1978. Predicting rainfall erosion losses. US Dept. Agric. Handbk. no. 537.

Wolman, M.G. 1977. Changing needs and opportunities in the sediment field. Wat. Resour. Res., 13(1), 50-54.

Wright, A.C. 1987. A model of the redistribution of disaggregated soil particles by rainsplash. Earth Surf. Process. Landf., 12(6), 583-596.

Yalin, M.S. 1963. An expression for bed-load transportation. J. Hydraul. Div., Am. Soc. Civ. Engrs., 89(HY3), 221-250.

Yang, C.T. 1973. Incipient motion and sediment transport. J. Hydraul. Div., Am. Soc. Civ. Engrs., 99(HY10), 1679-1704.

Yoon, Y.N. and Wenzel, H.G. 1971. Mechanics of sheet flow under simulated rainfall. J. Hydraul. Div., Am. Soc. Civ. Engrs., 97(HY9), 1367-1386.

Young, R.A. and Onstad, C.A. 1982. The effect of soil characteristics on erosion and nutrient loss. In: Walling, D.E. (editor) Recent developments in the explanation and prediction of erosion and sediment yield, Intl. Ass. Hydrol. Sci. Publ. no. 137, 105-113.

Young, R.A. and Wiersma, J.L. 1973. The role of rainfall impact in soil detachment and transport. Wat. Resour. Res., 9(6), 1629-1636.

Zingg, A.W. 1940. Degree and length of land slope as it affects soil loss in runoff. Agricultural Engineering, 21(2), 59-64.

APPENDIX A - DETERMINATION OF THE MOMENTUM SQUARED

A.1 MOMENTUM SQUARED FOR DIRECT RAINFALL

Assuming the Marshall and Palmer (1948) raindrop size distribution to be appropriate, the number of drops per m^3 having diameters between d and d+Δd is given by n(d)Δd, where

$$n(d) = n_0 \, e^{-\lambda d} \tag{A.1}$$

with $n_0 = 8x10^6$ (m^{-4}); $\lambda = 4.1x10^3 \, (3.6x10^6 I)^{-0.21}$ (m^{-1}); I = rainfall intensity (m s^{-1}); d = drop diameter (m).

The number of drops with diameter between d and d+Δd falling on a 1-m^2 area of land per second is n(d)ΔdV, where V is the terminal velocity of a raindrop of diameter d+Δd/2 (m s^{-1}). The terminal velocity can be calculated from the following function, fitted by Mualem and Assouline (1986) to the data of Laws (1941) and Gunn and Kinzer (1949)

$$V = 9.5 \left[1 - e^{-\left[\frac{d+\Delta d/2}{1.77x10^{-3}}\right]^{1.147}} \right] \tag{A.2}$$

The total square of momenta for each drop with a diameter between d and d+Δd, M(d), is the product of the number of drops falling per m^2 per second and their momenta squared, i.e.

$$M(d) \;=\; n(d)\,\Delta d\, V \left[\frac{\pi(d+\Delta d/2)^3}{6} \rho \, V\right]^2 \tag{A.3}$$

where ρ = density of water.

Using equations A.1 and A.2, equation A.3 was numerically integrated between diameters of 0.1 and 6.1 mm with steps of 0.2

mm. The calculations were repeated for rainfall intensities from 1 mm h^{-1} to 250 mm h^{-1} using a step of 1 mm h^{-1}. These data were then used to determine the coefficient and exponent for the model

$$M_R = \alpha\ I^{\beta} \tag{A.4}$$

where M_R = momentum squared per unit area per unit time interval ((kg m $s^{-1})^2$ m^{-2} s^{-1}); I = rainfall intensity (m s^{-1}); α, β = coefficient and exponent. A least squares curve fitting algorithm was used, with the curve segmented into the regions shown in Table A.1 based on analysis of correlation coefficients. The number of regions chosen results from balancing the requirements of optimising the goodness of fit criteria and keeping the table small for rapid searching during the SHESED simulations.

Table A.1 Parameters and correlation coefficients for the relationship between momentum squared and rainfall intensity (equation A.4)

Intensity, I (mm h^{-1})	α	β	Correlation coefficient
$0 \le I < 10$	3214.9	1.6896	0.9998
$10 \le I < 50$	583.4	1.5545	1.0002
$50 \le I < 100$	133.1	1.4242	0.9983
$100 \le I < 250$	29.9	1.2821	1.0007

Using a similar method, Styczen and Høgh-Schmidt (1988) determined exponent values of 1.63 for rainfall intensities below 100 mm h^{-1}, and 1.43 for rainfall intensities between 100 and 250 mm h^{-1}.

A.2 MOMENTUM SQUARED FOR LEAF DRIP

To facilitate the computations and reduce the data requirements, it is assumed that the process of soil detachment by leaf drip impact can be simulated using a *representative* leaf drip diameter falling from a representative canopy height. The evapotranspiration component of the SHE supplies the drainage rate, DRAINA (in m s^{-1}), for each grid rectangle at the current time step. This rate applies to the full grid rectangle and not just the area below the canopy. DRAINA includes leaf drip (large coalesced droplets), leaf splash (small shattered droplets) and stem flow; therefore DRAINA values have to be adjusted by multiplying by the input parameter DRIP% which is the proportion of drainage falling as leaf drip. Suggested values for the leaf drip diameter, fall height and DRIP% are presented in Table 4.2.

For a grid rectangle the total volume of leaf drip falling per unit area per unit time is the product of DRAINA and DRIP%. Assuming a representative leaf drip diameter of d (m), the total number of leaf drips per m^2 per second, n_d, is given by the total volume of leaf drips per m^2 per second divided by the volume of one leaf drip, i.e.

$$n_d = \frac{\text{DRAINA DRIP\%}}{(\pi d^3/6)} \tag{A.5}$$

The total momentum squared per m^2 per second is given by the product of the momentum squared of one leaf drip and n_d, i.e.

$$M_d = \left[\frac{V\rho\pi d^3}{6}\right]^2 \frac{\text{DRIP\% DRAINA}}{(\pi d^3/6)} \tag{A.6}$$

where M_d = total momentum squared for leaf drip per unit area per unit time ($(kg\ m\ s^{-1})^2\ m^{-2}\ s^{-1}$); ρ = density of water ($kg\ m^{-3}$); V = leaf drip fall velocity ($m\ s^{-1}$).

All terms on the right hand side of equation A.6 are known except the leaf drip fall velocity. This is mainly a function of drip diameter and fall height and for turbulent flow conditions the following theoretical equation has been derived by Epema and Riezebos (1983)

$$V = \left[\frac{M}{\beta} g \left(1 - e^{(-2X\beta/M)}\right) \right]^{\frac{1}{2}} \qquad \text{(A.7)}$$

where V = velocity ($m\ s^{-1}$); M = mass of the leaf drip (kg); β = friction constant; g = acceleration of gravity ($m\ s^{-2}$); X = fall distance (m).

The friction constant can vary with both drip diameter and fall height, and, based on graphs presented by Epema and Riezebos, the following expressions were obtained to characterise β

$$\begin{aligned} M/\beta &= 2200\ d && \text{if } d \le 3.3 \text{ mm} \\ M/\beta &= 1640\ d + 1.93 && \text{if } d > 3.3 \text{ mm and } X < 7.5 \text{ m} \qquad \text{(A.8)} \\ M/\beta &= 660\ d + 5.14 && \text{if } d > 3.3 \text{ mm and } X \ge 7.5 \text{ m} \end{aligned}$$

where d = drip diameter (m).

For drip diameters less than 2 mm the above method over-estimates the fall velocities, however this is of minor importance as representative leaf drips are likely to be of a diameter of at least 4 mm (see Table 4.2).

Thus the momentum squared can be calculated from equations A.6, A.7 and A.8 if the leaf drip fall height, drip diameter, rate of canopy drainage and proportion of canopy drainage falling as leaf drips are known.

APPENDIX B - TRANSPORT FORMULAE

B.1 SHIELDS CURVE

The Shields curve is a graphical relationship giving the critical dimensionless shear stress, F_{*c}, as a function of the particle (or boundary) Reynolds number, R_*, where

$$F_{*c} = \frac{\tau_c}{(\rho_s - \rho)gD} \tag{B.1}$$

$$R_* = \frac{V_* D}{v} \tag{B.2}$$

$$V_* = \left[\frac{\tau}{\rho} \right]^{0.5} \tag{B.3}$$

where τ_c = critical shear stress; ρ_s = sediment density; ρ = water density; g = acceleration due to gravity; D = sediment particle diameter; V_* = shear velocity; τ = shear stress (τ = $\rho g h S$, where h = water depth; S = water surface slope); v = kinematic viscosity of water.

Values on the Shields curve correspond to critical conditions for initiation of motion; the region below the curve represents no motion. The Shields curve is shown in Fig. B.1 along with the extension of the curve to small particle sizes by Mantz (1977). For use in the SHESED program the curve has been approximated by the set of equations shown in Table B.1. For a given value of the particle Reynolds number, the equations shown in Table B.1 can be used to calculate the critical dimensionless shear stress, F_{*c}, and thus, from a simple rearrangement of equation B.1, the critical shear stress, τ_c.

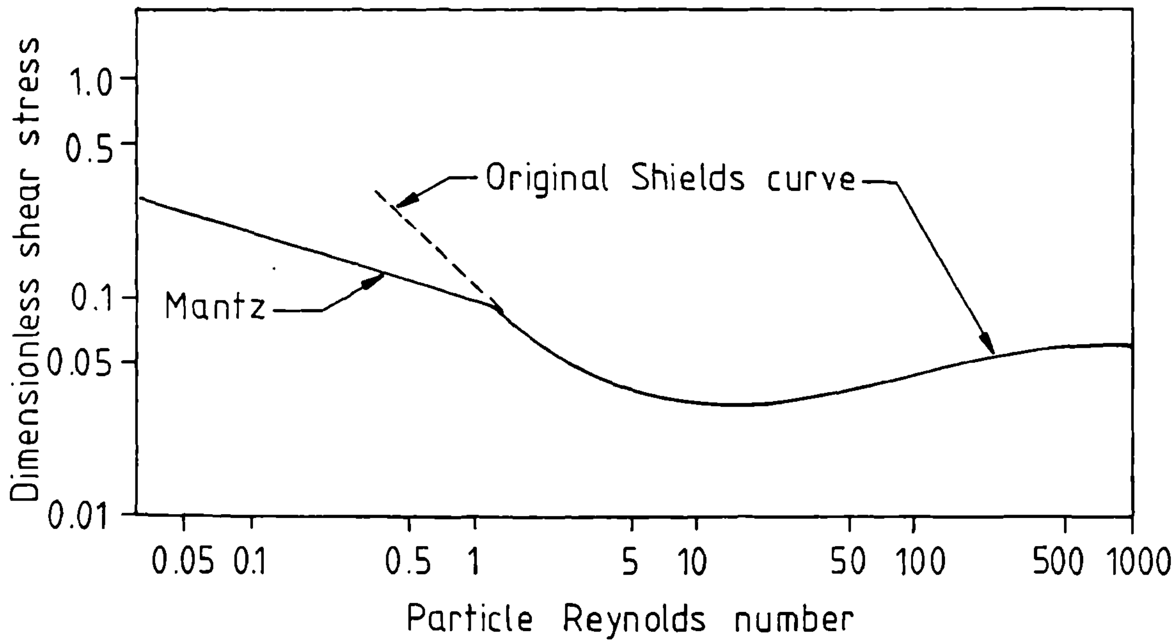

Fig. B.1 Shields curve as extended by Mantz (1977).

Table B.1 Equations to approximate the extended Shields curve

Range of validity of a and b	$F_{*c} = aR_*^b$	
	a	b
$0.03 < R_* \leq 1.0$	0.10	-0.30
$1.0 < R_* \leq 6.0$	0.10	-0.62
$6.0 < R_* \leq 30$	0.033	0
$30 < R_* \leq 135$	0.013	0.28
$135 < R_* \leq 400$	0.030	0.10
$400 < R_*$	0.056	0

B.2 YALIN (1963) BED LOAD EQUATION

The Yalin bed load equation is an excess shear type equation derived from an analysis of saltating particles and calibrated using a limited experimental data set. The Yalin equation is

$$G = WV_{*}D\ 0.635\ \delta\ \left[1 - \frac{1}{a\delta} \log_e(1 + a\delta)\right] \tag{B.4}$$

with

$$\begin{aligned} \delta &= \frac{F_{*}}{F_{*c}} - 1 && \text{if } F > F_{*c} \\ \delta &= 0 && \text{if } F \le F_{*c} \end{aligned} \tag{B.5}$$

$$a = 2.45\ s^{-0.4}\ (F_{*c})^{0.5} \tag{B.6}$$

$$s = \frac{\rho_s}{\rho} \tag{B.7}$$

where G = volumetric sediment transport rate; W = width of flow; V_{*} = shear velocity (equation B.3); D = sediment diameter; F_{*} = dimensionless shear stress (equation B.1); F_{*c} = critical dimensionless shear stress from the Shields curve (see Section B.1); s = specific gravity of sediment; ρ_s = density of sediment; ρ = density of water.

B.3 ENGELUND-HANSEN (1967) TOTAL LOAD EQUATION

The Engelund-Hansen equation was developed by equating the work done by the drag forces of the flow to the potential energy gained by particles as they move up the face of a dune. The form of the equation used in SHESED is

$$G = \frac{0.05\ W\ V^2\ h^{1.5}\ S^{1.5}}{(s - 1)^2\ D\ \sqrt{g}} \tag{B.8}$$

where G = volumetric sediment transport rate; W = width of flow; V = water velocity; h = flow depth; S = water surface slope; s = specific gravity of sediment (equation B.7); D = sediment diameter; g = acceleration due to gravity.

The suggested applicability of the Engelund-Hansen equation is for $\sqrt{(D_{75}/D_{25})} < 1.6$ and for a mean fall diameter greater than 0.15 mm.

B.4 ACKERS-WHITE (1973) TOTAL LOAD EQUATION

The Ackers-White equation was developed by determining the appropriate form of the equation from physical considerations and dimensional analysis, but used empirical data to determine the various coefficients. The calculation procedure for the Ackers-White equation, as used in SHESED, is described below.

(1) Determine the dimensionless sediment diameter, D_{gr}

$$D_{gr} = D \left[\frac{g(s - 1)}{v^2}\right]^{\frac{1}{3}} \tag{B.9}$$

where D = particle diameter (Ackers and White (1973) advise the use of the D_{35} size); g = acceleration due to gravity; s = specific gravity of sediment (equation B.7); v = kinematic viscosity of water.

(2) Determine the transition exponent, n, the initial motion parameter, A, and the coefficient and exponent in the sediment transport function (c and M respectively)

For $D_{gr} > 60$

$$n = 0 \qquad (B.10)$$

$$A = 0.17 \qquad (B.11)$$

$$M = 1.5 \qquad (B.12)$$

$$c = 0.025 \qquad (B.13)$$

For $60 \geq D_{gr} \geq 1$

$$n = 1 - 0.56\log_{10}D_{gr} \qquad (B.14)$$

$$A = \frac{0.23}{\sqrt{(D_{gr})}} + 0.14 \qquad (B.15)$$

$$M = \frac{9.66}{D_{gr}} + 1.34 \qquad (B.16)$$

$$c = 10^{(2.86\log_{10}D_{gr} - (\log_{10}D_{gr})^2 - 3.53)} \qquad (B.17)$$

(3) Determine the particle mobility, F_{gr}

$$F_{gr} = \frac{V_*^n}{\sqrt{(gD(s-1))}} \left[\frac{V}{\sqrt{(32)}\log_{10}(\frac{10h}{D})} \right]^{1-n} \qquad (B.18)$$

where V_* = shear velocity (equation B.3); V = mean flow velocity; h = depth of flow.

(4) Determine the dimensionless sediment transport rate, G_{gr}

$$G_{gr} = c\left[\frac{F_{gr}}{A} - 1\right]^M \qquad \text{if } A < F_{gr}$$

$$G_{gr} = 0 \qquad \text{if } A \geq F_{gr} \qquad (B.19)$$

(5) Determine the volumetric sediment transport rate, G,

$$G = \frac{Q\ G_{gr} D\ (V/V_*)^n}{h} \tag{B.20}$$

The suggested applicability of this equation is for $D_{gr} \geq 1$ and for flows with Froude numbers less than 0.8.

B.5 DAY (1980) MODIFICATION TO THE ACKERS-WHITE EQUATION

The Day extension to the Ackers-White total load equation seeks to account for the effects of particle exposure and shielding on the initiation of movement of nonuniform bed material. The procedure, as used in SHESED, is presented below. (For an explanation of the notation see Section B.4.)

(1) Determine the D_{16}, D_{50}, and D_{84} sizes of the bed material (this will be of the active layer for SHESED channel computations).

(2) Determine the critical diameter, D_A, which is the size fraction in a nonuniform bed which would begin to move at the same flow conditions as would a uniform bed of size D_A.

$$D_A = 1.62\ D_{50} \left[\frac{D_{84}}{D_{16}}\right]^{-0.28} \tag{B.21}$$

(3) Determine the dimensionless grain size for the critical diameter

$$(D_{gr})_A = D_A \left[\frac{g(s - 1)}{v^2}\right]^{\frac{1}{3}} \tag{B.22}$$

(4) Determine the initial motion parameter for D_A

$$A = \frac{0.23}{\sqrt{(D_{gr})_A}} + 0.14 \qquad \text{if } (D_{gr})_A < 60$$
$$A = 0.17 \qquad \text{if } (D_{gr})_A > 60 \tag{B.23}$$

The remaining steps in the procedure are repeated for all size fractions present.

(5) Determine the initial motion parameter for the current size fraction, m, of diameter D_m

$$A_m = A[0.4(D_m/D_A)^{-0.5} + 0.6] \tag{B.24}$$

(6) Determine n, M and c for the size fraction m, using $(D_{gr})_m$ and the equations in Section B.4.

(7) Determine $(F_{gr})_m$ from equation B.18.

(8) Determine $(G_{gr})_m$ from equation B.19.

(9) Determine G_m from equation B.20 and multiply this by the proportion of size fraction m in the potential sediment load. Here, the potential sediment load consists of sediment entering the node region from overland flow and upstream inflow, in addition to sediment in the active bed layer, but excludes sediment of silt and clay sizes.

The Day procedure should not be extrapolated below a $\sqrt{(D_{84}/D_{16})}$ value of about 1.4, because, as $\sqrt{(D_{84}/D_{16})}$ tends towards unity (uniform bed material), D_A does not tend towards D_{50}. In SHESED the Day modification is not used if $\sqrt{(D_{84}/D_{16})}$ is less than 1.4. Also, extrapolation above a $\sqrt{(D_{84}/D_{16})}$ value of about five or above a D_m/D_A value of about four is not recommended.

APPENDIX C - PROCEDURE TO UPDATE THE ACTIVE AND PARENT LAYERS

The following procedure, based on volumetric considerations, is used to update the active and parent layer size distributions of the channel bed material at the end of each time step. The procedure is presented here for one channel node but will be repeated for all nodes.

First some definitions: PA_m = proportion of sediment size fraction m in the active layer; PP_m = proportion of sediment size fraction m in the parent layer; AD = active layer thickness; PD = parent layer thickness; SD = total depth of bed material (= AD + PD); Δz_m = depth of erosion (-ve) or deposition (+ve) for size fraction m over the time step Δt; $\Sigma\Delta z$ = the summation of Δz_m over all size fractions; D_{99} = sediment diameter for which 99% of the original (i.e. at time = 0) parent layer sediment particles are finer. The superscripts n and n+1 refer to quantities determined at the start and end of the time step respectively.

The bed material depth and the active and parent layer depths at the end of the time step are given by

$$SD^{n+1} = SD^n + \Sigma\Delta z \tag{C.1}$$

$$AD^{n+1} = D_{99} \quad \text{if} \quad D_{99} \le SD^{n+1}$$

$$\tag{C.2}$$

$$AD^{n+1} = SD^{n+1} \quad \text{if} \quad D_{99} > SD^{n+1}$$

$$PD^{n+1} = SD^{n+1} - AD^{n+1} \tag{C.3}$$

The methods for calculating the new proportions in the active and parent layers depend on whether net deposition or erosion occurred during the time step. For net deposition ($\Sigma\Delta z \geq 0$)

$$PA_m^{n+1} = \frac{PA_m^n\, AD^n + \Delta z_m}{AD^n + \Sigma\Delta z} \tag{C.4}$$

$$PP_m^{n+1} = \frac{PP_m^n\, PD^n + PA_m^{n+1}\, (PD^{n+1} - PD^n)}{PD^{n+1}} \tag{C.5}$$

For net erosion ($\Sigma\Delta z < 0$)

$$PA_m^{n+1} = \frac{PA_m^n\, AD^n + \Delta z_m + PP_m^n\, (AD^{n+1} - AD^n - \Sigma\Delta z)}{AD^{n+1}} \tag{C.6}$$

$$PP_m^{n+1} = \frac{PP_m^n\, PD^n + PP_m^n\, (PD^{n+1} - PD^n)}{PD^{n+1}} \tag{C.7}$$

However if all the sediment is eroded from a layer then obviously the proportions of sediment in that layer are zero, i.e.

$$PA_m^{n+1} = 0 \quad \text{if} \quad AD^{n+1} = 0 \tag{C.8}$$

and

$$PP_m^{n+1} = 0 \quad \text{if} \quad PD^{n+1} = 0 \tag{C.9}$$

APPENDIX D - CAUSE OF THE NEGATIVE CONCENTRATIONS IN THE NUMERICAL SOLUTION OF THE ROUTING SCHEMES

The finite difference solutions of the hillslope and channel sediment continuity equations will, under certain ciroumstances, produce physically meaningless negative sediment concentrations. The cause of these negative concentrations are investigated in this appendix for the simplified case of a single channel link (Fig. D.1(a)) with no influx of sediment from hillslope processes, no available sediment stored on the channel bed, and only one particle size present, which is fine enough to be transported at the same velocity as the water and which the water can always transport (i.e. a very high transport capacity). These simplifications are introduced only to facilitate the explanation of the negative concentrations; the same conclusions will be reached for the more general case.

With the assumptions described above, and neglecting the diffusion term, the partial differential equation for conservation of sediment mass in channels (equation 5.1) can be written

$$\frac{\partial(AC)}{\partial t} + \frac{\partial(ACV)}{\partial x} = 0 \qquad (D.1)$$

where A = cross-sectional flow area; C = volumetric sediment concentration; V = water velocity (= sediment velocity); t = time; x = distance.

As the sediment transport rate G = ACV, and using the finite difference approximation shown in Fig. 4.2, equation D.1 becomes

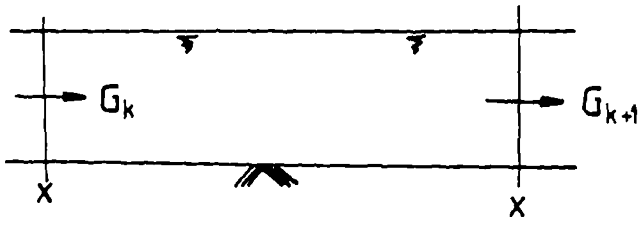

(a) Simple channel link

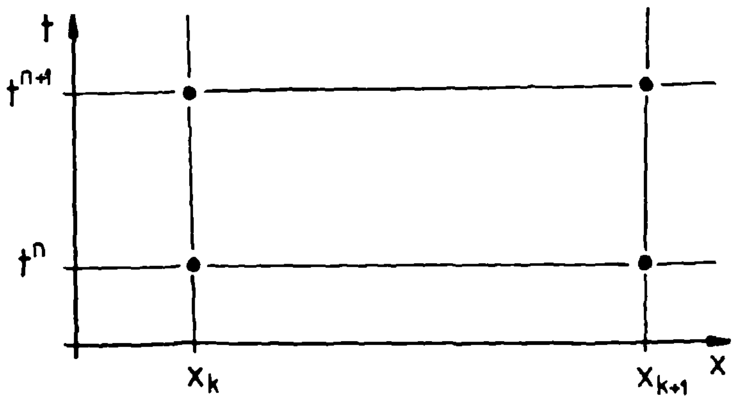

(b) Finite difference grid

Fig. D.1 Schematic representation of a channel link and the finite difference notation.

$$\frac{1}{\Delta t}\left[\ \phi[(AC)_{k+1}^{n+1} - (AC)_{k+1}^{n}] + (1-\phi)[(AC)_{k}^{n+1} - (AC)_{k}^{n}]\ \right]$$

$$+\ \frac{1}{\Delta x}\left[\ \theta[\ G_{k+1}^{n+1} - G_{k}^{n+1}] + (1-\theta)[G_{k+1}^{n} - G_{k}^{n}]\ \right] = 0 \qquad (D.2)$$

where Δt = computational time step (s); ϕ = space weighting factor; θ = time weighting factor; Δx = distance step (= length of the river link); n and n+1 refer to variables evaluated at the start (t^n) and end ($t^n + \Delta t$) of the time step respectively; k and k+1 refer to variables evaluated at the upstream (x_k) and downstream ($x_k + \Delta x$) ends of the link respectively (see Fig. D.1(b)).

Rearranging equation D.2 and noting that $G_{k+1}^{n+1} = (ACV)_{k+1}^{n+1}$ leads to

$$C_{k+1}^{n+1} = \Bigg[\ \Delta x\left[\ \phi\ (AC)_{k+1}^{n} - (1-\phi)\ (AC)_{k}^{n+1} + (1-\phi)\ (AC)_{k}^{n}\ \right]$$

$$+\ \Delta t\left[\ \theta\ G_{k}^{n+1} - (1-\theta)\ G_{k+1}^{n} + (1-\theta)\ G_{k}^{n}\ \right]\Bigg]$$

$$/\ [\Delta x\phi A_{k+1}^{n+1} + \Delta t\theta(AV)_{k+1}^{n+1}] \qquad (D.3)$$

If the case where $\phi = \theta = 0.5$ is considered, and the sediment supply to the link at time t^{n+1} is zero (i.e. $G_{k}^{n+1} = (ACV)_{k}^{n+1} = 0$), equation D.3 can be written

$$C_{k+1}^{n+1} = \left[\ \overbrace{\frac{\Delta x}{2}\left[\ (AC)_{k+1}^{n} + (AC)_{k}^{n}\ \right]}^{[1]} + \overbrace{\frac{\Delta t}{2}\,G_{k}^{n}}^{[2]} - \overbrace{\frac{\Delta t}{2}\,G_{k+1}^{n}}^{[3]}\ \right]$$

$$/\ [\frac{\Delta x}{2}\,A_{k+1}^{n+1} + \frac{\Delta t}{2}\,(AV)_{k+1}^{n+1}] \qquad (D.4)$$

The first term in the numerator of equation D.4, term [1], represents the volume of sediment present in the link at time t^n; the second, term [2], represents the summation of the influx of sediment into the link over the time interval Δt; and the third, term [3], represents the flux of sediment out of the link at time t^n (multiplied by $\Delta t/2$). As all the variables on the right hand side of equation D.4 are always positive, negative values of C_{k+1}^{n+1} can be predict only if [3] > ([1] + [2]). This corresponds to the situation when the supply of sediment ([1] + [2]) is less than that required to satisfy mass balance (using positive concentrations only) from a trapezoidal integration with intervals which must correlate with the positions x_k and x_{k+1} of the finite difference grid. This is explained further with the aid of Fig. D.2. The idealised 'actual' variation in the sediment discharge over time is represented by the line a-b-d, and shows that in this case of limited supply of sediment, all available sediment will have been transported from the link at the time represented by the point b (i.e. before t^{n+1}). However, as the finite difference scheme is based on the determination of values at fixed grid points, with a linear variation between grid points, the path a-b-d cannot be followed. The finite difference solution must follow the path a-c-e, which conserves total sediment mass but involves the introduction of a physically-meaningless negative concentration (point e).

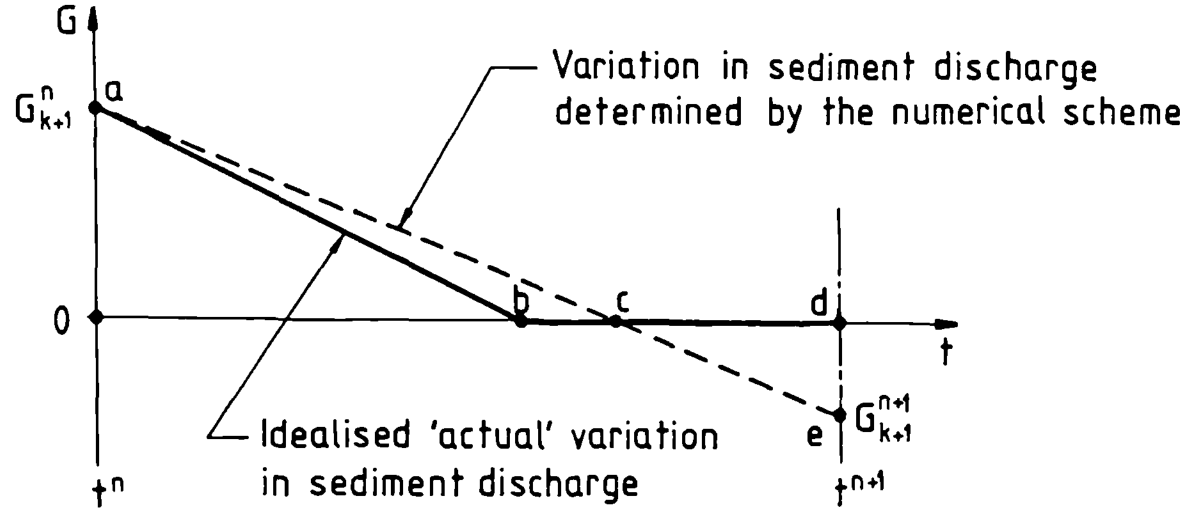

Fig. D.2 Graph showing the cause of the negative concentrations.

The conservation of mass is represented by the areas between the time-axis and the lines a-b-d and a-c-e. The total available volume of sediment is equal to the area between the time-axis and the idealised 'actual' variation in sediment discharge (i.e. the area abo), this volume of sediment is equal to the area between the time-axis and the variation in sediment discharge calculated by the finite difference scheme, i.e. the algebraic sum of the areas aco and cde (a negative area).

APPENDIX E - STRUCTURE OF SHESED

The SHESED program is designed as a separate module in the SHE hydrological modelling system, and is run after the main SHE software. Once a satisfactory calibration is achieved for water flows, the SHE is used to generate four unformatted data files containing catchment segmentation and set up data, and time series of precipitation rates, canopy drainage, and overland and channel water depths and flowrates. SHESED reads the SHE produced initialisation data file and the SHESED data file and does some preliminary calculations in the initialisation phase. This is followed by the simulation phase calculations. First the SHE produced data files are read to determine the values of hydrological variables for the current time step. Next the program loops over all the overland flow grid rectangles to calculate the erosion/deposition and sediment transport rates for all the grid rectangles. The final stage of the main calculations involves looping over the channel links to determine the erosion/deposition and sediment transport rates for all channel nodes/links. Before incrementing the time and repeating the simulation calculations, mass balance calculations are done and selected results are sent to the main results and plotting output files (see Fig. E.1).

The SHESED program is written in structured Fortran77 and consists of about 3600 lines of code (a third of which are comments) in a total of 30 routines. The execution times for the applications presented in this thesis varied between about 1 and 100 seconds of CPU time on an Amdahl 5860 mainframe computer.

Full documentation has been prepared under another project for the Natural Environment Research Council, Water Resource Systems Research Unit at the University of Newcastle upon Tyne.

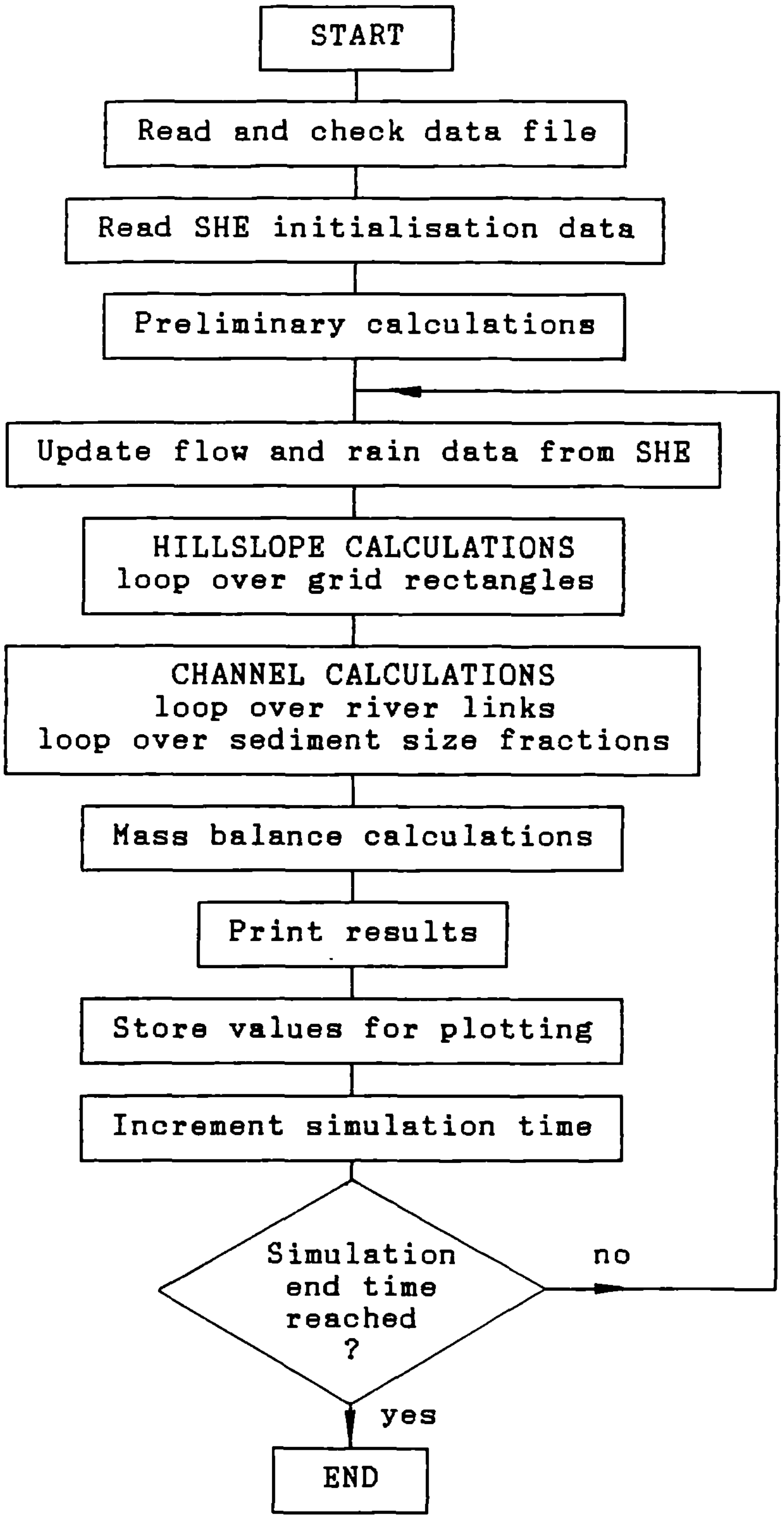

Fig. E.1 Program flow diagram

APPENDIX F - DATA REQUIREMENTS OF SHESED

Data are made available to SHESED either by being passed from the SHE software or through the SHESED data file. The data transferred from the SHE consist of initialisation data (e.g. catchment segmentation, vegetation and soil type distributions) and simulation data (time series of water flow rates and depths, rainfall rates and canopy drainage). The SHE data requirements were discussed in Section 3.3.1. The contents of the SHESED data file are listed below, although exact requirements will depend on the application.

(a) Simulation start and end times.

(b) Computational time step (can vary through the simulation).

(c) Printing selection:

- printing time step (can vary)
- results to print
- results for plotting
- debugging values

(d) Soil data for each soil type:

- particle size distribution and size fraction diameters and densities
- surface porosity
- raindrop soil detachment coefficient
- overland flow soil detachment coefficient

(e) Vegetation data for each canopy vegetation:

- representative fall height for leaf drip
- proportion of canopy drainage falling as leaf drip
- representative leaf drip diameter

(f) Ground cover density for each grid rectangle.

(g) Local values of the exponent and coefficient in the relationship between rainfall intensity and momentum squared, or an indication that the default values (as determined from the Marshall-Palmer raindrop size distribution) are to be used.

(h) Depth of any initially loose soil for each overland flow grid rectangle.

(i) Channel data for each computational node/link:

- bed material size distribution and size fraction diameters and densities for the active and parent layers
- active bed width
- thickness of loose bed material
- bed porosity
- initial sediment transport rates and particle size distributions

(j) Choice of sediment transport capacity equation for overland and for channel calculations.

(k) Data for channel sediment inflows to the catchment either as a and b in $G = aQ^b$ or as a time series of transport rates. The size distribution is also needed.

(l) If the channel segmentation is such that flows upslope will occur, then a renumbering of the channel links has to be input. This defines the flow direction and is used in the ordering of the numerical solution of the channel sediment continuity equation.